2019

CHARACTERIZATION OF NOVEL CYP26B1-INHIBITOR, DX314, FOR THE TREATMENT OF KERATINIZATION DISORDERS

Joachim Gwenn-Stephan Veit

CHARACTERIZATION OF NOVEL CYP26B1-INHIBITOR, DX314, FOR THE TREATMENT OF KERATINIZATION DISORDERS

BY

JOACHIM GWENN-STEPHAN VEIT

B.S. Molecular and Cellular Biology,
University of Illinois, Urbana-Champaign, IL, 2011

Dissertation

presented in partial fulfillment of the requirements for the degree of

Doctor of Philosophy
Pharmaceutical Sciences and Drug Design

University of Montana
Missoula, MT

May 2019

Approved by:

Scott Whittenburg, Dean of The Graduate School
Graduate School

Philippe J. Diaz, Chair
Department of Biomedical and Pharmaceutical Sciences

Erica L. Woodahl
Department of Biomedical and Pharmaceutical Sciences

Keith K. Parker
Department of Biomedical and Pharmaceutical Sciences

Kasper B. Hansen
Department of Biomedical and Pharmaceutical Sciences

Travis J. Wheeler
Department of Computer Science

Veit, Joachim G.S., Ph.D. Spring 2019
Pharmaceutical Sciences and Drug Design

Characterization of Novel CYP26B1-inhibitor, DX314, for the Treatment of Keratinization Disorders

Chairperson: Philippe J. Diaz

Our skin, particularly the barrier provided by the epidermis, functions as our primary protection from the harsh environment. It protects us from dangerous pathogens, allergens, ultraviolet radiation, and mechanical injury, as well as playing a major role in fluid and thermal regulation. Disruption of skin functions can lead to life-threatening consequences due to increased risk of infection, trans-epidermal water loss, and allergen sensitization. Many common skin disorders often result in a disrupted skin barrier placing patients at risk of complications.

Retinoic acid (RA) is a major component of the vitamin A pathway, which critically controls multiple skin functions including cell proliferation and differentiation, barrier maintenance and immune regulation. Retinoid-based therapies have successfully been used to treat various skin disorders, such as ichthyosis and Darier's disease, however, the prevalence of adverse effects, including dry skin, irritation, redness, photosensitivity, and barrier dysregulation, can result in complications and poor compliance. Novel, selective, retinoic acid metabolism blocking agents (RAMBAs), intended to minimize adverse effects and improve patient outcomes, have been designed and synthesized by our lab.

In these studies, we first investigated whether our novel RAMBA, DX314, can potentiate the effects of RA, via inhibition of the RA-metabolizing enzyme, CYP26B1, in healthy human epidermis models. By studying the gene expression effects of RA, DX314, and two previous-generation RAMBAs (liarozole and talarozole), we show that DX314 does potentiate the effects of RA. Additionally, by studying its effect on epidermal histology and transepithelial electrical resistance, we discovered that DX314 displays a unique skin barrier-reinforcing property. In our second series of studies, we investigated DX314's therapeutic potential in Darier's disease and ichthyosis. These results confirm DX314's ability to potentiate RA, and its barrier-reinforcing properties, in diseased skin models and suggest that DX314 has potential as a novel therapeutic agent for keratinization disorders.

Together, the studies within this dissertation show our next-generation RAMBA, DX314, is a strong candidate for further drug development in the context of keratinization disorders. If successful, DX314 could fulfill the therapeutic need for an efficacious, selective RAMBA, providing improved patient outcomes and quality of life, with greatly reduced adverse effects relative to current treatment options.

Acknowledgements

The completion of my doctoral studies has been a long, difficult, and fulfilling adventure, the success of which was only possible with the help of many incredible people.

First and foremost, I would like to dedicate this work to my incredible spouse Kate, whose support throughout this journey I undoubtably credit to my success. I cannot understate how critical your strength and encouragement were. You are the reason I continued to push through obstacles, I love you.

I must also credit and extend my gratitude to my advisor, Philippe Diaz for all his support and advice. I cannot thank him enough for his confidence in me as I established a functional biology lab within his chemistry-focused team, as well as his support in sending me to various conferences and a 3-month international lab exchange. Thank you for facilitating my growth and education over the past five years.

Thank you to all my committee members; Erica Woodahl, Keith Parker, Kasper Hansen, and Travis Wheeler; for all the time, advice, and support you have given me throughout the years. I could not have asked for a better committee to guide me.

I want to extend out a special thanks to Yves Poumay at the University of Namur. Your generous invitation to join your lab for three months as I learned lab techniques from such an established and knowledgeable expert in the field, was one of the most educational and vital experiences to my studies. Without your momentous help and resources, as well as the help of rest of the team (especially Valérie De Glas and Benoît Balau), this work would never have become what it is today.

Additionally, I would like the recognize our project collaborators Amy Paller and Haoming Liu at Northwestern University for all their help with the ichthyosis keratinocyte monolayer and organotypic raft studies.

I would also like to thank all the lab members which have assisted me at various points throughout the process including, but not limited to; Emily Berglund, Joanna Kreitinger, Desiree Mendez, Nicolas Guilloteau, Nicholas Wageling, Benjamin Uhlenbruck, and Fanny Astruc-Diaz. Thank you all for your assistance in various studies, compound synthesis, and general advice, all while graciously accommodating my occasional venting.

I extend my gratitude to the various donors and funding agencies who have made this research possible: The University of Montana Graduate School and the Department of Biomedical and Pharmaceutical Sciences; the Center for Biomolecular Structure and Dynamics who provided funding for the project, and awarded me the 2017 Graduate Research Fellowship; The National Institutes of Health for the grant awards contributing to this research; DermaXon for awarding me their 2018 Graduate Research Fellowship; and Glenmark Pharmaceuticals for donating the Aquaflux AF200 evaporimeter, as well as George Kramer at Biox Systems who facilitated the donation.

Last, but certainly not least, I must thank my loving parents; Catherine and Eberhard. Your hard work, support, and patience were instrumental in allowing me the opportunities which have brought me to this point.

Table of Contents

List of Figures

1. Introduction

2. DX314 Potentiates the Effects of RA, While Protecting Barrier Function in Reconstructed Epidermis

3. DX314 as a Potential Therapeutic in Keratinization Disorders

List of Tables

1. Introduction

2. DX314 Potentiates the Effects of RA, While Protecting Barrier Function in Reconstructed Epidermis

List of Third Party Copyrighted Material

Figure Number	Publisher	License Number
Figure 1.1	John Wiley and Sons	4606680766115
Figure 1.2 (left)	John Wiley and Sons	4606620180670
Figure 1.2 (right)	John Wiley and Sons	4606611448338
Figure 1.3	Elsevier	4606630114712
Figure 1.4	Springer Nature	4606630776515
Figure 1.5	Springer Nature	4606631204611
Figure 1.6	John Wiley and Sons	4606641010025
Figure 1.11	Elsevier	4606690534887
Figure 1.12	John Wiley and Sons	4606590968295

List of Abbreviations

AD	atopic dermatitis
ADH	alcohol dehydrogenase
ALDH	aldehyde dehydrogenase
AMP	antimicrobial peptide
ANOVA	analysis of variance
AP	activator protein
AQP	aquaporin
ARAT	acyl-CoA:retinol acyltransferase
ARNT	aryl hydrocarbon receptor nuclear translocator
ARP	actin-related protein
***at*RA**	all-trans retinoic acid
BAM	binary alignment map
BHLH	basic helix-loop-helix
BSA	bovine serum albumin
C1orf	chromosome 1 open reading frame
CASP	caspase
CE	cornified envelope
CLDN	claudin
CRABP	cellular retinoic acid binding protein
CRBP	cellular retinol binding protein
CRCT	cysteine rich C-terminal
CRNN	cornulin
CSV	comma-separated value
CYP	cytochrome P450
DD	Darier's disease
DMSO	dimethyl sulfoxide
DNA	deoxyribonucleic acid
DSC	desmocollin
ECM	extracellular matrix
EDC	epidermal differentiation complex
EDTA	ethylenediaminetetraacetic acid
EGF	epidermal growth factor
EHF	ETS homologous factor
ELF	E74 like ETS transcription factor
ERBB	Erb-B2 Receptor Tyrosine Kinase
Erk	extracellular signal-regulated kinases
FBS	fetal bovine serum

FDA	food and drug administration
FDR	false discovery rate
FGF	fibroblast growth factor
FLG	filaggrin
GATA	GATA binding protein
GRHL	grainyhead like transcription factor
GTF	gene transfer format
HBEGF	heparin-binding EGF-like growth factor
HE	hematoxylin and eosin
HGNC	HUGO gene nomenclature committee
HIC	HIC ZBTB transcriptional repressor
HKGS	human keratinocyte growth supplement
HRNR	hornerin
IF	immunofluorescence
IFNG	interferon gamma
IHC	immunohistochemistry
IL	interleukin
ILK	integrin-linked kinase
IPA	ingenuity pathway analysis
IVL	involucrin
JAK/STAT	janus kinases/signal transducer and activator of transcription
JAM	junctional adhesion molecules
KG	keratohyalin granules
KGF	keratinocyte growth factor
KLF	kruppel-like factor
KLK	kallikrein related peptidase
KRT	keratin
LAMB	laminin subunit beta
LCE	late cornified envelope
LI	lamellar ichthyosis
LOR	loricrin
LRAT	lecithin:retinol acetyltransferase
LXR	liver X receptor
MAPK	mitogen-activated protein kinases
MEIS	Meis homeobox
NFE	nuclear factor, erythroid
NR	nuclear receptor
NRIP	nuclear receptor interacting protein
OCLN	occludin

P/S	penicillin/streptomycin
PBS	phosphate buffered saline
PKC	protein kinase C
PPAR	peroxisome-proliferator-activated receptor
RA	retinoic acid
RABL	rab-like protein
RAL	retinal
RalDH	retinal dehydrogenase
RAMBA	retinoic acid metabolism blocking agents
RAR	retinoic acid receptor
RARE	retinoic acid response element
RARRES	retinoic acid receptor responder
RB1	retinoblastoma-associated protein
RBP	retinol binding protein
RE	retinyl esters
RHE	reconstructed human epidermis
RHOGDI	RHO protein GDP dissociation inhibitor
RNA	ribonucleic acid
ROL	retinol/vitamin A
ROR	RAR-related orphan receptor
RPTN	repetin
RT qPCR	real-time quantitative polymerase chain reaction
RXLI	recessive x-linked ichthyosis
RXR	retinoid X receptor
S100	S100 calcium binding protein
SAM	sequence alignment map
SB	stratum basale
SC	stratum corneum
SDR	short-chain dehydrogenases/reductases
SG	stratum granulosum
SMARC	SWI/SNF-related matrix-associated actin-dependent regulator of chromatin
SPINK	serine protease inhibitor kazal-type
SPR	small proline-rich protein
SS	stratum spinosum
SSWL	subsurface water loss
STRA	stimulated by retinoic acid
TCHH/THH	trichohyalin
TEER	transepithelial electrical resistance

TEWL	trans-epidermal water loss
TGF	transforming growth factor
TGM	transglutaminases
THOP	thimet oligopeptidase
TJ	tight junction
TLR	toll-like receptor
TNF	tumor necrosis factor
TP53	tumor protein p53
TR	thyroid receptor
TREM	triggering receptor expressed on myeloid cells
TTR	transthyretine
UV	ultraviolet
VDR	vitamin D receptor
WASP	Wiskott–Aldrich Syndrome protein
Wnt	wingless/integrated
ZO	zona occludens

1. INTRODUCTION

1.1 HUMAN SKIN

Our skin primarily functions as a critical barrier between our internal tissues and the harsh external environment. It provides protections against pathogens, allergens, ultraviolet (UV) radiation, mechanical and chemical insults, as well as playing a major role in fluid regulation and thermal homeostasis. Beyond the protective nature of the skin, it also provides important sensory (tactile feedback via dermal nerve endings), metabolic (vitamin D synthesis), and energy storage functions (subcutaneous adipocytes)[1]. Disruption of these critical skin functions, whether by disease pathology or physical destruction (e.g. severe burns, abrasions), can result in major complications for patients. These consequences include increased risk of infection, trans-epidermal water loss (TEWL), and allergen sensitization[2–4].

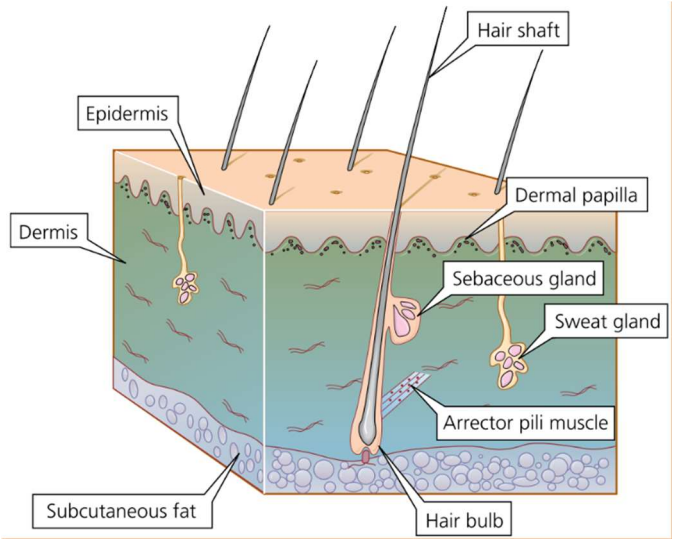

Figure 1.1: Illustration of primary skin structures. Including the hypodermis (subcutaneous fat), dermis, epidermis, and other major skin structures such as sebaceous glands, hair follicles, and sweat glands.
Source: Graham-Brown et al. (2016), with permission from John Wiley and Sons (lic. #: 4606680766115)

1.1.1 ANATOMY OF THE SKIN

Human skin can be divided into three primary layers: the most internal layer is the hypodermis, the middle layer is the dermis, and the external layer is referred to as the epidermis (Figure 1.1).

1.1.1.1 HYPODERMIS

The hypodermis, also referred to as subcutaneous tissue, is the innermost layer of the skin below the dermis and above skeletal muscle. It is primarily composed of adipocytes, collagen, and blood vessels which together function as thermal insulation, energy storage, and protection from mechanical trauma[5,6]. The thickness of this layer is highly variable across individuals and its specific location.

1.1.1.2 DERMIS

The dermal layer of the skin is localized between the hypodermis and the epidermis, ranges between 0.3mm (eyelids) and 3mm (back) thick and is primarily composed of connective tissue. This layer is divided into two regions known as the papillary dermis and the reticular dermis. The aptly named papillary layer contains dermal papilla, localized just below the epidermis, which provide resistance to shear stress. The remaining reticular layer accounts for most of the dermis and provides structural and elastic support. Other structures found within the dermis include sweat glands, hair follicles, sensory receptors such as Meissner's and Pacinian corpuscles, free nerve endings, and sebaceous glands (Figure 1.1).

The primary cell types found within the dermis include fibroblasts, mast cells (specialized secretory cells), macrophages (phagocytic cells), and various T cells (immune cells)[7]. Fibroblasts (the major cell type of the dermis) are responsible for the synthesis of

the dermal matrix which consists of approximately 70% collagen with some elastin, as well as a mucopolysaccharide gel which fills the inter-fibrous spaces and functions as a hydrogel to facilitate diffusion of fluids, nutrients, and other essential components. The highly diverse fibroblast populations within the dermis also produce several growth factors (e.g. keratinocyte growth factor (KGF), hepatic growth factor) as well as many cytokines (e.g. interleukins (IL)-1α/β, IL-8).

The dermis is highly innervated, which allows for its role in pain, itching, and tactile sensations. A critical function of the dermis is to support the epidermis by providing essential nutrients. Due to the lack of blood supply to the epidermis, the richly vascularized dermis provides a supply of nutrients and oxygen to the epidermis via diffusion[1,5,6,8].

1.1.1.3 EPIDERMIS

The exterior layer of the skin is the epidermis [*epi-* (on top of, Ancient Greek) the dermis] which functions as our foremost barrier between internal tissues and the environment. The epidermis is composed of a stratified squamous epithelium composed of several distinct layers. Thick skin (found on palmar and plantar surfaces) has an epidermal thickness of 0.8-1.5mm, while thin skin (majority of our skin) has an epidermal thickness ranging from 0.07-0.15mm[1].

The primary cell type found in the epidermis are keratinocytes (constituting >90% of the epidermal cell population[1]) which undergo carefully controlled differentiation to form the stratified epithelium of the epidermis. The four layers of the epidermis from the most internal to the most external are; the stratum basale (SB, basal layer), stratum spinosum (SS, spinous layer), stratum granulosum (SG, granular layer), and the stratum

corneum (SC, corneal layer) (Figure 1.2). Melanocyte cells, also found within the epidermis, are responsible for production of melanosomes, which contain the dark pigment melanin. Melanin provides essential protection from UV radiation by absorbing harmful high energy photons and preventing them from causing permanent damage to cellular DNA. Langerhans cells are antigen-presenting cells, originating from monocytes, which provide immunologic defense within the skin[1,5,6,8].

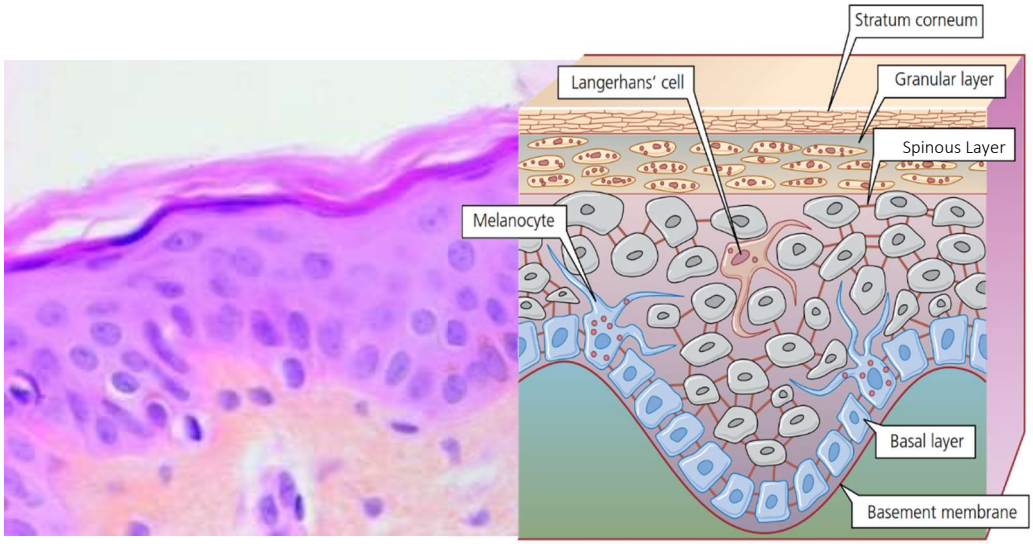

Figure 1.2: The human epidermis. Human skin section (left) showing dermal collagen (yellow) and epidermal keratinocytes (pink/purple), merged with an illustration of the epidermis (right). The four distinct layers of the epidermis (basal, spinous, granular, and corneal) can be seen in both images.
Adapted from: left, Frankart et al. (2012); right, Graham-Brown et al. (2016), with permission from John Wiley and Sons (lic. #: 4606620180670, 4606611448338)

1.1.1.3.1 EPIDERMAL STRATIFICATION

Stratification and maintenance of the epidermis is the result of a careful regulation of keratinocyte differentiation and proliferation. Proliferating keratinocytes originate from

keratinocyte stem cells found in the basal layer of the epidermis. As these keratinocytes undergo the process of terminal differentiation, they migrate upwards to sequentially form the suprabasal layers. Each of these layers have unique, critical characteristics and morphologies (Figure 1.3). *In vivo*, the differentiation process from basal to corneal keratinocytes is estimated to take approximately 14 days, where they remain for about another 14 days as corneocytes before subsequent desquamation (shedding of the outermost layer). The total skin rejuvenation cycle takes around 28 days[5,6,8,9].

1.1.1.3.2 STRATUM BASALE

The basal layer, also called the stratum basale, is the innermost layer of the epidermis found directly above the dermis. This layer is composed of 1-3 layers of undifferentiated, cuboidal keratinocytes which can either replenish basal cell populations, or undergo terminal differentiation. Melanocytes, which produce the UV-absorbing melanosomes, are also found within this layer and account for 5-10% of basal cells.

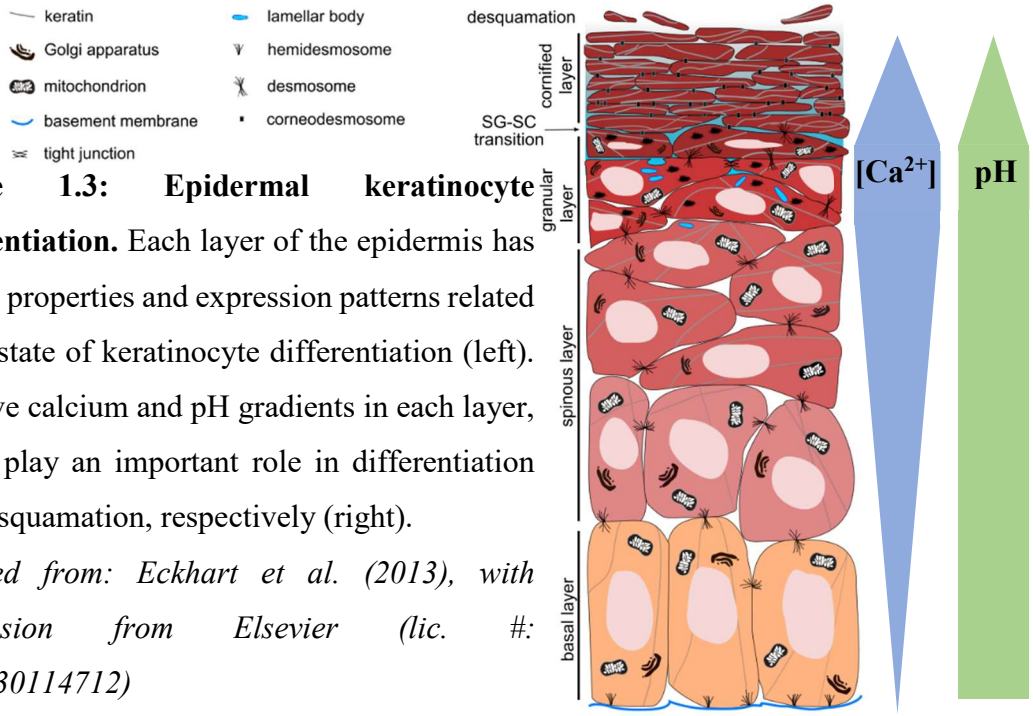

Figure 1.3: Epidermal keratinocyte differentiation. Each layer of the epidermis has unique properties and expression patterns related to the state of keratinocyte differentiation (left). Relative calcium and pH gradients in each layer, which play an important role in differentiation and desquamation, respectively (right).
Adapted from: Eckhart et al. (2013), with permission from Elsevier (lic. #: 4606630114712)

Basal stem cell populations are responsible for maintaining epidermal homeostasis. Several hypothesis on the mechanisms of this are available, however, the currently favored of them suggests a combination of symmetric and asymmetric cell division[10–13]. This hypothesis states that stem cells can either self-renew (symmetric), differentiate (symmetric), or asymmetrically divide, to maintain stem cell populations while generating differentiating keratinocytes for the suprabasal layers (Figure 1.4).

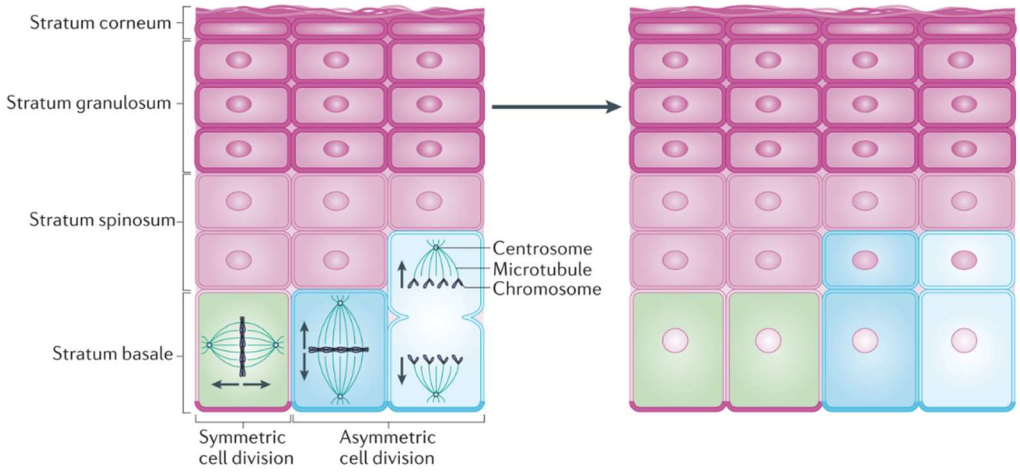

Figure 1.4: Cell division of basal keratinocytes. Representation of symmetric and asymmetric cell division thought to be the mechanisms responsible for epidermal maintenance by basal keratinocytes.
Adapted from: Simpson at al. (2011), with permission from Springer Nature (lic. #: 4606630776515)

The extracellular matrix (ECM) interface separating the basal epidermis from the underlying dermis is known as the basement membrane zone. Polarized basal keratinocytes produce intracellular intermediate filaments (keratins 5 and 14), which provide an anchor for integrin complexes (hemidesmosomes). These hemidesmosomes provide the necessary attachment to the laminin- and collagen-containing basement membrane[5,13,14]. Proper

attachment at the dermal-epidermal junction is mechanistically complex, but essential to the skin's ability to provide a functional barrier.

1.1.1.3.3 STRATUM SPINOSUM

Just above the stratum basale lies the 8-10 cell deep[1] stratum spinosum (spinal layer) of the epidermis. Once basal keratinocytes have been committed to terminal differentiation, they lose their columnar appearance and become increasingly polygonal as they form the spinal layer.

In addition to keratinocytes, 2-8% of the cells within the spinous layer are dendritic Langerhans cells[1]. Langerhans cells are monocyte-derived, antigen-presenting cells originating from bone marrow, which play a critical role in the immunologic functions of the skin. Once an antigen has been captured, Langerhans cells may migrate to the peripheral lymph nodes to present it to the appropriate T cell, or activate resident T cells within the epidermis[15], to initialize the required immunologic response[16].

The name of this layer originates from the appearance of spinous keratinocytes when stained with hematoxylin and eosin (HE) dyes and viewed under a microscope. The staining process causes the cells to shrink, while the cadherin-based desmosomes keep the cells bound to each other, resulting in "spines" forming at each interface. Desmosomes, tethered by intracellular keratin filaments, are intercellular connections between keratinocytes forming strong, shear-resistant bonds within the tissue.

As keratinocytes integrate into the spinous layer, genes for the fibrous protein keratins (KRT) found in proliferating basal keratinocytes (KRT5 and KRT14) are turned

off, and expression of KRT1 and KRT10 takes over. For this reason, KRT1 and KRT10 gene expression is often used as a marker of keratinocyte differentiation[13,14].

1.1.1.3.4 STRATUM GRANULOSUM

The next stage of differentiation forms the 3-5 cell thick granular layer, named after the dark-staining keratohyalin granules (KG) found within the keratinocytes of this layer. Keratohyalin granules contain pro-filaggrin which undergoes proteolysis to become to the keratin-aggregating protein filaggrin (FLG). These aggregated keratins make up a flexible matrix which also contains involucrin (IVL) and loricrin (LOR). IVL and LOR are structural proteins which play an important role in the cornification process needed to create to the stratum corneum[5,9,17].

The stratum granulosum is the primary location of epidermal tight junctions (TJ, can also be found in hair follicles[18]) which are critical barrier components responsible for controlling paracellular fluid and ion diffusion, and protecting against pathogen penetration. Tight junctions are composed of intercellular claudins (CLDN), occludin (OCLN), and junctional adhesion molecules (JAM), scaffolded to intracellular zonula occludens (ZO) proteins linked to the cell's actin cytoskeleton (Figure 1.5)[13,19–21].

The careful regulation of calcium ions in the epidermis plays a major role in regulating keratinocyte differentiation. A calcium gradient, with the highest concentrations found in the stratum granulosum and concentrations decreasing both above and below, is tightly controlled to maintain proper function[22] (Figure 1.3). Elevated calcium levels activates enzymes in the protein kinase C (PKC) family which will downregulate KRT1

and KRT10, while upregulating IVL, LOR, and transglutaminases (TGM)[23] expression, which in addition to FLG, are used as markers of late keratinocyte differentiation.

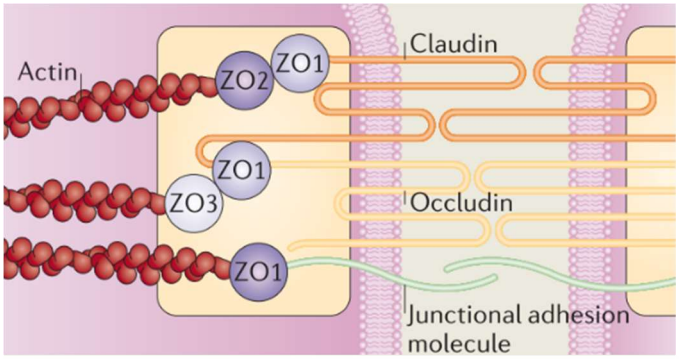

Figure 1.5: Structure of tight junctions found in the stratum granulosum. Tight junctions play an important role in skin barrier function by preventing paracellular diffusion through the granular layer of the epidermis**.**

Source: Simpson at al. (2011), with permission from Springer Nature (lic. #: 4606631204611)

Morphologically, granular keratinocytes undergo a characteristic flattening and observable degradation of their nuclei and organelles. Lipid- and hydrolase-secreting lamellar bodies being to form and produce an extracellular "mortar" at the granular-cornified transition[24]. The drastic changes seen in the granular layer prepare the keratinocytes for their final transition into the stratum corneum by a process known as cornification.

1.1.1.3.5 CORNIFICATION AND THE STRATUM CORNEUM

The outermost layer of skin, and terminal destination for keratinocytes, is the stratum corneum, also referred to as the corneal layer. In a process that began in the granular layer, keratinocytes undergo a distinct type of programmed cell death called cornification. The nucleus and other organelles (i.e. mitochondria, Golgi apparatus,

ribosomes, endoplasmic reticulum) are degraded and replaced by structural proteins and other corneal layer components.

FLG, formed within the granular keratinocytes, aggregate keratin filaments which causes the keratinocytes to collapse into organized sheets of flattened polyhedral cells named corneocytes. Proteins such as IVL, LOR, trichohyalin (TCHH), and small proline-rich proteins (SPR) are expressed and cross-linked by TGMs to form a cornified envelope (CE) on the cytoplasmic side of the cell membrane. The CE of each corneocyte is linked to neighboring CEs via modified desmosomes, referred to as corneodesmosomes, to form tight bonds within the stratum corneum. Lamellar bodies secrete their lipid- and enzyme-rich contents (e.g. ceramides, sterols, phospholipids) which function as a "mortar" between the layers of protein-rich corneocyte "bricks" (Figure 1.6)[9,17,25].

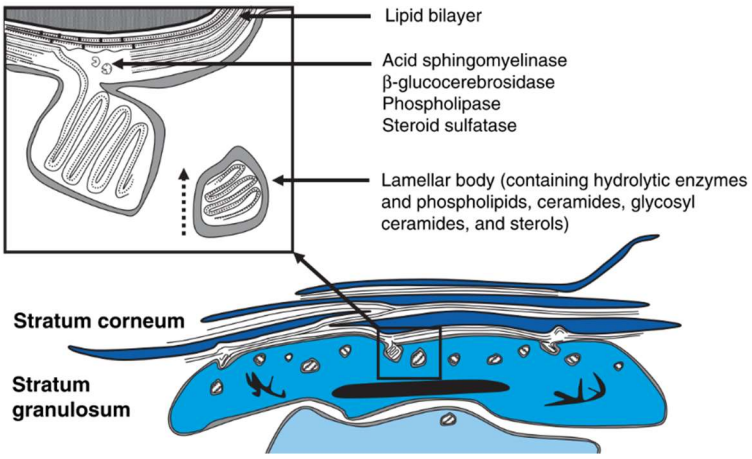

Figure 1.6: Lamellar body secretion during the formation of the stratum corneum. Lamellar bodies originating in the stratum granulosum release lipids and enzymes, which play critical roles in barrier function, into the stratum corneum where they act as an inter-corneocyte "mortar".
Adapted from: Proksch et al. (2008), with permission from John Wiley and Sons (lic. #: 4606641010025)

The stratum corneum is highly variable in thickness depending on location and can be anywhere from 15 (upper arm) to hundreds (palms and soles) of layers thick[1]. Considering the thick and tightly bound, hydrophobic makeup of the corneal layer, it is no surprise that it also plays a major role in skin barrier function.

As epidermal tissue is constantly being rejuvenated, a mechanism to make way for new tissue is necessary. The process of desquamation refers to the controlled shedding of corneocytes from the outermost layers of the stratum corneum. As corneocytes migrate from the deeper, denser corneal layers (stratum compactum) to the upper corneal layers (stratum disjunctum), they undergo compositional changes which promote desquamation[6]. One such change is a shift in the equilibrium of proteases and protease inhibitors, which allows for proteolysis of corneodesmosomes and shedding of those corneocytes. This balance is thought to be controlled by the pH gradient found in the corneal layer. The stratum compactum maintains a fairly neutral pH, ideal for protease and inhibitor function, however, the stratum disjunctum is markedly more acidic (pH 4-6)[26,27], which reduces protease inhibitor effectiveness[28]. (Figure 1.3) Although protease function is also decreased by the low pH, they are less effected than protease inhibitors, so the resulting desquamation is gradual and well controlled.

1.1.1.4 SKIN BARRIER FUNCTION

As previously discussed, the major function of the epidermis is maintaining a proper barrier between internal tissues and the external environment. The barrier can be divided into two major categories; the inside-outside barrier, consisting of fluid, ion, and

thermal homeostatic mechanisms, and the outside-inside barrier, protecting internal tissues from pathogens, allergens, UV radiation, mechanical, and chemical insults.

As the outermost layer, the stratum corneum is the skin barrier's first line-of-defense. The tightly bound layers of corneocytes and extracellular lipids provide a hydrophobic and difficult to penetrate barrier which contributes to both inside-outside (fluid regulation), and outside-inside (penetration) protections. The SC also contains antimicrobial peptides (AMPs), cytokines, antioxidants, and many other components that provide additional protections essential to the barrier function (see Section 1.1.1.3.5).

In addition to regulating desquamation, the previously mentioned acidic environment of the skin surface aids in processing barrier lipids and discourages pathogenic bacteria proliferation in favor of the normal skin flora[26].

Tight junctions found on the apical side of keratinocytes in the stratum granulosum are another significant component of the epidermal barrier. These cell-cell junctions tightly bind keratinocytes together forming a paracellular barrier not only to xenobiotics and pathogens, but also passively regulating bi-directional fluid and ion permeability[29] (see Section 1.1.1.3.4).

The pathogen-directed skin barrier components are the first line of defense protecting our internal tissues from infection. The presence of a healthy skin microflora has recently gotten more recognition as an important exogenous component of the skin barrier. By outcompeting pathogenic microbes on the surface of the skin our microflora decreases our risk of infection[30]. Keratinocytes also produce antimicrobial peptides

(AMPs, *e.g.* β-defensins and cathelicidins), delivered from lamellar bodies, which protect against bacteria, viruses, parasites, and fungi[31]. Finally, if an antigen gets past these initial protections, whether through barrier deficiency or physical injury, it is the role of spinous, antigen-presenting Langerhans cells to activate an immunological response (see Section 1.1.1.3.3).

Epidermal cytokines released by keratinocytes also play a role in maintaining the skin barrier by activating signaling cascades in response to insults. Cytokines such as IL-1α/β, tumor necrosis factor (TNF)α, IL-17α, IL-34, IL-24, and others, will activate the repair process of damaged tissue and induce a pro-inflammatory signal[30,32,33].

The interaction between individual components contributing to the homeostatic mechanisms which maintain the barrier are important to consider as well. Studies have found that the corneal barrier and granular tight junctions will compensate for decreased function of the other (*e.g.* increase in TJs when corneum is disrupted[34] or a denser, thicker corneum in claudin-1 deficient mice[35]). Studies have also found interactions between the immune barrier and the corneal and granular barriers being able to compensate for, or activate, when the other is deficient[32,36–38].

1.1.1.4.1 MEASURES OF EPIDERMAL BARRIER FUNCTION

There exist several established methods to assess epidermal barrier function, both *in vitro* and *in vivo*, which allow researchers and physicians to quantify changes in barrier function.

Transepithelial electrical resistance (TEER) is a common, non-destructive methodology used to measure barrier function *in vitro*. It functions by placing an electrode

above and below a tissue immersed in culture media (Figure 1.7) acting as an electrolyte, and applying a weak alternating current (10μA) which allows for a measure of electrical resistance (ohm, Ω) across the tissue. By subtracting out the resistance of an empty cell culture insert, the specific resistance of the tissue itself can be determined. This resistance is directly related to the freedom of ion to flow through the tissue via paracellular (controlled by tight junctions) and transcellular pathways. A decrease in TEER corresponds to decreased resistance to ion permeability across the tissue, and therefore a weaker epithelial barrier.

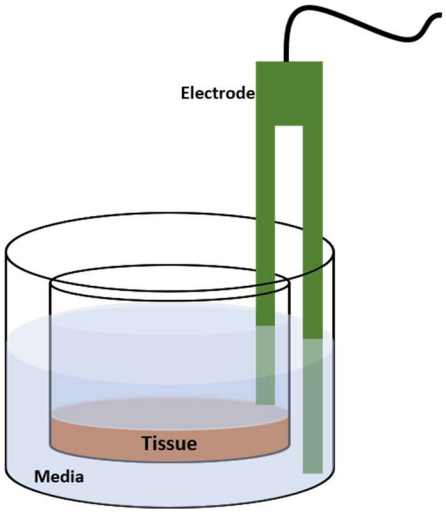

Figure 1.7: Illustration of TEER electrode placed in measurement position. Using electrode placed on either side of a tissue submerged in culture media, we can determine the electrical resistance across the tissue as measure of tissue barrier integrity.

Trans-epidermal water loss (TEWL) is another non-invasive measure of barrier integrity which, unlike TEER, can be used both *in vivo*[39] and *in vitro*[40]. As implied, TEWL is a measure of the passive diffusion of water across the epidermis, which is directly related the skin's inside-outside barrier function. The TEWL instrument used in these studies (Biox Aquaflux AF200) utilizes a sealed condenser chamber, which is placed over the tissue in an airtight manner (Figure 1.8). The chamber contains a chilled (-7.65°C) condenser plate to control the humidity within the chamber, as well as relative humidity

and temperature sensors between the condenser and the epidermis. As water vapor diffuses from the tissue surface to the condenser, the sensors calculate water vapor flux over time. To correct for the initial skin surface water loss (SSWL), which could contaminate the data, TEWL is measured over a period of 60-90s and once a steady state threshold has been achieved the water flux is recorded as mass of water per area over time (typically g/m^2h). Although TEWL is a useful tool to measure barrier integrity, it is inherently sensitive to subtle external influences. Care must be taken to maintain constant ambient humidity and temperature and ensure the surface of the tissue is thoroughly dried before measurement.

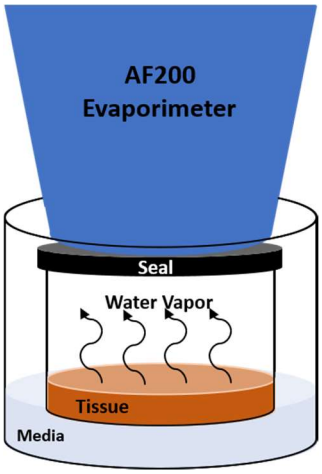

Figure 1.8: Illustration of TEWL measurement device on reconstructed epidermis. An evaporimeter measures water flux through the tissue. TEWL is used *in vivo,* or *in vitro* (shown here), to assess skin barrier integrity based on water permeability.

Other methods to measure barrier function include chemical permeation assays. A low-binding, low-molecular weight chemical can be applied to the surface of the tissue and the amount that is able to permeate into the media below can be quantified. Fluorescent dyes are commonly used for this type of assay and can also be used to visualize dye penetration by fluorescent microscopy of tissue cross-sections. A downside is this type of assay is the invasive nature of chemical treatments, which may affect the tissue in unpredictable ways. These assays are typically performed in independent, single-use

studies, whereas TEER or TEWL can be measured multiple times at several stages of tissue growth, or at various treatment times, in most studies without interfering with other downstream assays.

1.2 DISEASES OF THE SKIN

Since the skin plays such a major and critical role in protecting us from the insults of our environment, it is no surprise that skin diseases can have a devastating effect on patient health and quality of life. As previously discussed, maintaining healthy skin involves a series of carefully regulated, complex biological process for proper function. Even seemingly minor perturbations of many of these processes can result in severe disease states requiring medical intervention. Untreated skin diseases can result in increased infection risk, severe irritation, allergen sensitization, dehydration, vitamin D deficiency, thermal dysregulation, UV-damage, and psychological distress[8].

1.2.1 CONGENITAL ICHTHYOSIS

Congenital ichthyoses are a group of hereditary keratinization disorders. Keratinization is the process of keratinocyte differentiation, referring to the formation of keratin filaments. Originally derived from the Greek word for fish ("ichthys"), ichthyosis can cause skin to resemble fish scales due to improper cornification (Figure 1.12a[41]).

Congenital ichthyosis covers a wide gamut of related disorders and as such, there are many possible genetic causes attributed to the disease (Table 1.1[42]). Some forms, such as ichthyosis vulgaris and recessive x-linked ichthyosis (RXLI), are more common (1/300 and 1/2,500 respectively), while others, such as lamellar ichthyosis (LI) and bullous ichthyosis, are fairly uncommon (1/100,000 and 1/300,000 respectively)[43]. Severity is also

highly variable with less severe forms, such as ichthyosis vulgaris, having low mortality, while other forms, such as harlequin ichthyosis, resulting in neonatal survivability as low as 56%[44]. Symptoms can include dry skin (xerosis), redness and irritation (erythema), scaling and blisters, abnormal thickening of the skin (hyperkeratosis), and other problematic conditions[43].

Type	OMIM	Gene
Ichthyosis vulgaris	146700	FLG
X-linked ichthyosis	308100	STS
Congenital ichthyosiform erythroderma, Nonbullous (nbCIE)	242100	TGM1, ALOXE3/ALOX12B
Epidermolytic hyperkeratosis (bullous ichthyosis, bCIE)	113800	KRT1, KRT10
Harlequin-type ichthyosis	242500	ABCA12
Ichthyosis bullosa of Siemens	146800	KRT2
Ichthyosis hystrix, Curth-Macklin type	146590	KRT1
Hystrix-like ichthyosis with deafness	602540	GJB2
Lamellar ichthyosis, type 1	242300	TGM1
Lamellar ichthyosis, type 2	601277	ABCA12
Lamellar ichthyosis, type 3	604777	CYP4F22
Lamellar ichthyosis, type 4	613943	LIPN
Lamellar ichthyosis, type 5	606545	ALOXE3
Autosomal Recessive Congenital Ichthyosis	615023	CERS3

Table 1.1: Major types of congenital ichthyosis by culprit gene. Ichthyosis can be caused by many different genetic components. A disruption in any of the critical factors involved in the complex process of keratinization can result in dysfunction and medical complications. *Source: Online Mendelian Inheritance in Man (OMIM, https://omim.org).*

Current treatment options for these disorders typically target a combination of three strategies; hydration, lubrication, and keratolysis[43]. The two former strategies focus on mitigating symptoms, while the latter (often via retinoid treatment) targets the underlying biological mechanisms the diseases. Retinoid-related treatments (further discussed in Section 1.3) function as keratolytics and reduce hyperkeratosis, keratinocyte hyperproliferation, and excessive corneocyte production. Unfortunately, this treatment mechanism can result in adverse effects, including additional barrier dysfunction, and often require additional treatment with antimicrobials.

1.2.2 DARIER'S DISEASE

Darier's disease (DD, keratosis follicularis) is a rare (between 1 in 36,000 and 1 in 100,000[45]), autosomal dominant skin disorder characterized by disrupted intercellular adhesion (acantholysis) and abnormal keratinization (dyskeratosis). DD is caused by a mutation in the ATP2A2 gene which encodes a calcium transporter (SERCA2)[46] found in the endoplasmic reticulum of keratinocytes. Due to the importance of calcium ion gradients in skin development, epidermal homeostasis is consequently disrupted in DD. This results in abnormal keratinocyte differentiation, poor intercellular adhesion, and dark, crusty skin lesions, which together cause severe itching, pain, and increased risk of infection.

DD is treated similarly to other keratinization disorders; emollients and corticosteroids to address irritation, retinoids to control dyskeratosis[47–49], and antibiotics which may be used during flare ups. Retinoids such as isotretinoin (*13-cis*-retinoic acid), adapalene, tazarotene, acitretin, and others, have been used in the treatment of DD via topical and oral formulations[45,47,49,50].

1.2.3 ATOPIC DERMATITIS

Atopic dermatitis (AD) is a common chronic inflammatory skin disease (affects 15-30% of children and 2-10% of adults) with recently increasing prevalence[51]. AD patients present with xerosis, itching (pruritus), lesions of erythema which increase the risk of infection, and atopy (a genetic tendency to develop allergen sensitization)[52]. Since there are no specific markers for AD, diagnosis can be difficult and is typically done by looking for a defined set of clinical manifestations[53], including early onset age and the symptoms previously mentioned.

Noted features of AD are barrier dysfunction, measured by increased TEWL, inflammation, and immune dysfunction. It is currently unknown if one may lead to the other, but it is clear they are closely linked to each other and both genetic and environmental factors contribute to AD[54,55]. Mutations in barrier proteins, such as FLG and SPINK5, as well as immune factors such as IL- 4 & 13, toll-like receptor 2 (TLR2) and others have been associated with AD[56,57].

Like congenital ichthyosis, current AD treatment options are limited and often target symptoms rather than the underlying causes. Moisturizers and emollients hydrate the skin and mitigate TEWL, cortical steroids and calcineurin inhibitors target inflammation, and in severe cases, immunosuppressants are also used. Finally, ceramide and lipid-based formulations can be used to partially restore some barrier function lost in AD.

1.2.4 OTHER SKIN DISEASES

There exists such a wide gamut of different skin diseases that discussing the field of dermatology in its entirety is not feasible in this summary. This section will provide a very brief description of a few other skin disorders, primarily focusing on those that respond to retinoid-related treatments.

Psoriasis is a common (3% of western population[8]) inflammatory autoimmune skin disease. Interactions between keratinocytes, T cells, cytokines and chemokines all contribute to psoriasis. Psoriatic epidermis displays keratinocyte hyperproliferation, specifically increased stratum basale and stratum spinosum thickness (acanthosis), and inflammatory cell accumulation. There are several subtypes (plaque, guttate, inverse, pustular, erythrodermic, and others) and their symptoms include skin redness/irritation,

itching (pruritus), lesions, pain, and increased risk of infection. Treatments for psoriasis vary but often include combinations of steroids, vitamin D, phototherapy (UV exposure), immunosuppressants, emollients, retinoids, and most recently, various biologics[8,58,59].

Acne vulgaris is a skin condition that nearly everyone has had some direct experience with, particularly during adolescence (~90% of teenagers have acne[60]). Acne is caused by the blockage of sebaceous glands resulting in inflammation and lesions (blackheads, whiteheads, pimples, etc.). Processes that contribute to this include abnormal keratinocyte proliferation/desquamation, overproduction of sebum, bacterial infection (Propionibacterium Acnes), and inflammation[60]. Acne, like most externally presenting skin diseases, not only causes physical detriments, but also has a significant mental health component which can cause great suffering for affected patients. Treatments include retinoids, antibiotics, hormone therapies, and cleansing agents (salicylic acid, benzoyl peroxide) aimed at desquamation, clearing blockages, and/or reducing bacterial infection[60].

1.3 RETINOIDS AND RELATED COMPOUNDS

The term retinoid refers to the class of compounds chemically related to vitamin A. Vitamin A specifically refers to retinol (ROL), while retinoids include the entire family of bioactive metabolites and precursors of ROL including, but not limited to, retinal (RAL), retinoic acid (RA), and the various synthetic analogs acting on endogenous retinoid pathways (Figure 1.9). Due to the pleiotropic nature of retinoid biopathways, and their essential and diverse cellular functions, retinoids are ubiquitously required in all stages of human development. Vitamin A and its active metabolites play an essential role in many biological processes including, but not limited to; vision, immunity, reproduction, metabolism, neurologic function, development, and cellular differentiation[61].

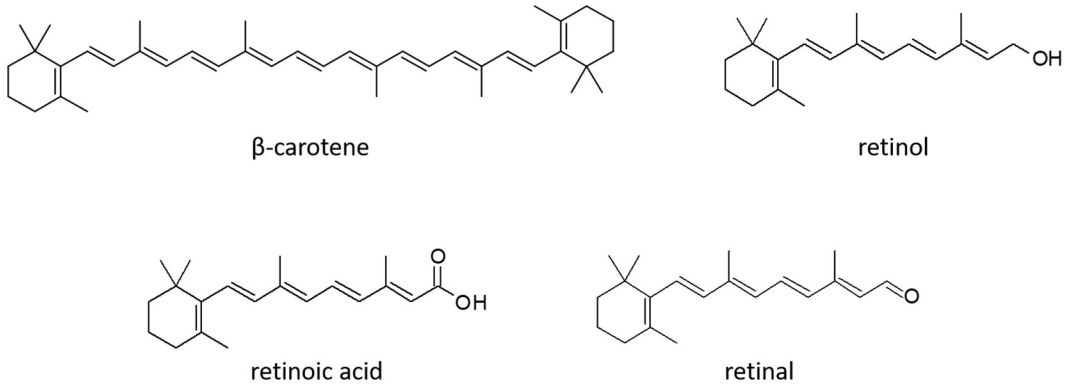

Figure 1.9: Common retinoids in the vitamin A family.
Also showing the dietary retinal precursor, β-carotene.

1.3.1 RETINOID TARGETS AND MECHANISMS

Endogenous retinoids display a complex and essential role in many biological processes and many of these roles still consist of incompletely defined mechanisms. A review of 1,191 publications found over 532 genes that appear to be regulated by RA[62].

This vast breadth of regulatory effects RA exerts on gene expression illustrates how extensively retinoids contribute to our biology.

The primary targets of retinoids are nuclear receptors (NRs) including retinoic acid receptors (RARs) and retinoid X receptors (RXRs) which, when activated, regulate gene transcription. RARs consist of three subtypes, each with multiple isoforms (α1/2, β1/2/3/4/1', and γ1/2), and can be activated by either *all-trans* retinoic acid (*at*RA) or *9-cis*-RA. RXRs also consist of three subtypes, each with multiple isoforms (α1/2, β1/2, and γ1/2), but are only known to be activated by the *9-cis* form of RA (whether or not *9-cis* RA is the bona fide ligand is still up for debate)[63]. RARs form heterodimers with RXRs, which will bind to specific DNA sequences called RA response elements (RAREs) found in the regulatory regions of their target genes. RXRs can form a very diverse range of active dimers as either homodimers or heterodimers with other NRs such as thyroid receptor (TR), liver X receptor (LXR), peroxisome-proliferator-activated receptors (PPARs), vitamin D receptor (VDR), and many others[63] (Figure 1.10).

Recent discoveries have also revealed that RA can bind other NRs such as PPARβ/δ, while other studies have found evidence of antagonistic interactions via RAR-related orphan receptor β (RORβ) and other NRs[61]. Further complicating the genomic effects of RA is the deep involvement of coregulators (coactivators and corepressors), which interact with RA-interacting NRs, and the variable sequences and geometries of RAREs contributing to gene regulation[63]. RARs also display protein-protein interactions with activator protein-1 (AP-1), a transcription factor regulating expression of cytokines,

growth factors, metalloproteases, and many other targets. The RAR/RXR/AP-1 complex acts to repress the expression of both RAR and AP-1 regulated genes[64] (Figure 1.10).

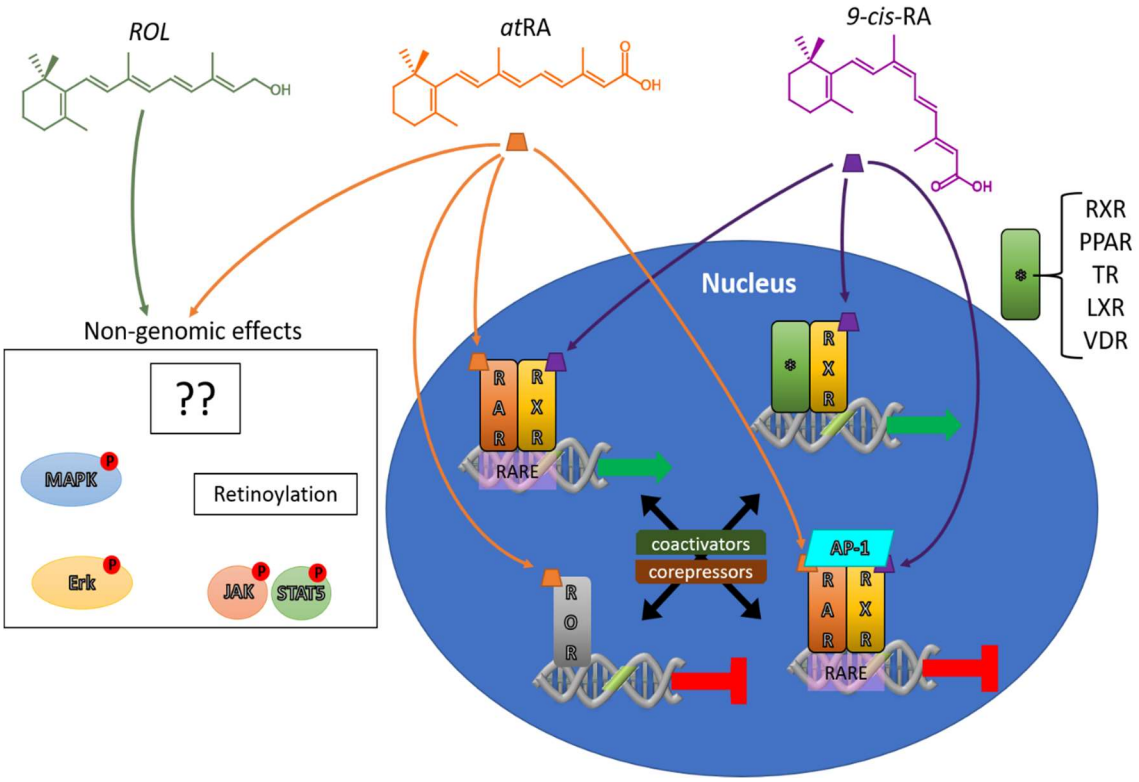

Figure 1.10: Illustration of some targets and biopathways of endogenous retinoids. Both genomic and non-genomic effects, many of which remain poorly understood, play a role in the biological effects of retinoids.

In addition to the genomic effects discussed above, retinoids also display non-genomic effects, an area of study which still requires significant research to properly define and comprehend. Studies have shown that RA can activate several kinase cascades including some mitogen-activated protein kinases (MAPKs) and extracellular signal-regulated kinases (Erk)[65]. ROL has also be found to activate Janus kinases/signal transducer and activator of transcription 5 (JAK/STAT5)[61]. RA can also affect post-translational protein modifications in a process called retinoylation[66] (Figure 1.10).

1.3.1.1 RETINOIDS IN THE SKIN

Retinoids are found ubiquitously, and play many critical roles, in our bodies. Within the skin, the roles of retinoids include regulation of keratinocyte proliferation, differentiation, apoptosis, and maintaining barrier and immune functions[67]. Endogenous levels of retinoids can vary greatly from one individual to another; approximate concentrations in healthy humans are ~2-4nM *at*RA and ~800nM ROL in the skin[68], 4-14nM *at*RA and 1-2μM ROL in serum[69].

RARγ and RARα are both found in the skin, although the levels of RARα are much lower. RXRs are more abundant than RARs with RXRα being the most common subtype in the skin. Unsurprisingly, the most commonly found RAR/RXR dimer pair within the skin appears to be the RARγ-RXRα complex[70].

Many cytokeratins (KRT5/6/14/17)[71], the RA-transporting protein CRABP-II[72], the RA-metabolizing enzyme cytochrome P450 (CYP)26A1[73], and many other genes expressed in the skin, contain RAREs within their promotor regions. There are many other genes, including heparin-binding EGF-like growth factor (HBEGF), KRT1/2/4/10, CYP26B1, and others, which are not known to contain RARE promotors, but are clearly regulated by retinoids. A study investigating the effects of retinoids on the expression of 475 skin-related genes in reconstructed human epidermis found 44 genes were variably expressed[74]. In addition to the genomic effects of retinoids, non-genomic targets such as AP-1 (antagonized by RA and RARs) play an important role in epidermal differentiation[75].

The role of retinoids in skin barrier function include regulating epidermal permeability, keratinocyte differentiation[76], sebum production[77], and apoptosis[78]. Studies

have found that disrupting retinoid-related receptors in the skin results in epidermal dysregulation[79,80]. Transgenic mice with complete loss of function of the RA-metabolizing enzyme CYP26B1, leading to abnormally high RA levels, show decreased expression of barrier proteins and barrier dysfunction[81]. Inhibition of retinoid signaling has also been shown to cause disruption of the lipid barrier[82]. These studies, and many others showing both increased and decreased retinoid signaling will disrupt barrier formation, together illustrate a so-called "goldilocks" zone of retinoid signaling in the skin.

Retinoids also play an important role in maintaining epidermal immune functions (previously discussed in Section 1.1.1.3) which contribute to the skin's role in regulating pathogen/allergen exposure and mediating inflammation. RAR and RXR pathways are also involved in T helper cell development[83–85] and retinoids are known to regulate cytokine and chemokine levels[86,87].

Due to the robust effects of retinoids in many skin functions, they are commonly used in the treatment of many skin diseases (see Section 1.2). Keratinization and epidermal proliferation disorders such as congenital ichthyosis[41,49,88], psoriasis[89–91], Darier's disease[47,48], and many others respond to retinoid treatment and continue to be studied within this context. Retinoids such as tretinoin, adapalene, and tazarotene are also used in the treatment of mild- to severe- acne[58]. Retinoids have also shown promise in treating inflammatory skin diseases such as atopic dermatitis[68]. Their ability to control cellular differentiation and apoptosis have also led researchers to study retinoids for the prophylaxis or treatment of skin cancers[58].

1.3.2 BIOSYNTHESIS, TRANSPORT & METABOLISM OF ENDOGENOUS RETINOIDS

Retinol (ROL) is primarily obtained via its dietary precursors: animal-origin retinyl esters (RE) and plant-origin carotenoids like β-carotene. Ingested dietary REs are hydrolyzed to ROL in the intestines, absorbed, and complexed with cellular retinol binding protein (CRBP)-II. Carotenoids are absorbed in the intestines, oxidized into retinal (RAL, which can complex with CRBP-II as protection from oxidation), and reduced to ROL via a retinal reductase. The ROL-CRBP-II complex can then interact with lecithin:retinol acetyltransferase (LRAT) which catalyzes esterification of ROL to RE. RE is then transported by chylomicron to the liver for long-term storage (50-80% of all the vitamin A in the body is stored as RE). ROL is transported in the blood by the plasma transport protein retinol binding protein (RBP), and delivered to its target cells[61,67] (Figure 1.11[66]).

Following uptake into keratinocytes, which is likely mediated by a cell surface RBP receptor, ROL binds CRBP-I which assists in stabilization and transport[92]. ROL will then either be metabolized to RE by LRAT or acyl-CoA:retinol acyltransferase (ARAT)[93], or reversibly converted to RAL by alcohol dehydrogenases (ADH) and short-chain dehydrogenases/reductases (SDR). RAL can then be irreversibly converted to retinoic acid (RA) by an aldehyde dehydrogenase (ALDH), namely, retinal dehydrogenase (RalDH)[94]. RA will then bind cellular retinoic acid binding protein (CRABP) I or II, which can facilitate either RA degradation or nuclear transport. CRABP has the highest affinity for *at*RA, with low and no affinity for *9-cis*-RA and *13-cis*-RA, respectively[95].

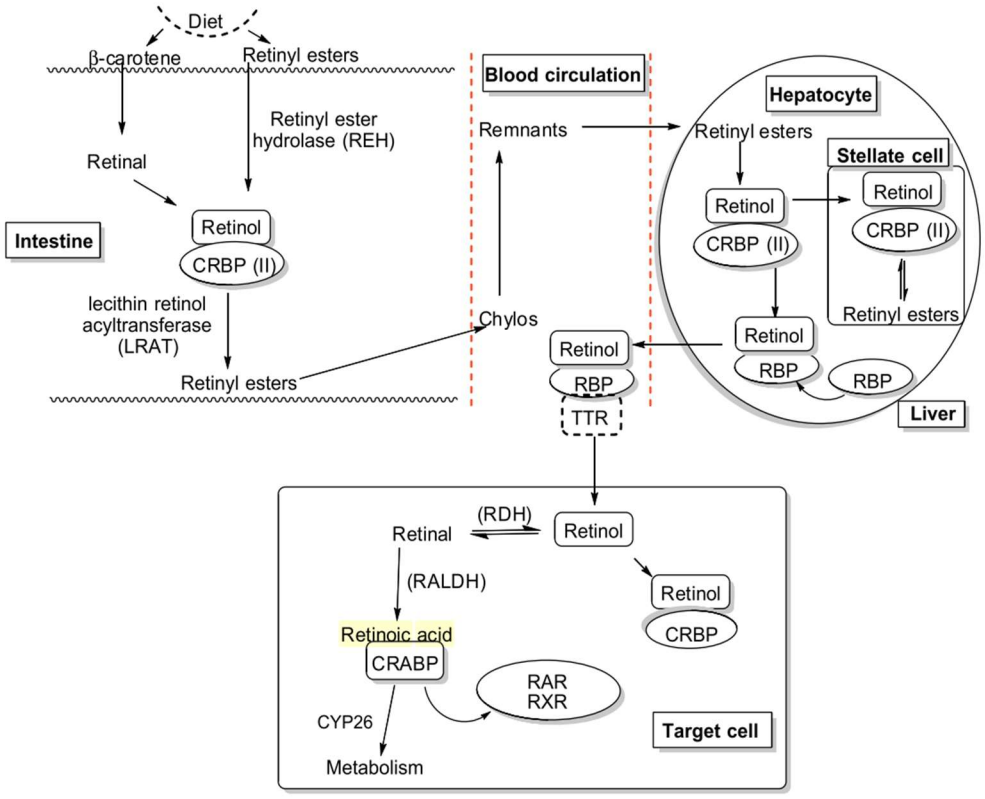

Figure 1.11: Absorption, transport, and processing of retinoids. Retinyl esters and β-carotenes found in our diet are intestinally absorbed, converted to retinol in the liver, then distributed to its target cells where it is converted to retinoic acid and exhibits its biological effects. CYP26 enzymes are responsible for the metabolism of retinoic acid. TTR, transthyretine; RBP, retinol binding protein; CRBP, cellular retinol binding protein; RDH, retinol dehydrogenase; RALDH, retinaldehyde dehydrogenase; RAR, retinoic acid receptor; RXR, retinoid X receptor.
Source: Das et al. (2014), with permission from Elsevier (lic. #: 4606690534887)

RA metabolism is catalyzed by heme-containing cytochrome P450 enzymes (CYPs), a superfamily of 57 [in humans] enzymes responsible for the metabolism of many endogenous and exogenous compounds, as well as an estimated 75% of marketed pharmaceuticals drugs[96]. The CYP26 family is the primary enzyme responsible for metabolism of RA, however, other non-RA-specific CYPs have also been reported to metabolize RA[97]. CYP26 enzymes (three human isoforms: CYP26A1, CYP26B1,

CYP26C1) are unique due to their selectivity for RA metabolism. CYP26 research has primarily focused on the CYP26A1 and CYP26B1 isoforms in part due to the low levels of CYP26C1 expression seen in adult human tissues[98]. *In vitro* and *in vivo* studies have shown autoinduction of CYP26A1 expression by RA[99–101], a mechanism generally accepted to be controlled by RAR/RXRs bindings to RAREs found in the promotor region of many RA-regulated genes[102,103]. CYP26B1 gene expression is also induced by RA, however, only CYP26A1's promotor has been found to contain a RARE[73]. Tissue distribution of each isoform varies (e.g. CYP26A1 is the primary hepatic isoform[97], CYP26B1 the primary brain isoform[98]), however, both can be found in skin tissue. Studies have found that CYP26A1 expression tends to be restricted to basal epidermal keratinocytes[104], while CYP26B1 has greater expression in the dermis and hair follicles than the epidermis[81].

1.4 RETINOIC ACID METABOLISM BLOCKING AGENTS

Retinoid therapies (available in oral and topical formulations) have successfully been used in the treatment of a variety of skin diseases (detailed in Section 1.2). These include endogenous retinoids like *all-trans* RA (tretinoin) and *13-cis* RA (isotretinoin), and synthetics including tazarotene, adapalene, and many others. Although retinoids are commonly used in clinical settings, the adverse effects of these drugs (e.g. skin irritation, dryness, photosensitivity, hyperlipidemia, hyperostosis, teratogenicity, and more)[58] can result in complications or noncompliance in many patients.

To address adverse effects and the issue of tolerance (resulting from autoinduction of its metabolism) by direct retinoid therapy, a new class of drugs called retinoic acid

metabolism blocking agents (RAMBAs) were developed. These act by blocking RA metabolism via selective inhibition of CYP26-mediated RA metabolism[105].

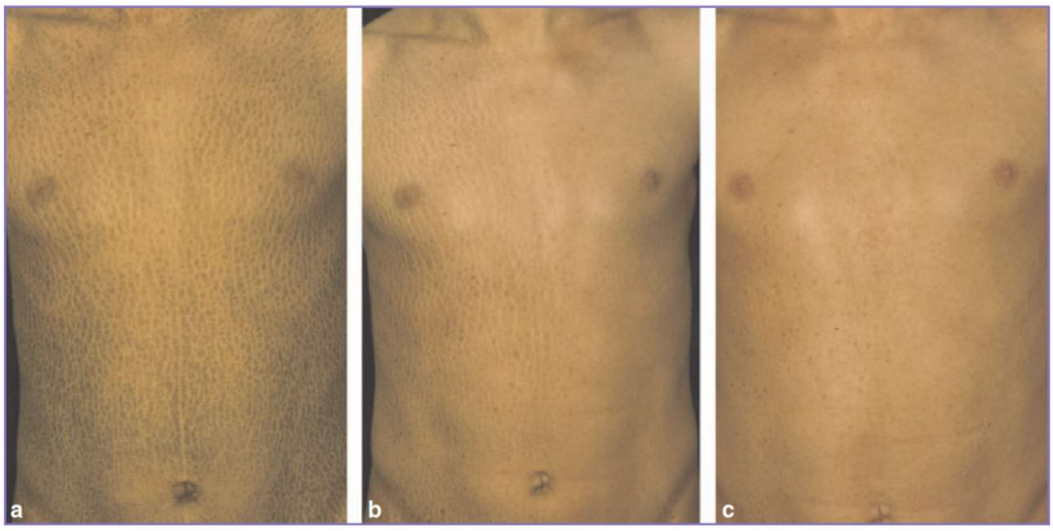

Figure 1.12: Non-erythrodermic lamellar ichthyosis patient treated with 5% topical liarozole showing marked improvement. (a) before treatment, (b) patient's left side treated with liarozole & patient's right side treated with vehicle only, (c) liarozole treatment on both sides.
Source: Lucker et al. (2005), with permission from John Wiley and Sons (lic. #: 4606590968295)

The antifungal agent ketoconazole was the first studied after it was found to inhibit CYP-mediated RA metabolism, however, its use was short lived due to off-target activity[106]. The first-generation of CYP26-specific RAMBAs such as liarozole (Figure 1.13), successfully inhibited the metabolism of RA[107] and showed great promise in treating several skin disorders[41,88,90,91,108,109] including psoriasis and ichthyosis (Figure 1.12[41]). Liarozole, although extensively studied and progressing to late-stage clinical trials, displayed non-specific effects including interference of hormone biosynthesis[106], which may be the reason they have not progressed to clinical use in the US. The more selective

and potent RAMBA, talarozole (R115866) (Figure 1.13), was synthesized to address the issues seen with liarozole[110]. Talarozole has also been shown to alter the expression of retinoid-related genes[111] and underwent several successful topical and oral clinical trials for the treatment of acne and psoriasis[89,112], however, development was halted in 2008, likely for budgetary reasons[113].

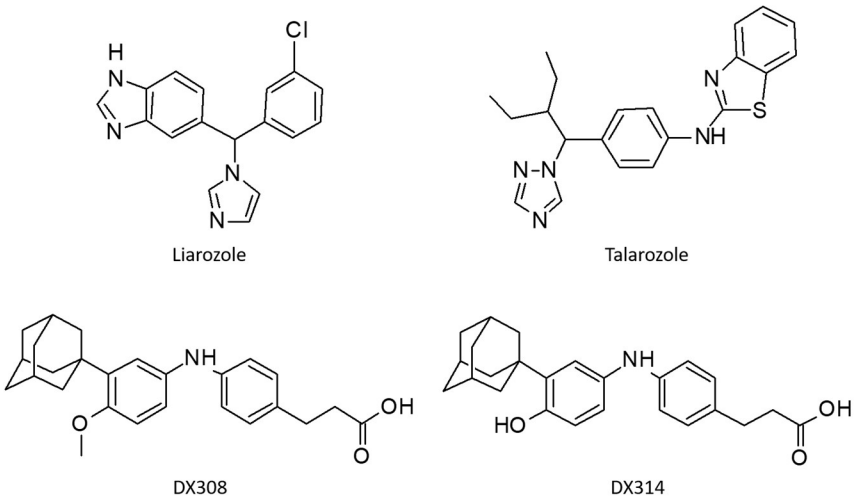

Figure 1.13: Structures of several RAMBAs. First-generation (top) and two of the novel candidate compounds developed by Diaz et al. (bottom). These next-generation RAMBAs lack the azole moiety found on the previous generations, which should reduce their off-target activity.

In response to this gap in the development of CYP26-inhibitors, Diaz et al., have synthesized and screened a library of compounds with varying selectivity for the different CYP26 isoforms[114,115] (Figure 1.13). The previous generation RAMBAs contain an azole moiety, which can interact with the heme found in all CYPs, is thought to contribute to their lack of specificity. The compounds developed by Diaz et al. aim to increase CYP26 specificity with a series of compounds lacking this azole moiety, then, by studying

candidates with varying the isoform specificity, elucidate the advantages each. Initial screening of several early development compounds showed high CYP26 specificity and potency, with little detectable direct activation of RAR[114].

1.4.1 CYP26B1-SELECTIVE RAMBA: DX314

DX314 (previously referred to as NMP314) is a novel CYP26B1-selective RAMBA previously described and patented[116] by Diaz et al. In these studies, we focus primarily on DX314 (Figure 1.13), a CYP26B1-selective compound with a 16-fold higher selectivity for CYP26B1 over CYP26A1, and no detected inhibition of CYP19 (estrogen synthase), in contrast to liarozole and talarozole (Table 1.2[114,116,117]). DX314's cytotoxicity was previously assessed (data not shown) in human keratinocyte, dermal papilla cell, and SH-SY5Y monolayer cultures, which found no evidence of significantly decreased cell viability within the dose ranges used in this study.

Table 1.2: Previous and novel RAMBA cytochrome P-450 IC_{50} values. CYP26A1 and CYP26B1 were expressed in SF9 cells and prepared as microsomal fractions. 100nM *9-cis*-RA was used as the substrate and formation of the metabolite *9-cis*-OH-RA was measured by HPLC. Estimated IC_{50} was determined by: $\mathbf{100\%} \cdot \frac{v_i}{v} = \left(\frac{v_i}{v}\right)_{min} \cdot \mathbf{100\%} + \frac{\left(\frac{v_i}{v}\right)_{max} - \left(\frac{v_i}{v}\right)_{min} \cdot \mathbf{100\%}}{1+10^{(I-\log IC_{50})}}$. CYP2C8, CYP3A4, and CYP19 inhibition assays were performed in pooled human liver microsomes using paclitaxel (4μM), midazolam (0.5μM), and estrone (1μM), as the respective substrates. Product formation was measured by LC-MS/MS. * = unpublished data.

	CYP26A1 IC_{50} (nM)	**CYP26B1 IC_{50} (nM)**	**CYP2C8 IC_{50} (nM)**	**CYP3A4 IC_{50} (nM)**	**CYP19 activity @ 1μM (%)**	**Reference (PMID)**
Liarozole	1,900 [3,200]	18 880*	480 [1,300]	10,000 [1,220]	16.2*	26918322[114] [28275201][161]
Talarozole	5.1 [4]	0.46	220	470	63.6*	26918322 [10734183][110]
DX314 (#39)	1,752	108	>1,000*	2,400*	102.1*	Patent[116]
DX308 (#38)	51	51	>1,000*	24,000*	98.5 (@ 0.1μM)*	Patent
DX385 (#44)	340	14,500	>1,000*	>50,000*	98.4*	Patent

2. DX314 POTENTIATES THE EFFECTS OF RA, WHILE PROTECTING BARRIER FUNCTION IN RECONSTRUCTED EPIDERMIS

2.1 INTRODUCTION

During initial studies, a library of several of candidate compounds having previously undergone *in silico* and *in vitro* CYP26-inhibition assays, were investigated for cytotoxicity and retinoid-responsive gene expression changes within simple monolayer keratinocyte cultures. Two compounds; DX308, and this study's focus DX314, were selected for further study. Here we focus on the characterization of DX314, which became our primary focus as it displayed the least evidence of non-specific biological effects.

The aim of these studies is to investigate whether DX314 can potentiate the effects of endogenous levels of *at*RA, and consequently mimic the desired biological effects seen in retinoid-based therapies, with minimal evidence of undesirable effects. For the purpose of these studies, a potentiation of *at*RA is defined as the ability of a compound cotreated with low-dose *at*RA to display: an effect significantly different from control given said effect can be seen when treating with *at*RA alone; an effect size larger than what is seen with low-dose (1nM) *at*RA alone; and in a manner mimicking the effects seen when treating with higher-dose *at*RA alone. A RAMBA displaying little or no effect on its own but displaying a potentiation of *at*RA when they are cotreated, implies the RAMBA acts by inhibiting the metabolism of *at*RA. This would result in identical initial doses of *at*RA producing a relatively increased effect in the presence of a RAMBA. These studies were performed in reconstructed human epidermis (RHE) grown using primary keratinocytes

from healthy adult donors. Use of *in vitro* 3D skin models provides significant improvements in study relevance to *in vivo* conditions relative to the traditional monolayer keratinocyte culture. Two independent studies (Table 2.1) characterizing the effects of DX314 in healthy RHE are presented here. The effects of *at*RA, as well as the well-studied RAMBA liarozole, are used to compare the therapeutic potential of DX314.

	Cells	Assays	Groups
Experiment 1	NAK209 NAK214 NAK219	qPCR	1
		Histology	2
		IHC/IF	2
		TEER	1, 2
Experiment 2	Gibco C00505C	RNAseq	3
		TEER	3
		IPA	3
		TEWL	4

Table 2.1: Outline of experiments performed during this study. IPA, Ingenuity Pathway Analysis; IHC/IF, Immunohistochemistry/ immunofluorescence; TEER, transepithelial electrical resistance; TEWL, trans-epidermal water loss.

2.2 METHODS

2.2.1 PRIMARY HUMAN KERATINOCYTES

Primary, human, adult, healthy, epidermal keratinocytes were used for all parts of this project. Adult, human epidermal keratinocytes (HEKa, Gibco, C-005-5C) were sourced from a 40yo female. NAK209 (48yo, female), NAK214 (37yo, male), and NAK219 (32yo, female) were generously donated to the project by our collaborator, Dr. Yves Poumay at the University of Namur, Belgium.

2.2.2 CELL CULTURE

The keratinocytes were previously isolated by the Poumay lab from skin biopsies as described[118–120]. Excess skin tissue from abdominoplasty was stored in a 4°C saline solution for transport to the lab. In a sterile culture hood, the tissue was placed into a petri dish containing solution A (10mM Glucose, 2mM KCl, 130mM NaCl, 1mM Na_2HPO_4, 3.3µM phenol red, 30mM HEPES, pH 7.2-7.4, 0.22µm sterile filtered) and cut into 1-2cm^2 sections. The sections are then transferred to a petri dish containing a 4°C trypsin solution (0.17% w/v trypsin, 50µg/mL gentamycin, 250ng/mL fungizone, and 250ng/mL ampicillin in solution A) and incubated overnight at 4°C. The dermis and epidermis are then separated using sterile forceps and the epidermis placed in solution A containing 2% dialyzed fetal bovine serum (FBS) for further dissociation by manual stirring. The suspension is then filtered through a 70µm cell strainer, centrifuged for 10min at 160rcf and 4°C, and resuspended in 10mL KGM-2 bullet kit (Lonza, CC3107) supplemented with gentamycin, fungizone, and ampicillin in the concentrations described above. The viable cell count is determined with a Countess automated cell counter (Invitrogen), then 46,000 cells/cm^2 are

plated in a 175cm^2 culture flasks containing 25µL FBS and 25mL KGM-2 supplemented with 0.5% penicillin/streptomycin (P/S, Corning, 30002CI). This is incubated undisturbed for 3 days in a 37°C, 5% CO_2, humidified incubator. The media is then replaced with Epilife Complete (Epilife media [Gibco, MEPI500CA], 1% HKGS [Gibco, S0015], 0.5% P/S), which is replaced every two days, and allowed to reach 50-60% confluence before subculturing or cryopreservation at 1e6 cells/mL in freezing media. (Epilife, 10% DMSO, 10% FBS).

Keratinocyte culture protocols were adapted from the protocol described by Poumay et al.[121]. Briefly, cryopreserved cells were thawed and seeded in cell culture flasks at 3000-12000 cells/cm^2 in KGM-2 (supplemented with 0.5% penicillin/streptomycin) and placed in a 37°C, 5% CO_2, humidified incubator for 24hrs. Media was then replaced with Epilife Complete, refreshed every 2 days, until ~60-70% confluence. The cells are then trypsinized (0.025% trypsin/0.01% EDTA), neutralized, counted, and used for RHE or autocrine monolayer culture.

2.2.2.1 RECONSTRUCTED HUMAN EPIDERMIS

The RHE protocol was adapted from the protocol described by Poumay et al.[118–120]. Briefly, 2.5mL of RHE Day 0 media (Epilife Complete with 1.5mM $CaCl_2$) is placed into each well of a 6-well cell culture plate. A 12mm diameter, polycarbonate membrane (0.4µm pore-size), cell culture insert (Millipore, PIHP01250), is then placed into each well using sterile tweezers. Keratinocytes (passage 3 or 4) are suspended in Epilife Complete at 4e5 cells/mL, and 500µL of this cell suspension is pipetted into each insert (resulting in 200k cells/insert). The plates are then placed in a 37°C, 5% CO_2, humidified incubator, and

left undisturbed for ~24hrs. The following day, the media is aspirated and replaced with 1.5mL RHE Day 1+ media (RHE Day 0 media with 10ng/mL human keratinocyte growth factor [Sigma, K1757] and 50µg/mL vitamin C), which was subsequently changed every two days for the remainder of the experiment. Any media remaining on the surface of each tissue is carefully aspirated to establish an air-tissue interface, which promotes differentiation and epidermal stratification. Drying of the RHE surface was done daily until the barrier is fully formed and media is no longer appearing on the tissue surface. RHEs were grown for a total of 11 days, treatments were started on day 7, refreshed day 9, and stopped on day 11 (Figure 2.1). All treatment groups (including controls) contained 0.1% DMSO as a vehicle to aid compound solubility. Preparation of any photosensitive compounds (*i.e.* retinoic acid) was performed in a dark culture hood with minimal ambient light. Following treatment, the RHEs were collected for RNA purification (Section 2.2.6.1) or histology (Section 2.2.5).

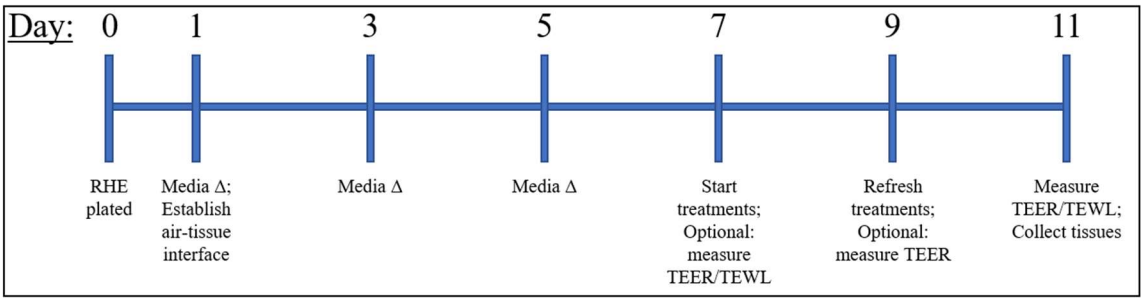

Figure 2.1: Timeline of RHE growth and treatment. Media Δ, media change; RHE, reconstructed human epidermis; TEER, transepithelial electrical resistance; TEWL, trans-epidermal water loss.

2.2.3 TEWL

A custom protocol was developed to allow for a minimally invasive and disruptive measurement of TEWL in viable RHE. This method was required to minimize physical

contact with the tissue surface, allow the tissue to remain within the insert, and to not interfere with downstream experiments, including TEER and histology on the same tissue. Typical *in vitro* methods to quantify TEWL either required the tissue to mounted to a Franz cell (which requires it to be removed from the insert), or use of an evaporimeter attachment, which makes direct contact with the tissue surface and could potentially damage the thin tissue. For this reason, we constructed flexible rubber seals (using gaskets and washers purchased at a local hardware store and assembled with a flexible silicone-based adhesive), which could be sterilized in a solution of 70% ethanol. This allowed the evaporimeter to form an airtight seal over the insert, ensuring any measured water flux must have diffused through the tissue (Figure 1.8). If both TEWL and TEER were measured within a single experiment, TEWL was measured first, followed by a minimum of 2hrs of recovery time in the incubator before TEER is measured. Because TEER requires each tissue to be submerged in media, the residual moisture from this assay would have interfered with the sensitive TEWL measure.

Plates were removed from the incubator and placed in the tissue culture hood with their lids slightly ajar for 15min to allow for adjustment to ambient humidity. Tissue surfaces were thoroughly checked for any moisture, and if needed, lightly dabbed with a sterile cotton swab. The plate was placed on a 37°C plate warmer to ensure consistent media/tissue temperature and promote diffusion and formation of water vapor at a physiologically relevant temperature. The custom rubber seal was fitted over the insert to form an airtight seal between the tissue and the AquaFlux AF200 evaporimeter (Biox) measurement head. TEWL was measured before (day 7) and after (day 11) treatment

(Figure 2.1), over 60-90s, as recommended by the manufacturer, until a steady state water flux was achieved. Due to the inherent sensitivity of TEWL measurements, after each tissue on a plate was measured once, they were sequentially measured a second time and the two values were combined into a single datapoint for statistical analysis.

2.2.4 TEER

The TEER protocol was adapted from a protocol developed by the Poumay lab, which was communicated by personal correspondence. Under sterile conditions, 4mL of Epilife media was placed into each well of a 6-well plate (a separate well for each unique treatment to prevent cross-contamination) and allow to come to room temperature. Use sterile tweezers to transfer an RHE into the media, then pipette 500µL of the underlying media into the insert (3.5mL of media remains in the bottom of the well). Allow the tissue to remain submerged for 30sec before inserting the sterile electrode (Millicell ERS-2) (Figure 1.7). Ideally, we would allow the TEER measure to come to a steady state before reading, however, we found that in many cases this could take in excess of 10min per tissue. We believe this is due to a slow diffusion of media into the tissue affecting the electrical resistance, thus causing the reading to continuously drift. For this reason, we arbitrarily choose a consistent 30sec measurement period for all tissues and recorded the TEER at the end of that period. After measurement, the media in the insert was aspirated and placed back into the well, the tissue surface was dried, and the RHE was placed back into its growth plate. TEER was measured before (day 7) and after (day 11) treatment, and occasionally halfway through (day 9) treatment (Figure 2.1).

2.2.5 HISTOLOGY

Preparation of RHE for histological analysis is described in the RHE protocols above[119,120]. Following treatment, RHEs were immediately placed in a fixing buffer, which consists of 4% formaldehyde and 1% glacial acetic acid. The following day, the tissues were dehydrated with sequential methanol washes (1x rinse, 1x 5min wash, 2x 10min wash), removed from the insert, briefly rinsed in toluene, then placed in fresh toluene bath for 1hr at room temperature. The tissue was then rinsed in liquified paraffin and transferred to fresh liquified paraffin at 58°C for 1hr to allow for complete toluene-paraffin exchange. Finally, the tissue was perpendicularly mounted in a mold containing fresh liquified paraffin, covered by a histology cassette, and allowed to solidify. A microtome was used to take 6µm vertical sections from a depth of at least 1.5mm into the 12mm diameter RHE. Sections were mounted to positively charged glass slides and allowed to dry before use.

Deparaffinization of the slides was performed in the following steps: 2x 3min toluene, 2x 3min methanol, 2x 3min 70% methanol, 10min circulating tap water rinse. The slides were then immediately used for hematoxylin-eosin (HE, Section 2.2.5.1) or immunohistological (Section 2.2.5.2) staining.

2.2.5.1 HEMATOXYLIN-EOSIN STAIN

Slides were sequentially exposed to the following baths: 3x 3min hematoxylin solution, 3min circulating tap water, 3min ethanol with 0.15% HCl, 10min circulating tap water, 2x 3min eosin solution, 3min circulating tap water, 3min 70% ethanol, 3x 3min isopropanol, 3min toluene. Coverslips were mounted, and the adhesive allowed to dry before imaging on an Olympus DX63 microscope with Olympus SC50 camera.

2.2.5.2 IMMUNOHISTOLOGY

Slides were sequentially exposed to the following: PBS rinse, 2x 3min 0.1M glycine in dH_2O, PBS rinse, then 1hr in PBS/BSA/Triton (PBS with 0.2% BSA and 0.02% Triton X-100). A hydrophobic marker was used to encircle the tissue and 50µL of primary antibody (diluted in PBS/BSA/Triton) was applied. The slides were placed in a humidity chamber and incubated for 1hr at room temperature. The slides were then rinsed three times in PBS/BSA/Triton before 1hr humidified incubation with 50µL of the respective secondary antibody. The slides were again rinsed three times in PBS/BSA/Triton before a 15min incubation with 50µL of Hoechst nuclear stain (diluted in PBS/BSA/Triton) followed by 3x 5min PBS rinses. Coverslips were mounted with Mowiol and the slides were stored at 4°C until imaged on an Olympus DX63 microscope with Olympus XM10 camera. Primary and secondary antibody sources and dilutions can be found below (Table 2.2).

Target	Species	Dilution	Source
IVL	Mouse	1:200	Invitrogen, I9018
CYP26A1	Mouse	1:50	Santa Cruz, SC53618
CYP26B1	Mouse	1:50	Santa Cruz, SC293493
FLG	Mouse	1:75	ThermoFisher MA5-13440
KRT10	Mouse	1:100	DAKO, M7002
KRT14	Mouse	1:50	Santa Cruz, SC58724
2°, HRP-conjugated (anti-mouse)	Horse	1:100	Vectastain, PK-4002
2°, Alexa Fluor 488-conjugated (anti-mouse)	Goat	1:1000	Life Technologies, A11001
Hoechst 33258, nuclear stain	-	1:100	Life Technologies, H3569

Table 2.2: Antibodies and dyes used for immunohistological staining.

2.2.6 DIFFERENTIAL GENE EXPRESSION

2.2.6.1 RNA ISOLATION

Following treatment, RHEs intended for RNA extraction were flash frozen at -80°C until use. RNA was isolated using the NucleoSpin RNA (Macherey-Nagel, 740955) kit, as recommended by the manufacturer. Variations from the standard protocol include: homogenization with 600µL (rather than 350µL) of RA1 lysis buffer, addition of 6µL of β-mercaptoethanol to RA1 to aid tissue lysis, and addition 600µL of 70% ethanol (rather than 350µL) during nucleic acid precipitation.

2.2.6.2 RT qPCR

Isolated RNA purity and concentration were measured by NanoDrop 2000c (Thermo Scientific) and integrity was confirmed by gel electrophoresis. For each reaction, 6.5µL of a mix containing; 100-200ng of template RNA, 50ng/mL oligo(dT)$_{12\text{-}18}$ (Life Technologies, 58862), and 0.5mM dNTP mix (Invitrogen, 10216018/10219012/10217016/10218014), were incubated at 65°C for 5min. 3.5uL of the Superscript III reverse transcriptase kit (Invitrogen, 18080044), which includes enzyme (56575), DTT (Y00147), and 5x first-strand buffer (Y02321), is then added to each well and incubated for 50min at 42°C, followed by 15min at 70°C. The cDNA was then diluted 1:10 with water. 2µL of cDNA was added to a 10µL real-time qPCR reaction, which used Takyon No ROX SYBR 2X MasterMix (Eurogentec, UF-NSMT-B0701) on a Roche Lightcycler 96 (activation: 3min - 95°C; 40 cycles: 10sec - 95°C, 20sec - 60°C, 30sec - 72°C). 500nM of each primer pair (Table 2.3), optimized for an annealing temperature of 60°C, was used for each reaction. RPL13a and 36B4 (RPLP0) were used as reference

genes. Every reaction was performed in technical duplicates. Due to limited access to donor tissue, and the low cellular passage number necessary for quality RHE, the qPCR results obtained during experiment 1 (Table 2.1) consists of pooled data from replicate experiments consisting of RHE from several donors. Because these independent replicates are subject to the interindividual variability in treatment response by each donor, we applied a method described by Willems et al.[122] to standardize the qPCR data, determine the fold-change in expression from control, and calculate the 95% confidence interval of the mean. Statistical analysis was done by one-way ANOVA with Dunnett's correction for multiple comparisons on the standardized values using GraphPad Prism 6.

Target	Forward	Reverse	Ref
36B4	5'-ATC AAC GGG TAC AAA CGA GTC-3'	5'-CAG ATG GAT CAG CCA AGA AGG-3'	121
RPL13a	5'-CTC AAG GTC GTG CGT CTG AA-3'	5'-TGG CTG TCA CTG CCT GGT ACT-3'	123
HBEGF	5'-TGG CCC TCC ACT CCT CAT C-3'	5'-GGG TCA CAG AAC CAT CCT AGC T-3'	121
IVL	5'-TGA AAC AGC CAA CTC CAC-3'	5'-TTC CTC TTG CTT TGA TGG G-3';	121
KRT10	5'-ATC GAT GAC CTT AAA AAT CAG ATT CTC-3'	5'-GCA GAG CTA CCT CAT TCT CAT AC-3'	*i*
KRT14	5'-CGA TGG CAA GGT GGT GTC-3'	5'-GGG TGA AGC AGG GTC CAG-3'	123
CYP26A1	5'-GGG AGA GCG GCT GGA CAT-3'	5'-TCC AAA GAG GAG TTC GGT TGA-3'	121
CYP26B1	5'-CCG CTT CCA TTA CCT CCC GTT C-3'	5'-CCA CCG CCA GCA CCT TCA G-3'	*ii*
FLG	5'-GGG CAC TGA AAG GCA AAA AG-3'	5'-CAC CAT AAT CAT AAT CTG CAC TAC CA-3'	123
TGM1	5'-GTC GTC TTC CGG CTC GAA-3'	5'-TCA CTG TTT CAT TGC CTC CAA T-3'	123
STRA6	5'-TCC CTG TGT TTG CTG CT-3'	5'-GAA CAG TCC CAG TAT CTT CCA G-3'	*iii*

Table 2.3: List of primers used for qPCR. Integrated DNA Technologies (IDT) assay IDs: *i* - Hs.PT.58.38635764, *ii* - Hs.PT.58.38517191, *iii* - Hs.PT.58.3346779.g.

2.2.6.3 RNA SEQUENCING & BIOINFORMATICS

RNA samples were sent to the University of Colorado's Genomics and Sequencing Core Facility (Denver) for library preparation and sequencing. Purity and concentration were measured with an Agilent Bioanalyzer (Agilent Technology). 200-500ng of RNA was used to prepare the Illumina HiSeq libraries according to manufacturer's instructions for the TruSeq Stranded RNA kit (Illumina). Sequencing was done as 2x 151bp paired end reads on the Illumina HiSeq4000.

Raw data was delivered to us as FASTQ files (two paired files per sample), which contained RNA sequences, each with a length of 151 bases (b), as well as a quality score metric (Q) per base read, which indicates the probability (P) that the respective nucleotide was incorrectly identified by the sequencer. This score is defined as: $Q = -10 \cdot \log_{10} P$. A sequence score ≥ 30 (indicating a $P \leq 0.001$) is typically considered acceptable for analysis. As delivered, sequencing across all samples had an average quality score of 35.2 (lowest quality sample scoring a mean of 34.9 across all sequences), with the total reads per sample averaging 12.4Gb (smallest sample size: 9.2Gb).

The bioinformatics pipeline we used was an adaptation of several previously described methods[124–130], and was applied in the following sequence: FastQC[130] (v0.11.5) → Trimmomatic[128] (v0.38) → FastQC → HiSat2[129] (v2.1.0) → SamTools[131] (v1.8) → StringTie[125] (v1.3.4d). FastQC analyzes the FASTQ files to determine the quality of the reads before, and after, trimming to ensure acceptable read quality for downstream analysis. Trimmomatic then processes each sequence within a set of paired FASTQ files to remove the adapter sequences, which were added to the RNA fragments during library

preparation for sample identification. Trimmomatic also applies quality filtering using a sliding window approach to, starting on the 5' end of the read, scan 4b fragments and trim the 3' end if any group falls below a mean quality score of 15. Trimmomatic was also instructed to remove any sequences trimmed below 36b from the dataset, which helps prevent false positives during alignment. Trimming resulted in an average of 0.57% (SD = 0.13%) of the paired sequences being dropped completely, 59.5% (SD = 11.7%) paired survivors, 39.5% (SD = 8.6%) forward only survivors, and 0.47% (SD = 0.09%) reverse only survivors. The resulting paired read outputs were used for alignment, while unpaired sequences were excluded from further analysis. The trimmed paired FASTQ files were reanalyzed in FASTQC to confirm sequence quality was maintained during trimming. The HiSat2 package was used to align each sequence to a reference human genome (H. sapien GRCh38 *genome_tran* index, provided by the HiSat2 developers[132] and indexed with the included shell script). HiSAT2 exports a sequence alignment map (SAM)-formatted file, which contains information on each alignment including: the sequence aligned, the location of each sequence within the genome, the quality of the alignment, the sequence length, and more. SamTools is then used to convert the text-based SAM file to a binary alignment map (BAM) file to allow annotation and qualification by the StringTie package. StringTie accepts a BAM file as well as a gene transfer format (GTF) file (also built by shell script included with the GRCh38 *genome_tran* index), which contains the names and locations of known genes, transcripts, introns, and exons in the reference genome. StringTie's network flow algorithm will also identify and account for various isoforms of a given gene, even if they are not explicitly defined in the user provided annotation. The final output of

StringTie provides a GTF-formatted count table containing the Ensembl ID for each transcript, as well as the number of matching sequences in the sample. The StringTie developers also provide a small script (prepDE.py), which was used to combine the individual GTF files to a single count table formatted as a comma-separated value (CSV) file, which contains one gene per row with the gene IDs in the first column, one sample per subsequent column, and the number of transcripts found during alignment in each corresponding cell.

This gene count table can then be imported by the R[133] (v3.5.2) package DESeq2[126,127,134] (v1.22.2) for differential expression analysis. DESeq2 was set up to group treatment replicates and determine the fold-change in gene expression from the control group for each treatment. BiomaRt[135] (v2.38.0) was then used to attach the HUGO Gene Nomenclature Committee (HGNC) gene symbols to each Ensembl ID. Finally, DESeq2 normalizes the raw read counts based on the differential read depth for each sample, applies logarithmic-fold change shrinkage to correct for effect size using the apeglm[136] (v1.4.2) algorithm, and computes the false-discovery rate (FDR) statistic with the default Benjamini-Hochberg correction for multiple comparisons. The final output consists of one CSV file per comparison (treatment) containing one gene per row (annotated with Ensembl ID and HGNC symbol) as well as the mean fold-change in expression and FDR statistic for each comparison. Individual treatments were then merged (by matching gene IDs) into a single CSV containing the fold-change in expression and FDR for every treatment group in the study.

Treatment groups & sample sizes: Control (0.1% DMSO, n = 5), 1nM *at*RA (n = 4), 100nM *at*RA (n = 4), 1000nM DX314 (n = 3), and 1000nM DX314 + 1nM *at*RA (n = 4). The scripts used for bioinformatic analysis can be found here: https://github.com/JGSV/DX314_Bioinformatics/.

2.2.6.3.1 PATHWAY AND REGULATOR ANALYSIS

The output of the procedure detailed above, which contains each treatment's mean fold-change in expression from control, and their respective FDR values, mapped to Ensembl IDs were imported into Ingenuity Pathway Analysis[137] (IPA, Qiagen) software for pathway analysis. This software utilizes an expert-curated knowledgebase containing millions of peer reviewed findings and datasets, to allow for in depth investigation into complex biological pathways, networks, regulators, and more. We selected to limit the IPA analysis (which used the most up-to-date database available as of January 20th, 2019) to only consider genes with an FDR ≤ 0.05 and a fold-change in expression greater than 1.5, or less than -1.5. IPA utilizes Fisher's exact test (we accepted the recommended significance cutoff of $p \leq 0.05$) to predict which canonical pathways and upstream regulators are activated, inhibited, or unaffected. IPA was instructed to only consider upstream regulators which fell under the following IPA-provided categories: "genes, RNA, proteins, and endogenous chemicals". The relative strength and direction of each prediction is given as a z-score. As per IPA's recommendation, a z-score of ≥ 2.0 was considered activated, while a z-score ≤ -2.0 was considered inhibited.

2.3 RESULTS

2.3.1 DX314 POTENTIATES THE EXPRESSION OF RETINOID-RESPONSIVE GENES WHEN CO-TREATED WITH NANOMOLAR *at*RA

In the first series of experiments, RHE made with primary keratinocytes from three adult donors were treated with variable doses of *at*RA or RAMBAs (DX314 or liarozole) with, or without 1nM *at*RA. Alterations in the mRNA expression of several genes related to keratinocyte differentiation or retinoid bioactivity were observed using real-time, quantitative polymerase chain reaction (RT-qPCR) (Figure 2.2). Due to inherently high interindividual and interexperimental variability, the raw data was standardized as described by Willems et al.[122] across independent experimental replicates. After treatment with *at*RA alone, an increase in HBEGF, CYP26A1 and CYP26B1 expression is observed. A subtle, yet significant, increase in expression is also observed in IVL at a dose of 100nM. Since culture media does not initially contain RA, RAMBAs alone should exhibit no effect if their action is through enhancement of RA concentration. We herein confirm that neither DX314 nor liarozole alone had significant effect on the expression of the genes analyzed in this study. On the contrary, we found that 1000nM DX314 combined with 1nM *at*RA was able to mimic the consequences of high dose *at*RA on the expression of every gene analyzed here. 100nM DX314 with 1nM *at*RA also achieved this effect on HBEGF and IVL. Liarozole with *at*RA was only able to significantly alter HBEGF and CYP26A1 expression but did so each dose studied. Overall, these results do appear to support the hypothesis that the RAMBAs potentiate the effect of low dose *at*RA on these genes,

however, we did experience a large variance in the replicates, which, we believe, was due to the inherent interindividual variability in response by different donors.

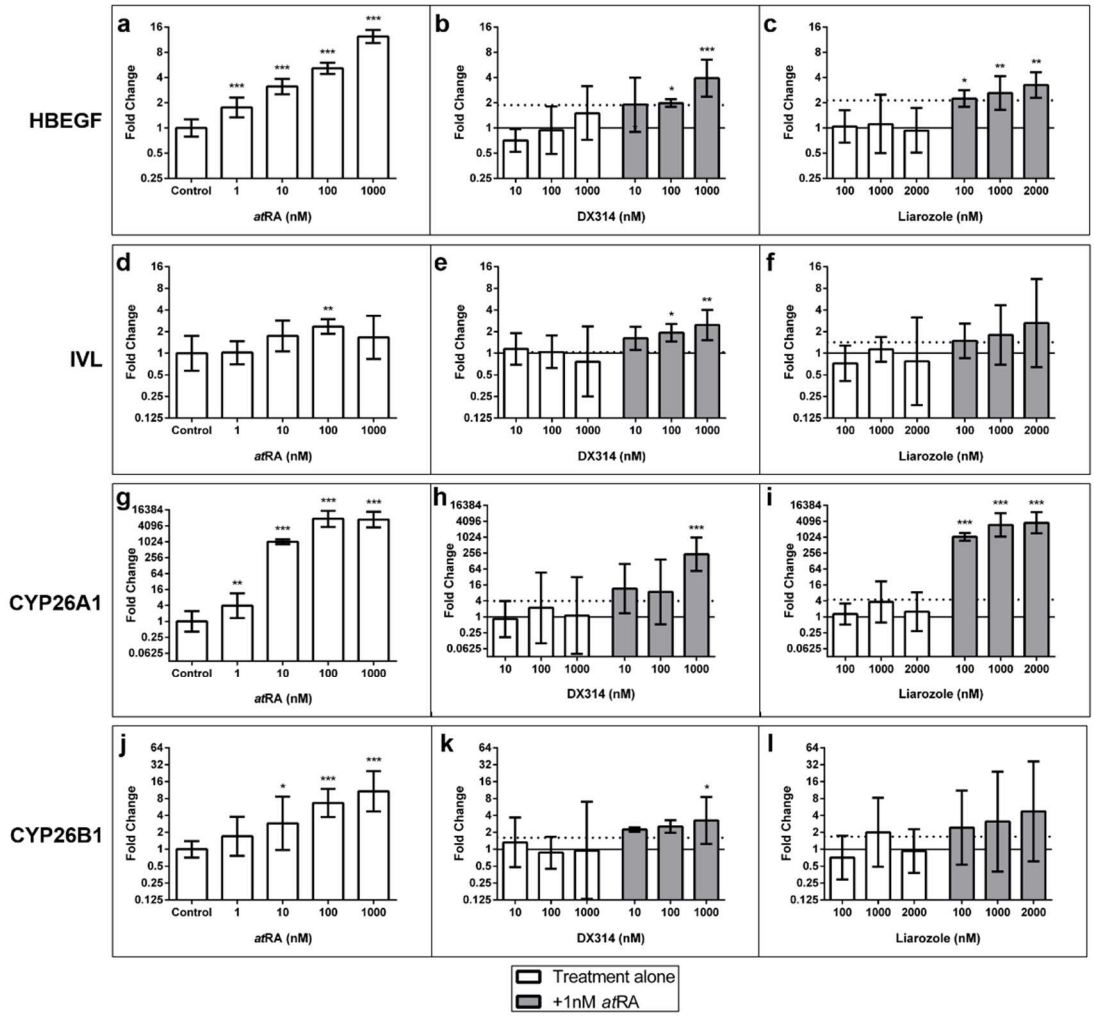

Figure 2.2: **Variable gene expression of RHE treated with *at*RA, RAMBAs.** Expression of HBEGF (a-d), IVL (e-h), CYP26A1 (i-l) and CYP26B1 (m-p) mRNA after 4-day treatment with *at*RA or RAMBAs, with (grey bars), and without (white bars), 1nM *at*RA. Data includes pooled results of RHE grown using keratinocytes from one of three donors. Solid line below shows control, while the dotted line shows 1nM *at*RA. Bars show mean ± 95% CI. Significance vs vehicle control determined by one-way ANOVA with Dunnett's correction for multiple comparisons on autoscaled values. *p≤0.05; **p≤0.01; ***p≤0.001. n = 4 in all groups except: 1000nM DX314 (with/without *at*RA) and 2000nM liarozole (with/without *at*RA); n=3. Note: CYP26A1 controls showed no detectible fluorescence after 40 qPCR cycles. To allow for presentation of data a target Ct value of 40 was assigned to undetected samples.

Immunohistochemical staining of the RHE shows IVL primarily localized in the upper layers of the epidermis in the control and 100nM DX314 treatment groups (Figure 2.3). 1nM and 100nM *at*RA, as well as 100nM DX314 + 1nM *at*RA, all show earlier IVL expression within the lower layers suggesting a modification of differentiation by *at*RA and supporting the potentiating effect of DX314. Immunostaining of CYP26A1 and CYP26B1 (Figure 2.4) were also performed but the results were disorganized and inconsistent with mRNA expression patterns. Irregularities and a lack of correlation between CYP26 mRNA and protein expression has previously been observed in *in vitro*[138] and *in vivo*[111,139] studies of RAMBA treated ichthyotic and healthy skin.

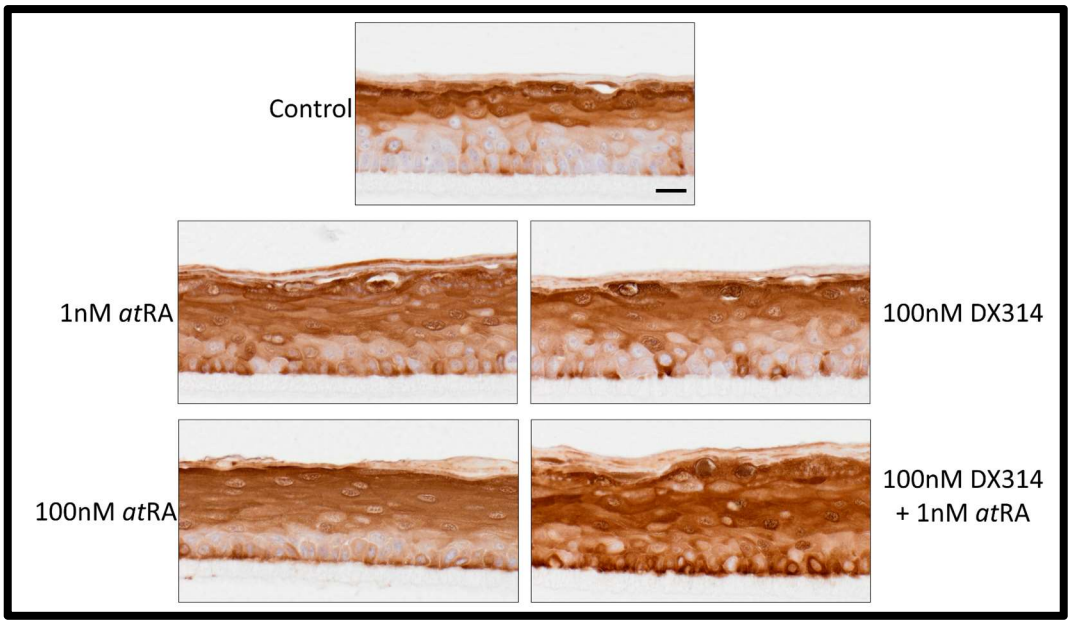

Figure 2.3: Changes in involucrin (IVL) localization by atRA, DX314. Comparison of healthy RHE processed for IHC detection of late differentiation marker, IVL, following a 4 day of treatment with *at*RA, DX314, or DX314 + *at*RA. Scale bar = 20µm.

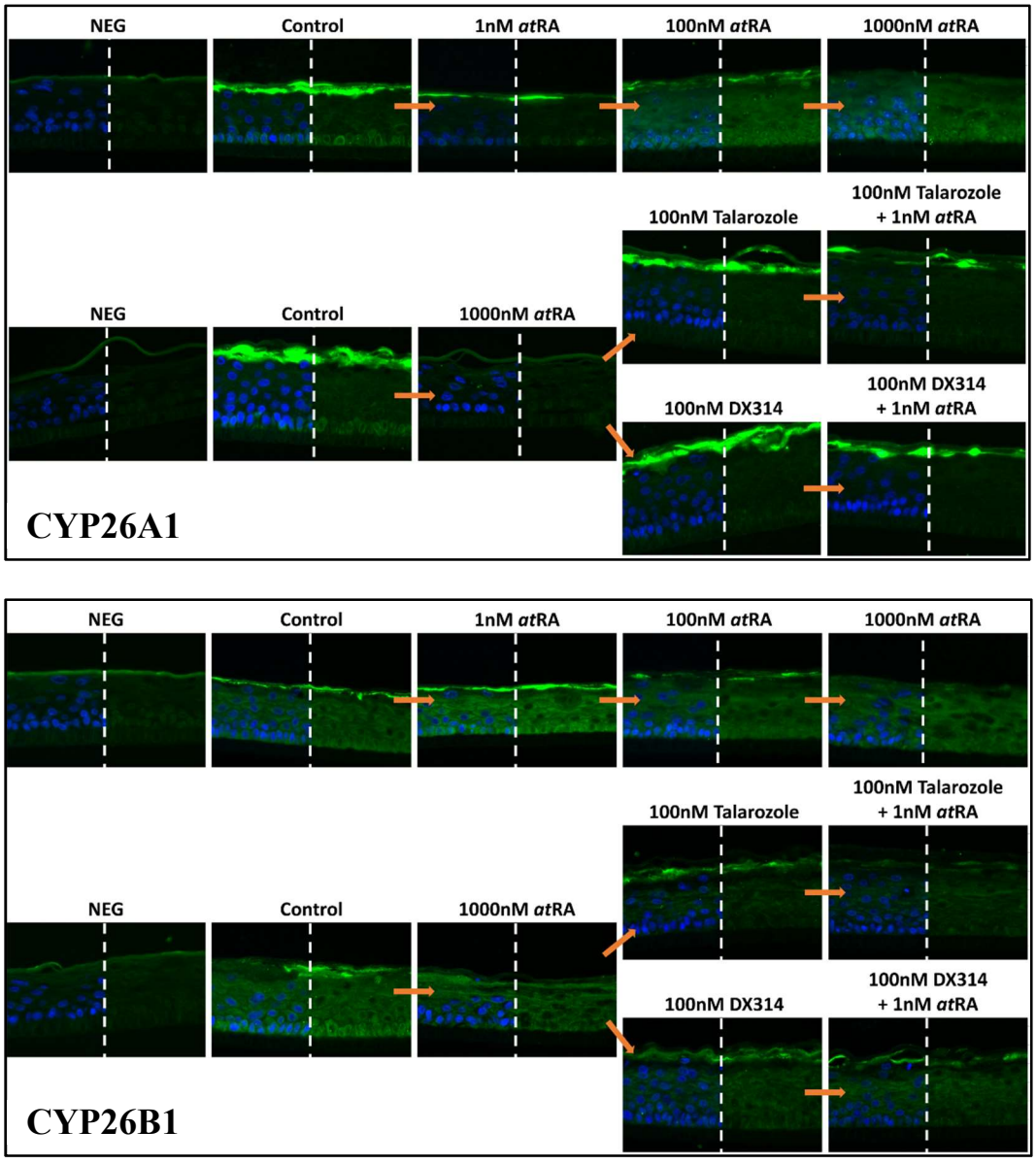

Figure 2.4: Immunofluorescent staining of CYP26 in healthy RHE. RHE were stained with antibodies targeting CYP26A1 (top, green), CYP26B1 (bottom, green), and a nuclear stain (blue).

To address the variance in gene expression seen in in the first series of experiments and confirm the ability of DX314 to potentiate the effects of low dose *at*RA, we designed the second series of experiments, to use a single source of healthy, primary keratinocytes

for all replicates. In this experiment, we performed RNA sequencing (RNAseq) which allows simultaneous investigation of all expressed transcripts in a sample and quantify differential expression across treatments. The RNAseq results confirm that 1000nM DX314 alone has no effect on HBEGF, IVL, CYP26A1 or CYP26B1 mRNA expression. However, DX314 conversely demonstrates potentiation of *at*RA effects when cotreatment is performed (Figure 2.5). We also present a gamut of known retinoid-responsive genes including several keratins (KRT)[71], lecithin:retinol acyl- transferase (LRAT)[93], retinol binding protein 1 (RBP1)[140], and cellular retinoic acid binding protein 2 (CRABP2)[141] which also show a potentiation of *at*RA by DX314. In the adjacent left column of the figure, we show whether a particular gene involves direct (green = RAREs present within promotor[71,100,142–148]), or indirect/unknown (white = no known RAREs in promotor) RA pathways. Overall, the RNAseq experiment displays gene expression patterns which provide strong evidence that DX314 inhibits *at*RA metabolism, thereby potentiating its effects.

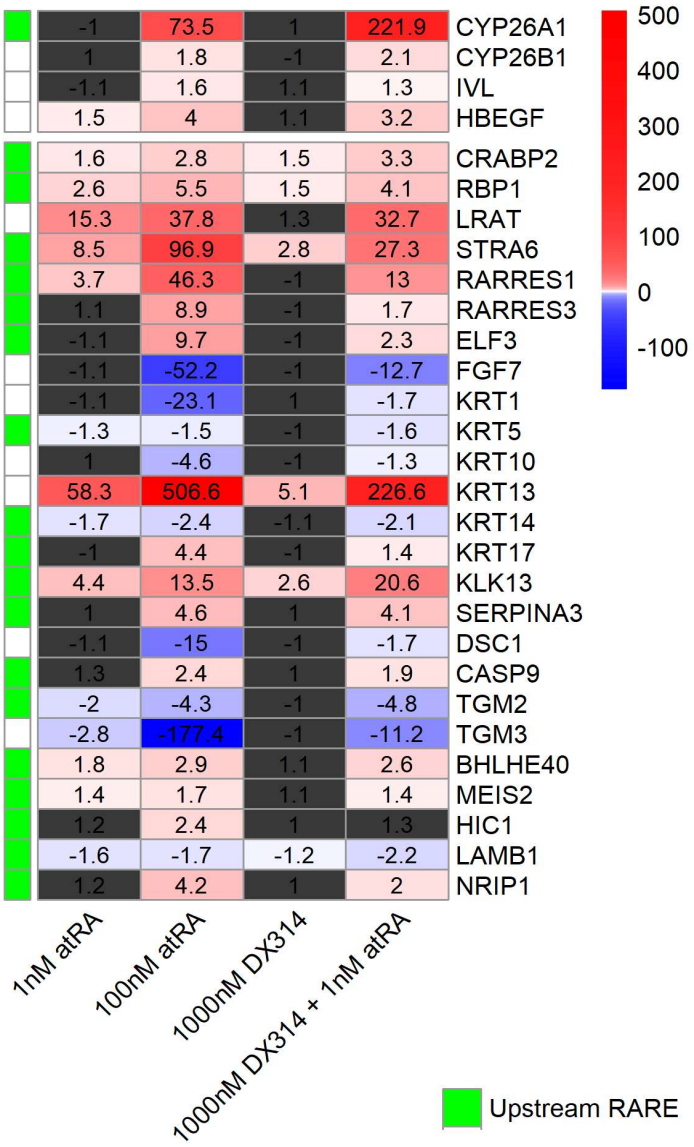

Figure 2.5: Gene expression by RNAseq in RHE treated with *at*RA, DX314. Fold-change in expression vs vehicle control. RHE treated with 1nM *at*RA (left column), 100nM *at*RA (middle-left column), 1000nM DX314 (middle-right column), or 1000nM DX314 + 1nM *at*RA (right column). Dark grey cells indicate a lack of statistical significance, while all colored cells are considered statistically significant (FDR $\leq$ 0.05). An adjacent green box indicates the gene shows evidence of RAR-mediated expression effects based on RA response elements (RAREs) found within the promotor region.

2.3.2 DX314 INDEPENDENTLY MITIGATES RHE BARRIER DISRUPTION

We measured the transepithelial electrical resistance (TEER) of RHE from the first series of experiments as a functional measure of barrier integrity. To account for the inherent variability across experiments and keratinocyte sources, the results of each independent run were pooled and normalized to their respective controls. We observed a significant decrease in TEER by *at*RA (Figure 2.6). Talarozole and liarozole alone showed no significant effect on TEER, while cotreatment with nanomolar *at*RA resulted in a significant decrease. Surprisingly, 1000nM DX314 showed an increase in TEER and there

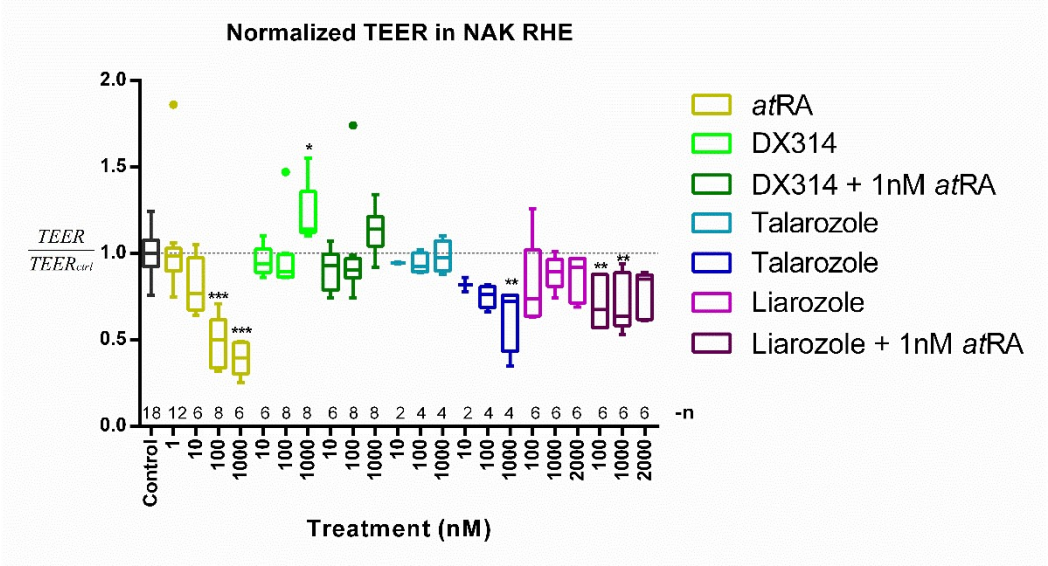

Figure 2.6: Normalized TEER of RHE treated with *at*RA, RAMBAs. Experiment 1 (groups 1 and 2) RHE following 4-day treatment with *at*RA or RAMBAs with, or without, *at*RA cotreatment. Data includes pooled results of 9 independent runs performed during experiment 1. Post-treatment TEER values were normalized to the control RHEs within each run. Graph shows Tukey's boxplot with outliers. Sample sizes (n) are shown above x-axis. Significance vs the vehicle control determined by one-way ANOVA with Dunnett's correction for multiple comparisons. *p≤0.05; **p≤0.01; ***p≤0.001

was no observed decrease in TEER when cotreated with *at*RA. This is despite our gene expression studies indicating a robust potentiation of *at*RA effects. TEER was measured again in the second series of experiments (Figure 2.7a), however, we found that the D11 (post-treatment) TEER in all groups, apart from 100nM *at*RA, exceeded the accuracy threshold of the instrument (accurate at ≤10,000Ω), so any differences could not be resolved. Despite the instrument limitation invalidating any conclusive analysis of the results, we believe the initial trends observed on D9 were consistent with, and certainly do not contradict, the observations of the first experiment.

Assessment of TEWL also proved problematic in this study. The experiment was performed twice, and the results combined for analysis. Although it initially appeared that DX314 treated RHE may have slightly reduced the average TEWL (Figure 2.7b), the experiment as performed did not find any statistically significant differences and conclusions could not be drawn.

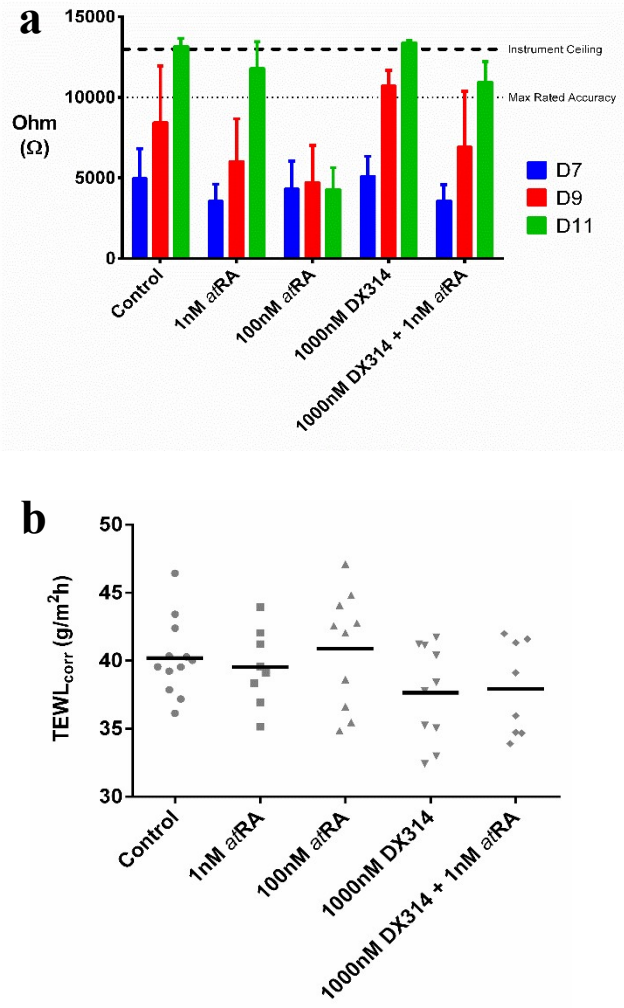

Figure 2.7: TEER and TEWL of RHE treated with *at*RA, DX314. (a) Raw TEER of RHE (experiment 2, group 3) following treatment with *at*RA or DX314 with, or without *at*RA cotreatment. Raw TEER of D7 (blue, before treatment), D9 (red, 2 days of treatment), and D11 (green, 4 days of treatment) are shown. Due to TEER measurements exceeding the accuracy limits of the instrument (rated at 10,000Ω, dotted line) in most samples, a proper analysis could not be performed. Bars show mean±SD. (b) Corrected TEWL values from two runs of RHE (experiment 2, group 4) treated with *at*RA or DX314 with, and without, *at*RA cotreatment. Black bar indicates mean, each point represents a single RHE. One-way ANOVA with Dunnett's correction for multiple comparisons showed no significant differences between control and any treatment.

Morphologically, *at*RA treated RHE showed a distinct disruption of normal tissue structure (Figure 2.8). Observed changes include a near total loss of the dark, FLG-containing, keratohyalin granules (KG) typically found in the stratum granulosum (SG), a shift in the stratum basale (SB) keratinocytes from a typical columnar appearance to a more rounded appearance (more closely resembling SS keratinocytes), a less nucleated stratum

spinosum (SS), and an overall unhealthy appearance. RHE treated with liarozole or talarozole alone showed no major histological changes, but RHE cotreated with nanomolar *at*RA resemble the RHE treated with high dose *at*RA. Similarly, DX314 causes no major changes in morphology when dosed alone, but unlike the other RAMBAs, we observed minimal disruption of normal morphology with *at*RA cotreatment (intact SG/KG, columnar SB keratinocytes, generally healthy tissue appearance). A replication study of these effects on RHE morphology by *at*RA and DX314 showed the same results (Figure 2.9). When we consider the gene expression profile showing a strong potentiation of low dose *at*RA by DX314, this finding seems to suggest that DX314 displays a subtle protective effect on epidermal integrity and may be able to mitigate the more aggressive adverse effects of *at*RA treatment.

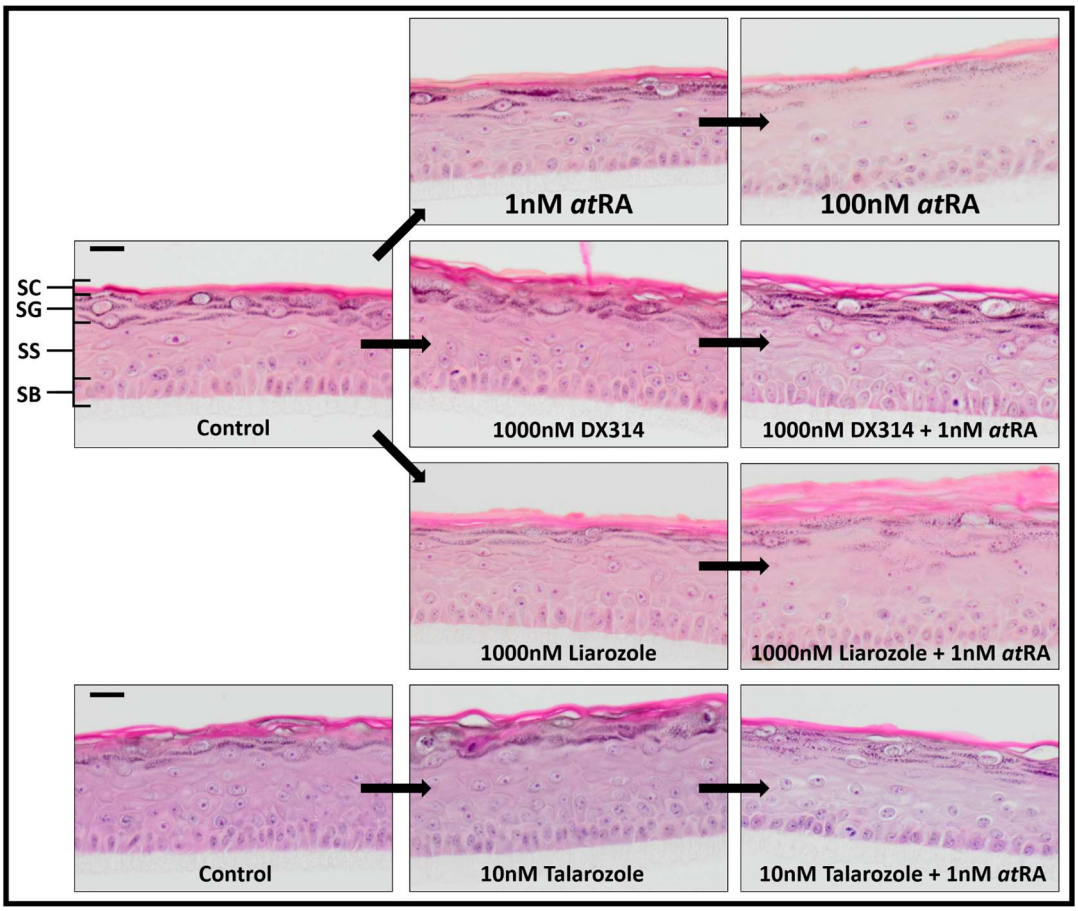

Figure 2.8: Morphological changes in RHE treated with *at*RA, RAMBAs. RHE (experiment 1, group 2) morphology changes after 4-day treatment. 6µm sections were stained with H/E. Control RHE consists of columnar keratinocytes in the stratum basale (SB, bottom layer), flattened cells in the stratum spinosum (SS, second layer), a thick stratum granulosum (SG, third layer) with many keratohyalin granules (KG, stain as a dark grainy texture within SG), and a relatively thin but tightly packed stratum corneum (SC, upper layer). Scale bars = 20µm.

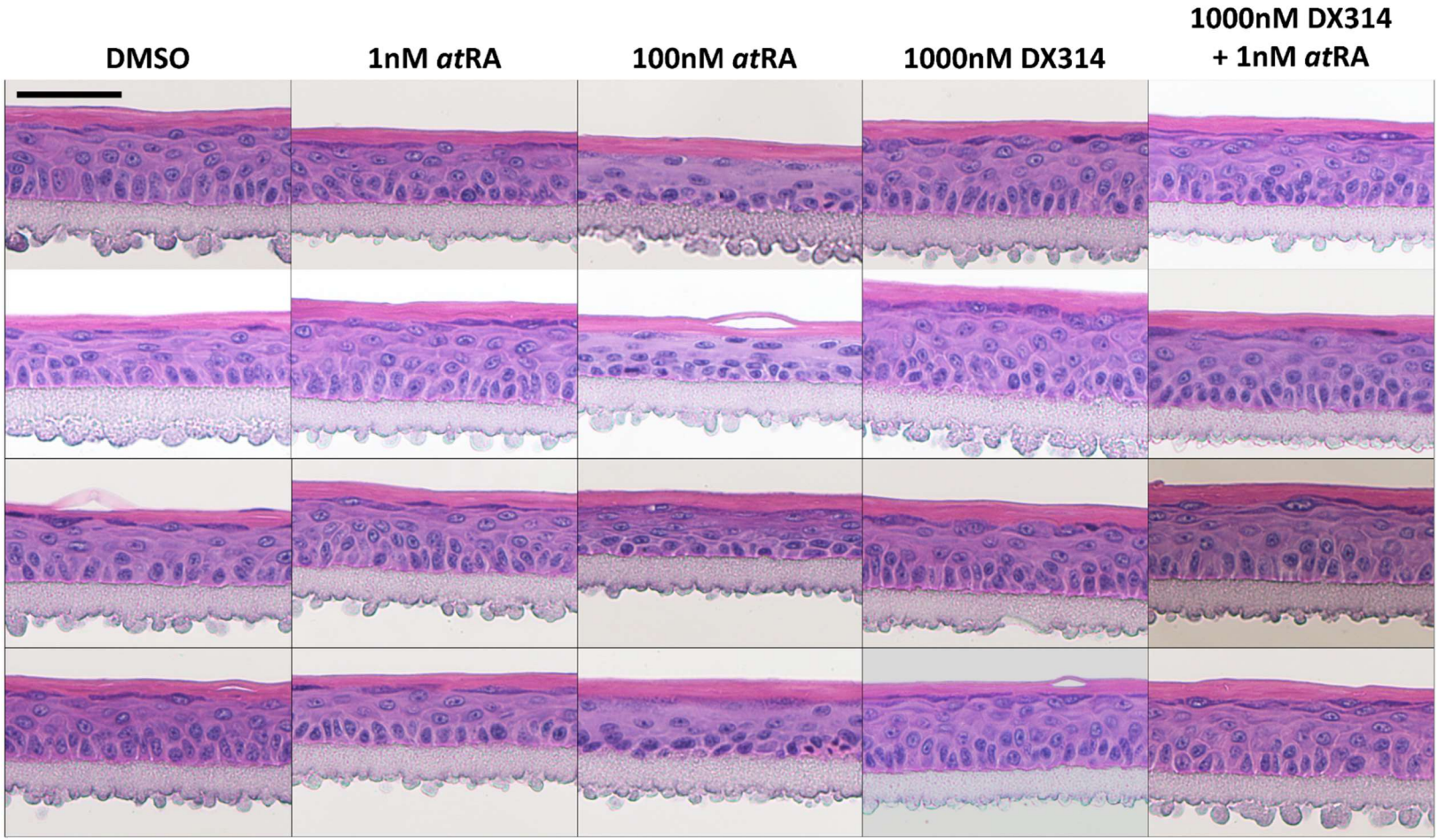

Figure 2.9: Replicate histology of healthy RHE treated with atRA, DX314. Images from a replication of the initial study to confirm morphological effects. Note that adjacent tissues in this experiment are not paired and replicates can be considered a uniform sample population. Scale bar = 50µm

The epidermal differentiation complex (EDC) is a cluster of genes, found on human locus 1q21, that are essential for epidermal differentiation[149]. We mapped the expression of these genes, as well as some known EDC gene expression regulators, to the RNAseq data we collected (Figure 2.10). Overall, the expression patterns appear to be consistent with observations of other retinoid-responsive genes previously discussed. However, we did observe that the expression of many genes in the cornified envelope precursor family were not affected by DX314 + *at*RA treatment despite a dramatic downregulation by high dose *at*RA. We speculate that a preservation of cornified envelope protein expression may be a factor contributing to the increase in TEER observed in DX314 treated RHE. Investigation into whether this observation directly contributes to the barrier effects we have shown should considered in future studies of DX314.

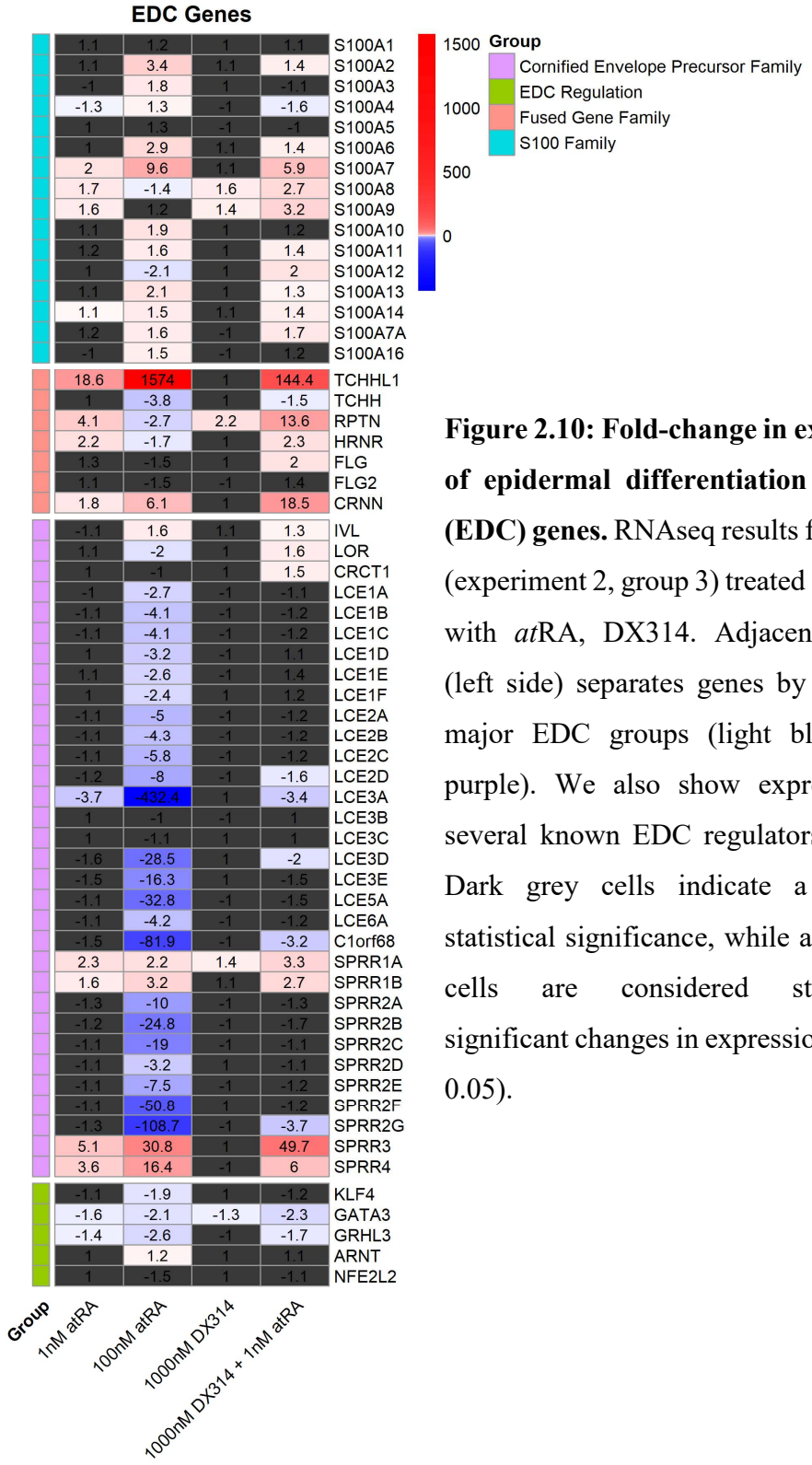

Figure 2.10: Fold-change in expression of epidermal differentiation complex (EDC) genes. RNAseq results from RHE (experiment 2, group 3) treated for 4 days with *at*RA, DX314. Adjacent column (left side) separates genes by the three major EDC groups (light blue, pink, purple). We also show expression of several known EDC regulators (green). Dark grey cells indicate a lack of statistical significance, while all colored cells are considered statistically significant changes in expression (FDR ≤ 0.05).

2.3.3 PATHWAY AND UPSTREAM REGULATOR ANALYSIS OF DX314 AND *at*RA

Data from the RNAseq study was then ingested into Qiagen's Ingenuity Pathways Analysis (IPA) software for *in silico* canonical pathway and upstream regulator analysis. We elected to use significance cutoffs of FDR ≤ 0.05 and fold-changes ≥ 1.5 or ≤ -1.5 to limit the number of genes used in the analysis. These cutoffs resulted in 1360, 5480, 169, and 3015 differentially expressed genes being considered for analysis of 1nM *at*RA, 100nM *at*RA, 1000nM DX314, and 1000nM DX314 + 1nM *at*RA, respectively. As per the recommendations, the pathway regulator predictions by IPA were considered significant if the Fisher's exact p-value was ≤ 0.05, and the z-score was ≥ 2.0 (predicted activation) or ≤ -2.0 (predicted inhibition).

The results of IPA's upstream regulator analysis were filtered to only include "genes, RNA, proteins, and endogenous chemicals", then sorted by overall |z-score| (Figure 2.11, left). As expected, the regulator with largest predicted activation was *at*RA (tretinoin), and the predicted activation scores displayed a pattern consistent with a potentiation of low-dose *at*RA by DX314 (i.e. there is no significant activation by DX314 alone, while DX314 with *at*RA results in a score exceeding that of *at*RA alone). Of the top 20 scoring regulators, only three weakly displayed any predicted activity by DX314 alone suggesting minimal effects by DX314 in the absence of *at*RA.

Canonical pathway analysis (Figure 2.11, right) found the overall most activated ("Integrin Signaling") and inhibited ("RhoGDI Signaling") pathways both display activation score patterns which suggest a potentiation of low-dose *at*RA by DX314.

Diagrams of these two signaling pathways, as well as the "RAR activation" pathway for each treatment can be found in the supplemental data (Supplemental Figure 1, Supplemental Figure 2, Supplemental Figure 3). Only a single pathway ("Neuroprotective Role of THOP1 in Alzheimer's Disease") was found to be modulated by DX314 alone, however the effect was weak with the z-score (= 2.0) just meeting the recommended cutoff threshold for significance.

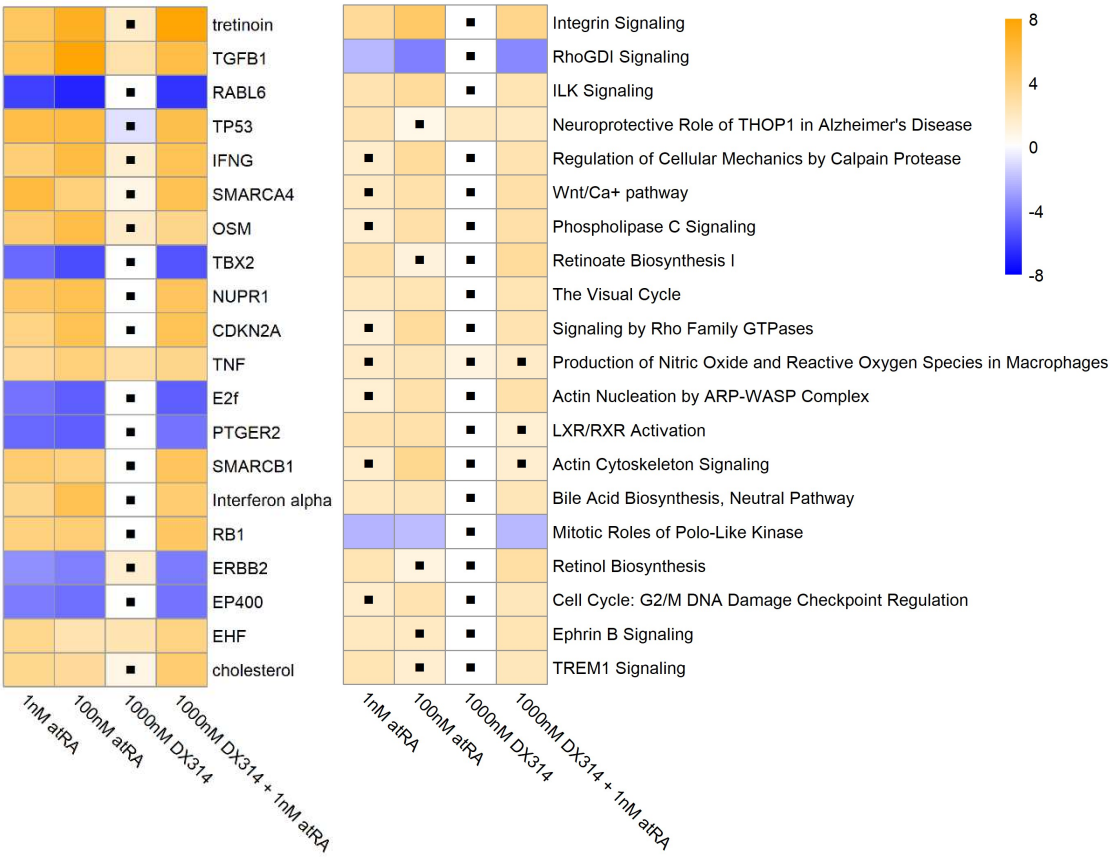

Figure 2.11: Pathway analysis of RNAseq profiles. (left) The top 20 highest scoring upstream regulators (including; genes, RNA, proteins, and endogenous chemicals) as predicted by IPA. (right) The top 20 highest scoring canonical pathways predicted by IPA. A positive z-score (orange) predicts activation, while a negative z-score (blue) predicts inhibition. A black dot indicates scores that did not meet the threshold for significance ($|z\text{-score}| \geq 2$).

2.4 DISCUSSION

Retinoids are well-established therapeutics for the treatment of many skin diseases[43,60,64]. Despite their efficacy, their use can often lead to adverse reactions in patients due to undesirable activity exacerbated by autoinduction of its metabolism and tolerance[58,150]. A strategy involving the use of RAMBAs, which target the RA-inactivating CYP26 enzyme, was developed to address these issues. Although preclinical studies and clinical trials did show their potential in treating certain skin disorders[41,88,112,121,151,89–91,107–111], first-generation RAMBAs such as liarozole, have not progressed past clinical trials, likely due to off-target activity[106]. Consequently, there remains a strong interest in highly selective RAMBAs, with low risk of adverse events, that could address the downsides of current treatments.

Here, we show our novel CYP26B1-selective RAMBA, DX314, can potentiate the effects of low-dose *at*RA in healthy RHE. We investigated the effects of *at*RA on several retinoid-responsive genes compared to DX314 or liarozole, when treated with, or without *at*RA at a nanomolar concentration (Figure 2.2). We confirmed an increase in HBEGF, CYP26A1, and CYP26B1 mRNA expression by *at*RA. Although the effect on IVL expression was less robust, we did see a significant increase in IVL expression by *at*RA at a dose of 100nM. Our experiments also show that, when used alone, neither RAMBA had a significant effect on the expression of these genes at any dose. DX314 was able to significantly potentiate *at*RA's effects on HBEGF, IVL, CYP26A1, and CYP26B1 expression. Liarozole with *at*RA was only able to significantly alter the expression of HBEGF and CYP26A1. Immunostaining confirms the effects of DX314 and *at*RA on IVL

localization (Figure 2.3), however CYP26A1 and CYP26B1 staining (Figure 2.4) was found to be irregular and not reflect mRNA expression. Because this anomaly has been previously reported in *in vivo* and *in vitro* studies of healthy and ichthyotic skin, we do not believe it conflicts with our conclusions[111,138,139].

In the initial experiments, replicates were done using RHE grown from different donors. This study design ensured that any observed effects must be robust enough not be overly sensitive to inter-individual differences, however, this also resulted in large variances across independent experimental runs.

For the design of the second series of experiments we chose to study DX314 and *at*RA in RHE using RNAseq and a single, independent source of primary keratinocytes for all replicates. This experiment confirmed the expression effects of *at*RA, the lack of effect with DX314 alone, and the *at*RA potentiating effect of DX314 on HBEGF, IVL, CYP26A1 and CYP26B1 expression (Figure 2.5). This experiment also allowed us to investigate the effects on many other genes of interest of which the overwhelming majority supported the *at*RA potentiation hypothesis. We observed this pattern in genes regulated by both direct (RARE-containing promotor), and indirect RA pathways. Based on these results, we conclude that DX314 can potentiate the effects of nanomolar *at*RA by inhibiting the metabolism of RA.

TEER is a useful method of assessing epidermal barrier integrity *in vitro*. Surprisingly, we found that RHE treated with 1000nM DX314 displayed a significant increase in TEER compared to control, and unlike liarozole or talarozole, no decrease in TEER when cotreated with low-dose *at*RA (Figure 2.5). Despite *at*RA robustly decreasing

TEER, and DX314 otherwise appearing to potentiate the gene expression effects of *at*RA, we did not observe deterioration of barrier function in RHE dosed with a cotreatment of DX314 and *at*RA. Replication studies of these TEER effects were inconclusive due to instrument limitations (Figure 2.7a), however, we believe the trends observed in the data show a pattern consistent with the previous observations. Morphologically, DX314 treated RHE appear to show significantly less disruption of the SG and KGs, and display an overall healthy appearance compared to high dose *at*RA or liarozole treated groups (Figure 2.8, Figure 2.9). We also found minimal changes in the expression of many corneal layer precursor transcripts within the EDC (Figure 2.10), despite a large decrease in expression by high-dose *at*RA, and most retinoid-responsive genes showing DX314 potentiating *at*RA's effects on gene expression. Whether or not DX314 does protect the skin barrier, while also retaining the therapeutic benefits of retinoids, remains to be seen and we cannot make a conclusive statement based solely on this study, however, we believe the observations made certainly merit further investigation. Additional *in vitro* and *in vivo* studies utilizing alternative measures of barrier integrity and function may provide additional insight into these unique observations.

Finally, we present the activity of upstream regulators (Figure 2.11, left) and canonical pathways (Figure 2.11, right) as predicted by IPA software. The top scoring upstream regulator was *at*RA (i.e. tretinoin) which showed an activation z-score of 5.04 and 6.90 for 1 and 100nM *at*RA, respectively. DX314 alone scored below the significance threshold at 1.70, but when cotreated with 1nM *at*RA scored 7.94. This result strongly suggests DX314 alone does not significantly affect known RA pathways, but potently

potentiates the effects of *at*RA in cotreated conditions. 16 of the top 20 scoring upstream regulators, and 14 of the top 20 scoring canonical pathways showed DX314 with low-dose *at*RA as having an absolute z-score larger than low-dose *at*RA alone. Overall, these results, in conjunction with the previously discussed data, provide further evidence of DX314's ability to potentiate the effects of nanomolar *at*RA.

We conclude that the results presented in this study show strong evidence that DX314, which is known to inhibit the RA-metabolizing enzyme CYP26B1, potentiates the effects of *at*RA in healthy RHE. We also show compelling evidence that DX314 may protect from epidermal barrier disruption by retinoids, and strongly believe these observations merit further study.

3. DX314 AS A POTENTIAL THERAPEUTIC IN KERATINIZATION DISORDERS

3.1 INTRODUCTION

Keratinization disorders refer to a class of skin disorders which induce a disruption of normal keratinocyte differentiation (keratinization) and resulting in abnormal skin development and function. In this study, we expand upon our previous research confirming DX314 will potentiate the effects of low-dose *at*RA, with minimal undesirable off-target activity. To determine if these effects will translate from healthy keratinocytes to the potentially unique responses of diseased keratinocytes, we investigated DX314 in two keratinization disorders which have an established clinical history of effective treatment by retinoids.

In the first series of experiments, we grew RHE using keratinocytes donated by a patient with Darier's disease (DD). Although RAMBAs have not specifically been investigated or used for treatment of this disease, retinoids, particularly *13-cis*-RA, have been used as an effective treatment in DD patients[47–49]. If the advantages of RAMBAs can be shown to be as effective as retinoids in DD, implementing their use may improve patients' outcomes and provide more treatment options to their physicians. For the second series of experiments, we studied the effects of DX314 on keratinocytes donated by congenital ichthyosis patients. The subtypes investigated in this study include two recessive x-linked ichthyosis (RXLI) donors (herein referred to as RXLI-1653 and RXLI-1658), and one lamellar ichthyosis (LI) donor (LI-173).

3.1 METHODS

3.1.1 PRIMARY HUMAN KERATINOCYTES

Darier's disease keratinocytes (DARK1) from a male child were donated to the project by our collaborator Dr. Yves Poumay at the University of Namur, Belgium. Recessive x-linked ichthyosis (RXLI) and lamellar ichthyosis (LI) keratinocytes were provided by Dr. Amy Paller at Northwestern University, Illinois. Keratinocytes from three ichthyosis patient donors were used in this study: RXLI-1653 (29yo, male), RXLI-1658 (13yo, male), and LI-173 (details not provided).

3.1.2 CELL CULTURE

Refer to Section 2.2.2.

3.1.2.1 MONOLAYER AUTOCRINE KERATINOCYTES

Culture of monolayer RXLI keratinocytes was performed by the Paller lab and is adapted from a method described by Poumay et al.[123]. In short, 25,000-50,000 keratinocytes (prepared as described in Section 2.2.2) are seeded in 6-well cell culture plates containing 2mL of Epilife Complete and placed in a 37°C, 5% CO_2, humidified incubator. The media is changed every two days until ~60% confluent, at which point the media is replaced with Epilife Autocrine (Epilife media, 0.5% P/S, 0.5µM hydrocortisone, 240µM L-histidine, 750µM L-isoleucine, 90µM L-methionine, 90µM L-phenylalanine, 45µM L-tryptophan, 75µM L-tyrosine), which does not contain any HKGS, for the remainder of the experiment. This autocrine formula allows for the investigation of epidermal differentiation markers, which can otherwise be affected by growth factors present in non-autocrine media, using monolayer keratinocyte cultures. The keratinocytes

continue to proliferate in autocrine conditions, and the media changed every two days, until 100% confluent. Once all the wells in an experimental group reach confluence, treatments are added to fresh Epilife Autocrine (final concentration of 0.1% DMSO as vehicle), applied to each well, and allowed to incubate for 20hrs. After the 20hr treatment, the media is aspirated from each well and 500µL of TRIzol (Thermo, 15596-018) is immediately added. The cells are homogenized, and the lysate is flash frozen at -80°C until shipped to us on dry ice for RNA isolation.

3.1.2.2 RECONSTRUCTED HUMAN EPIDERMIS

Refer to Section 2.2.2.1.

3.1.2.3 ORGANOTYPIC RAFTS

Organotypic rafts were grown by collaborators at the Paller Lab (Northwestern University) using a previously described protocol[152]. The protocol here is described per raft so all components were scaled according to the number of rafts within each experiment. For each raft, 4e5 J2-3T3 fibroblasts are suspended in 150µL of 10x reconstitution buffer (22µg/mL NaHCO3, 46µg/mL HEPES in 0.05N NaOH then 0.2µm sterile filtered). On ice, 150µL of 10x DMEM is then added, followed by 6mg of rat tail collagen I (BD, 354249), which is rocked gently until color changes to yellow indicating the solution is acidic. We then add 0.5N NaOH until the pH becomes neutral and the solution is brought up to 1.5mL (per raft) with sterile ddH2O. 1.5mL of the collagen suspension is added to a well of a 12-well plate and placed in a 37°C incubator for 30min to polymerize, after which an additional 3mL of media is added to the top of each plug. This is then incubated at 37°C for at least 24hrs before keratinocytes can be added. After 1-4 days, media is removed from

each plug and replaced with 1mL of E media [180µM adenine (Signa, A2786), 5µg/mL human recombinant insulin (VWR, 91077C), 5µg/mL human apo-transferrin (Sigma, T1147), 5µg/mL triiodothyronine T3 (Sigma, T6397), 0.25µg/mL Amphotericin B (Cellgro, 30003CF), 4nM L-glutamine (Sigma, G7513), 0.4µg/mL hydrocortisone (Sigma, H0888), 10ng/mL Cholera toxin (Sigma, C8052), 5% FBS (Fisher, SV30014.03), in 1:1 mix of DMEM HG (Sigma, D5671): DMEM/F-12 (Sigma, D6421)] supplemented with 5ng/mL EGF. For each raft, suspend 6e5 keratinocytes in 1mL E media + 5ng/mL EGF and add this suspension to the top of a collagen plug. The media is refreshed after 24hrs. After two days, a sterile spatula is used to transfer each raft to the top of a sterile metal grid in a 60mm plate. Enough media is added so that only the bottom of the raft is submerged, and an air-tissue interface is established on the surface (~4-5mL). The rafts are placed in an incubator and media is maintained every two days until the experiment is complete. As with the RHE, treatments (0.1% DMSO vehicle) are done over four days and refreshed after two days. Rafts intended for RNA isolation are then lysed in 500µL TRIzol and stored at -80°C until shipped to us on dry ice for RNA isolation.

3.1.3 TEWL

Refer to Section 2.2.3.

3.1.4 TEER

Refer to Section 2.2.4.

3.1.5 HISTOLOGY & IMMUNOSTAINING

Refer to Section 2.2.5.

3.1.6 DIFFERENTIAL GENE EXPRESSION

3.1.6.1 RNA ISOLATION

Isolation of RNA from RHE groups was performed as described in Section 2.2.6.1.

RNA obtained from monolayer and organotypic raft cultures were isolated using TRIzol (phenol-chloroform extraction) as described by the manufacturer. Variations from the standard protocol include chilling the sample following the addition of isopropanol to encourage nucleic acid precipitation, and the addition of a second chilled 75% ethanol wash prior to drying the pellet, which greatly improved consistency in RNA purity.

3.1.6.2 RT QPCR

DD RHE study was performed as described above (Section 3.1.6.2) Remaining groups in this study were done with several variations from the previously described method which are described here:

A 10µL reverse transcription was done with 100-200ng of template RNA using qScript cDNA Supermix (QuantaBio, 95048) with the following incubations: 5min 25°C, 30min 42°C, 5min 85°C. The cDNA was then diluted 1:10 with water and 2µL was added to a 10µL real-time qPCR reaction, which used PerfeCTa SYBR Green Supermix, Low-ROX (QuantaBio, 95056) on a Stratagene Mx3005P (Agilent Technologies) or CFX384 (Bio-Rad). Program is as follows (40 cycles): 30sec 95°C, 60sec 60°C, 60sec 72°C. Statistical analysis was done by one-way ANOVA with Dunnett's correction for multiple comparisons on the standardized (DD RHE), or raw dCt (remaining experimental groups), values using GraphPad Prism 6. Primers can be found above (Table 2.3).

3.2 RESULTS

3.2.1 DX314 IN DARIER'S DISEASE RHE

DD RHE were investigated by the same experimental methodologies used for the previously described healthy RHE studies (Section 0). As expected, *at*RA treatment produced an increase in HBEGF and CYP26A1 gene expression, and a decrease in KRT10 expression (Figure 3.1). The potent RAMBA talarozole significantly potentiated the effects of all genes analyzed, at all doses studied. DX314 was able to significantly potentiate effects of *at*RA on both KRT10 and CYP26A1 expression. However, despite indicating a higher average fold-change in HBEGF gene expression, RHE treated by DX314 with low-dose *at*RA did not reach the predefined threshold for statistical significance. Due to the precious nature of the DD keratinocytes, we were limited in the number of replicates which could be used for qPCR analysis which resulted in low statistical power. This small sample size likely explains the lack of a statistically significant change in HBEGF expression despite a significant modulation of this gene observed in our previous studies.

Histological analysis shows a*t*RA inducing robust morphological changes in DD RHE (Figure 3.2, left column) which reflected those seen in healthy RHE (Figure 2.8). RHE treated with a*t*RA showed a dramatic loss of the SB (and KGs typically contained within), denucleation and flattening of SS keratinocytes, and an overall unhealthy appearance. When treated alone, DX314 and talarozole showed no major morphological changes, however addition of nanomolar *at*RA shifted the appearance, most notably the SG/KG, to more closely resemble high dose *at*RA. Visualization of FLG localization (Figure 3.2, middle left column) shows, as we would expect, expression largely isolated to

the granular and corneal layers of the epidermis. Treatment with *at*RA results in a decrease in FLG staining relative to control. Talarozole alone displays similar FLG staining to control, while talarozole with *at*RA shows expression levels resembling high dose *at*RA. Conversely, DX314 appears to display significantly increased FLG relative to control, an observation which may contribute to the increase in TEER seen in the DX314-treated RHE from our previous study (Section 2.3.2). DX314 with 1nM *at*RA shows FLG levels mimicking those of high dose *at*RA which suggests DX314 is potentiating the effect of *at*RA on FLG staining. KRT14, a cytokeratin typically isolated to basal keratinocytes, shows decreased staining following *at*RA treatment, no significant change following treatment by DX314 or talarozole, and diminished expression when RAMBAs are cotreated with *at*RA (Figure 3.2, middle column). Finally, KRT10, a commonly used marker of epidermal differentiation typically localized within the suprabasal epidermis, shows delayed expression in *at*RA treated RHE. This seen as an apparent migration of KRT10 staining away from the lower layers, and more isolated to the apical layers of the epidermis (Figure 3.2, middle right column). When treated alone, the RAMBAs studied here show no change in KRT10 localization relative to control, however, when cotreated with low dose *at*RA, staining is diminished in the lower layers and only seen in the more apical layers. Overall, this study of DD RHE histology presents compelling evidence that DX314 potentiates the effects *at*RA and does so in a manner comparable to the well-studied RAMBA talarozole.

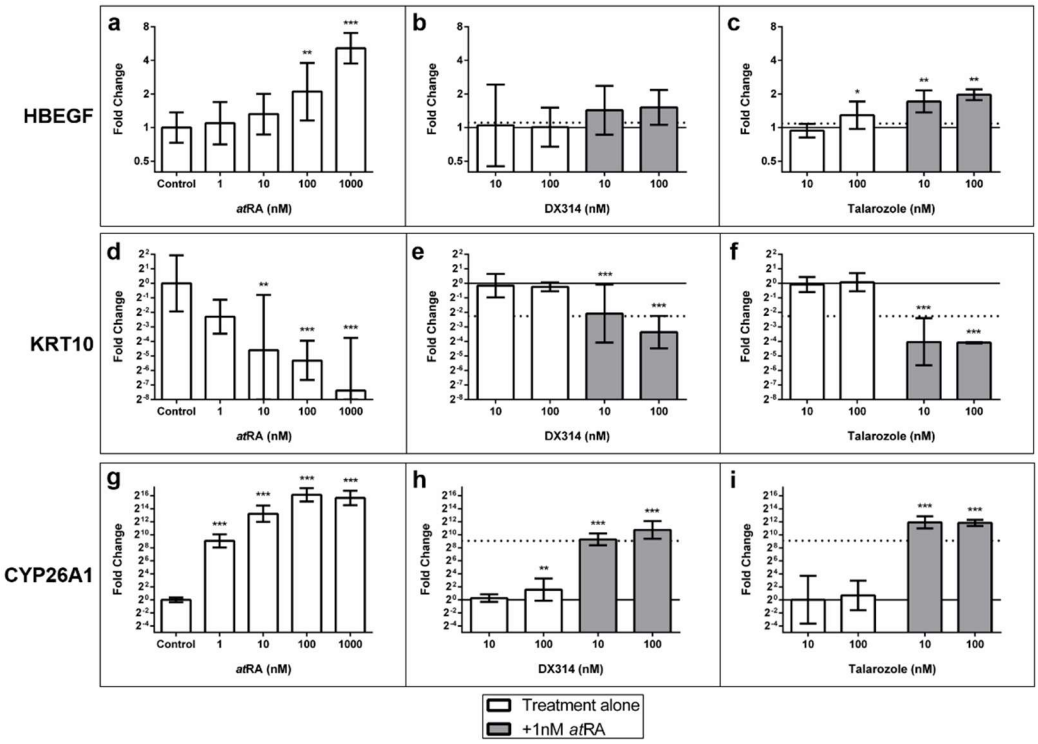

Figure 3.1: Gene expression in DD RHE treated with *at*RA, RAMBAs. Differential expression of HBEGF (a-c), KRT10 (d-f), and CYP26A1 (g-i) transcripts after 4-day treatment with *at*RA or RAMBAs, with (grey bars), and without (white bars), 1nM *at*RA. Solid line shows control and dotted line shows 1nM *at*RA RHE. Significant changes vs control determined by one-way ANOVA with Dunnett's multiple comparisons correction on autoscaled values. *p≤0.05; **p≤0.01; ***p≤0.001. Graphs show mean ± 95% CI. n = 3 per treatment. Note: CYP26A1 control showed no detectible signal after 40 cycles so a target Ct of 40 was assigned to any undetected samples.

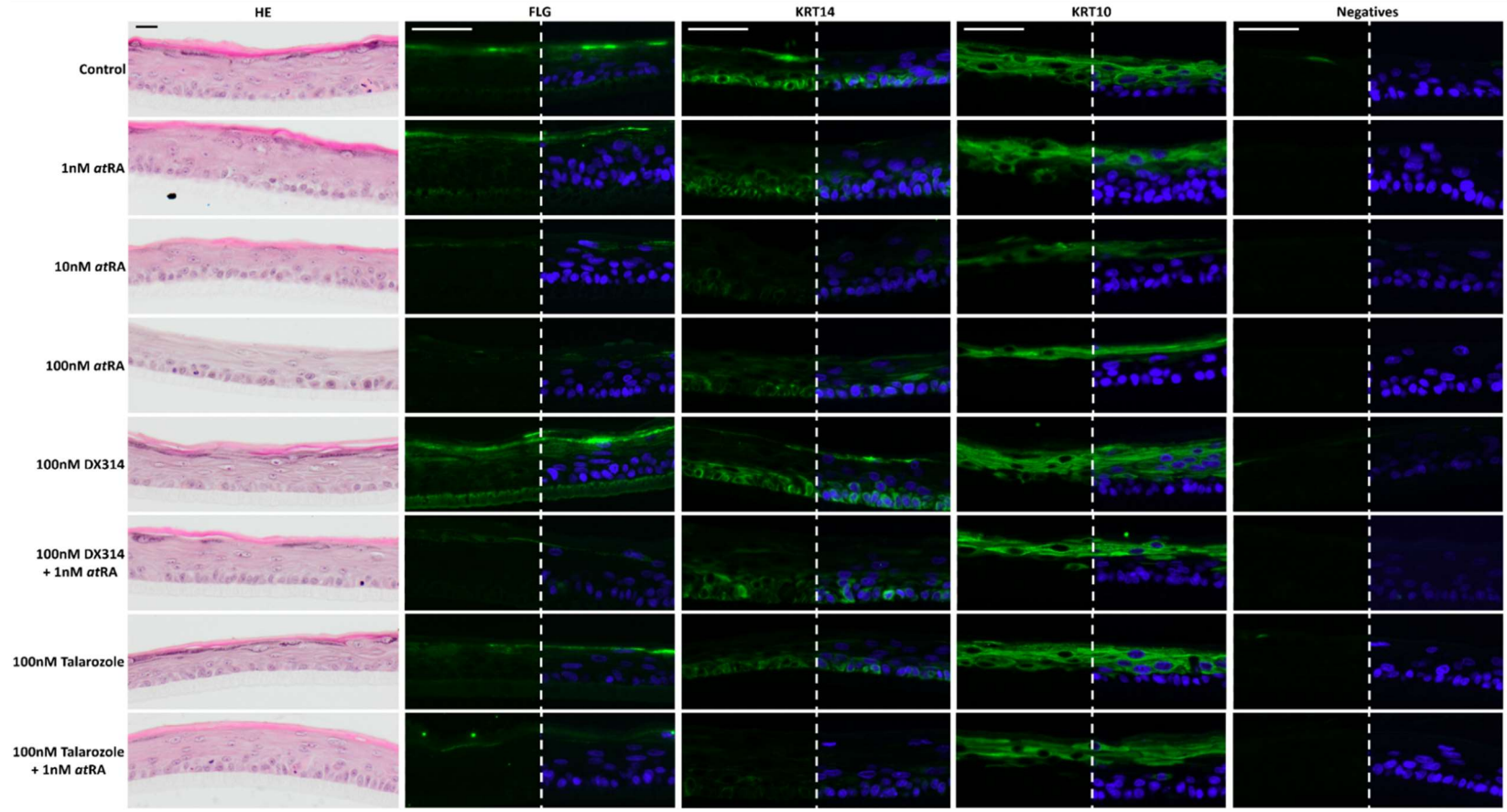

Figure 3.2: Histology of Darier's disease RHE treated with *at*RA, RAMBAs. HE (left), FLG (middle left), KRT14 (middle), KRT10 (middle right), and negative controls (right) are shown here. Left side of the tissue shows target protein (green) alone, left side of tissue shows cellular nuclei (blue) stain overlaid with target. Black scale bar = 20µm, white scale bar = 50 µm).

3.2.2 DX314 IN ICHTHYOTIC KERATINOCYTE CULTURES AND 3D EPIDERMIS

Recessive X-linked ichthyosis (RXLI-1658) patient keratinocytes were grown in monolayer cultures and differentiated under autocrine conditions. Cultures were treated for 20hrs with *at*RA or RAMBAs (DX314 or liarozole) with, and without, *at*RA cotreatment before RNA was extracted for subsequent RT-qPCR. RXLI-1658 monolayer cultures showed DX314 (100 and 1000nM doses) and liarozole (all doses) can potentiate the effect of 1nM *at*RA on the expression HBEGF and CYP26A1 (Figure 3.3) transcripts. DX314 only appeared to potentiate *at*RA's effect on KRT10 and FLG gene expression at the highest doses tested, however, we also found that 10nM DX314 alone increases their expression. This subtle, but significant, increase likely lessens the decrease in expression we would expect when inhibiting *at*RA metabolism. This may explain why only the highest DX314 dose displayed gene expression changes exceeding those of 1nM *at*RA alone.

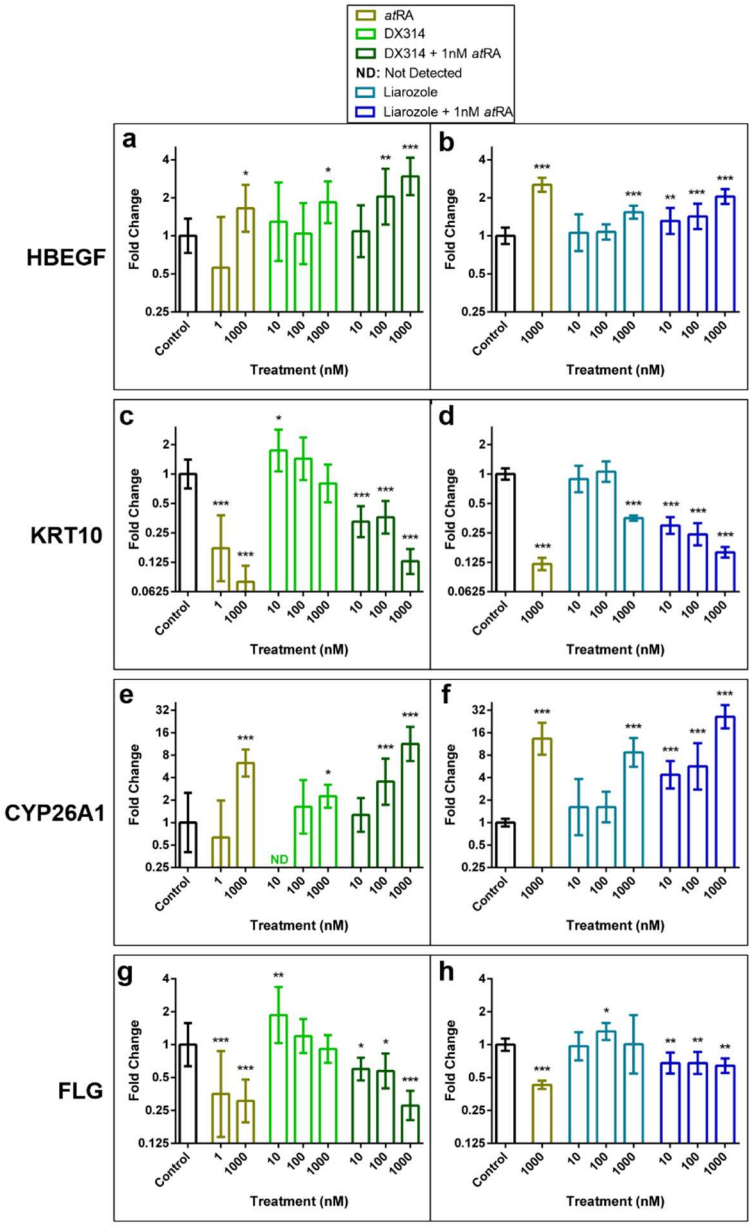

Figure 3.3: Gene expression effects in RXLI-1658 keratinocyte cultures. Keratinocytes from a patient with recessive x-linked ichthyosis (RXLI) were grown to confluence in autocrine conditions and exposed to a 20hr treatment before RT-qPCR was performed. Expression of HBEGF, KRT10, CYP26A1, and FLG genes are shown. Significant changes in expression vs control was determined by one-way ANOVA with Dunnett's correction for multiple comparisons on dCt values. *p≤0.05; **p≤0.01; ***p≤0.001. n = 3. Bars show mean ± 95% CI.

To investigate how DX314 would perform in RXLI organotypic skin models, rafts were grown using RXLI-1653 keratinocytes which were given a 4-day drug treatment before RT-qPCR was performed on the isolated RNA. Consistently with our previous studies, *at*RA induced an increase in HBEGF and CYP26A1 gene expression (Figure 3.4).

Contrarily to our previous observations, DX314 and liarozole appeared to slightly increase HBEGF gene expression in the absence of *at*RA. This unexpected effect was also seen on the expression of CYP26A1 transcripts when the rafts were treated with liarozole, but not DX314. However, when cotreated with low dose *at*RA, an unmistakable potentiating effect was still seen by both RAMBAs in both genes.

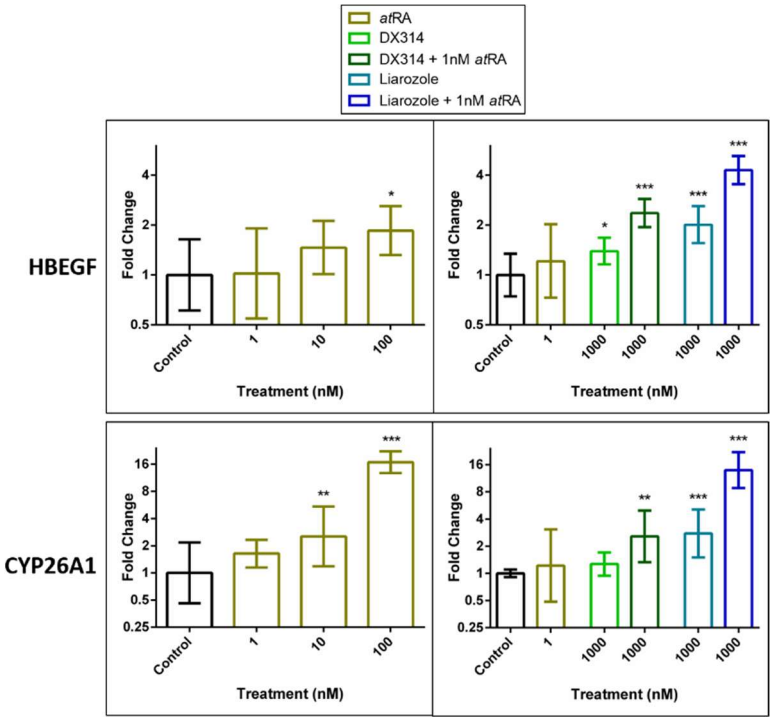

Figure 3.4: Gene expression in RXLI-1653 organotypic rafts. Rafts grown with keratinocytes from an RXLI patient were treated for 4-days. Expression of HBEGF and CYP26A1 genes was measured by RT-qPCR. Significant expression changes vs control was determined by one-way ANOVA with Dunnett's correction for multiple comparisons on dCt values. *p≤0.05; **p≤0.01; ***p≤0.001. n = 3 per treatment. Bars show mean ± 95% CI.

Our final study of DX314 in diseased keratinocytes was performed in RHE grown with lamellar ichthyotic (LI) donor keratinocytes. We analyzed the expression of several of the retinoid-responsive genes we had previously studied. As expected, CYP26A1, CYP26B1, HBEGF, and KRT10 transcripts displayed a change in expression by *at*RA (Figure 3.5). In agreement with our immunolabeling of DD RHE (Figure 3.2), *at*RA treatment decreased KRT14 mRNA expression in the LI RHE. Stimulated by retinoic acid-6 (STRA6), a gene with a strong RARE-mediated response to RA treatment, also saw a robust increase in expression by *at*RA. Expression of TGM-1, a transglutaminase responsible for cross-linking the structural proteins of the cornified envelope, was decreased by *at*RA. In all the genes investigated here, 1000nM DX314 alone had no effect on gene expression, however, unlike our previous studies, only CYP26A1 and STRA6 showed expression patterns suggesting a potentiation of low dose *at*RA by DX314. The effects of DX314 with lose-dose *at*RA do not appear to be significantly different from low dose a*t*RA alone for CYP26B1, HBEGF, TGM1 or KRT14 expression.

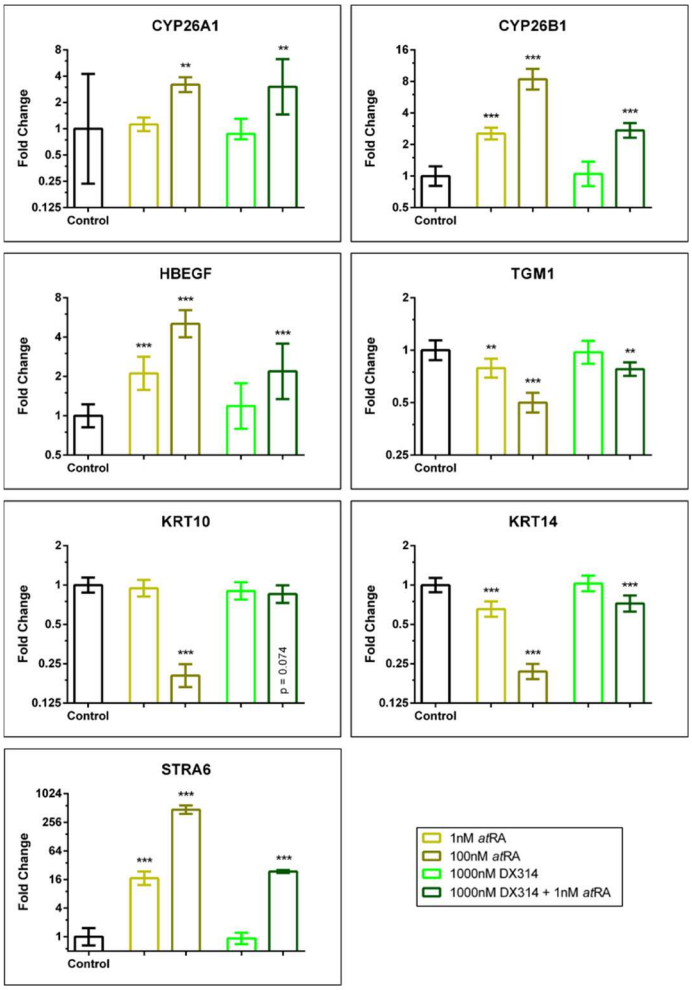

Figure 3.5: qPCR of LI-173 RHE treated with DX314, atRA. RHE were treated for 4 days before measuring relative changes in expression of several genes of interest by RT-qPCR. Significant expression changes vs control was determined by one-way ANOVA with Dunnett's correction for multiple comparisons on dCt values. *p≤0.05; **p≤0.01; ***p≤0.001. n = 3 per treatment. Bars show mean ± 95% CI.

In the same study of LI RHE, we concurrently investigated the effect treatments on TEER and TEWL to their effects on epidermal barrier integrity. As we originally discovered in healthy RHE (Figure 2.6), we see *at*RA decreased TEER, while DX314 independently increased TEER and mitigates *at*RA's effect on TEER when cotreated (Figure 3.6a). As a secondary measure of barrier function, we also measured the TEWL of the RHE following the 4-day treatment. In support of our TEER observations, we find *at*RA induces a robust effect on this measure of barrier function, however, we did not find that DX314 had any significant effect on TEWL, nor did it mitigate the effects of low-dose

*at*RA in cotreatment conditions (Figure 3.6b). Finally, since we simultaneously measured both TEER and TEWL on the same RHE, we analyzed the two metrics together to see if there exists a correlation between the two measures of barrier function. We show that, within the range of the TEER and TEWL values of these RHE, there exists an inverse linear relationship between the two, and each treatment tends to cluster with its replicates (Figure 3.6c).

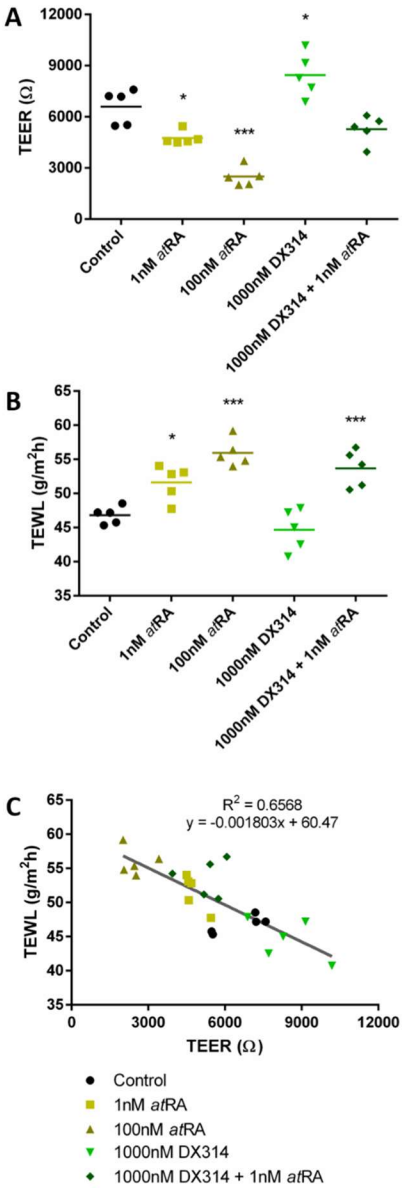

Figure 3.6: TEER and TEWL of LI RHE treated with DX314, atRA. Raw, post-treatment TEER (a), TEWL (b), and the linear correlation between the two (c) following treatment. Significant changes vs control determined by one-way ANOVA with Dunnett's correction for multiple comparisons. *p≤0.05; **p≤0.01; ***p≤0.001. n = 5 per treatment.

Investigating the treatment effects on RHE tissue morphology shows LI RHE reacting to a*t*RA and DX314 in a manner nearly identical to the changes seen in our studies of healthy and DD RHE. High dose *at*RA leads to a significant reduction in SG thickness and KG presence and displays an overall unhealthy appearance (Figure 3.7). RHE treated with DX314 with, and without low dose *at*RA, show minimal histological changes relative to control, although there does appear to be a slightly more continuous presence of KG across the SG.

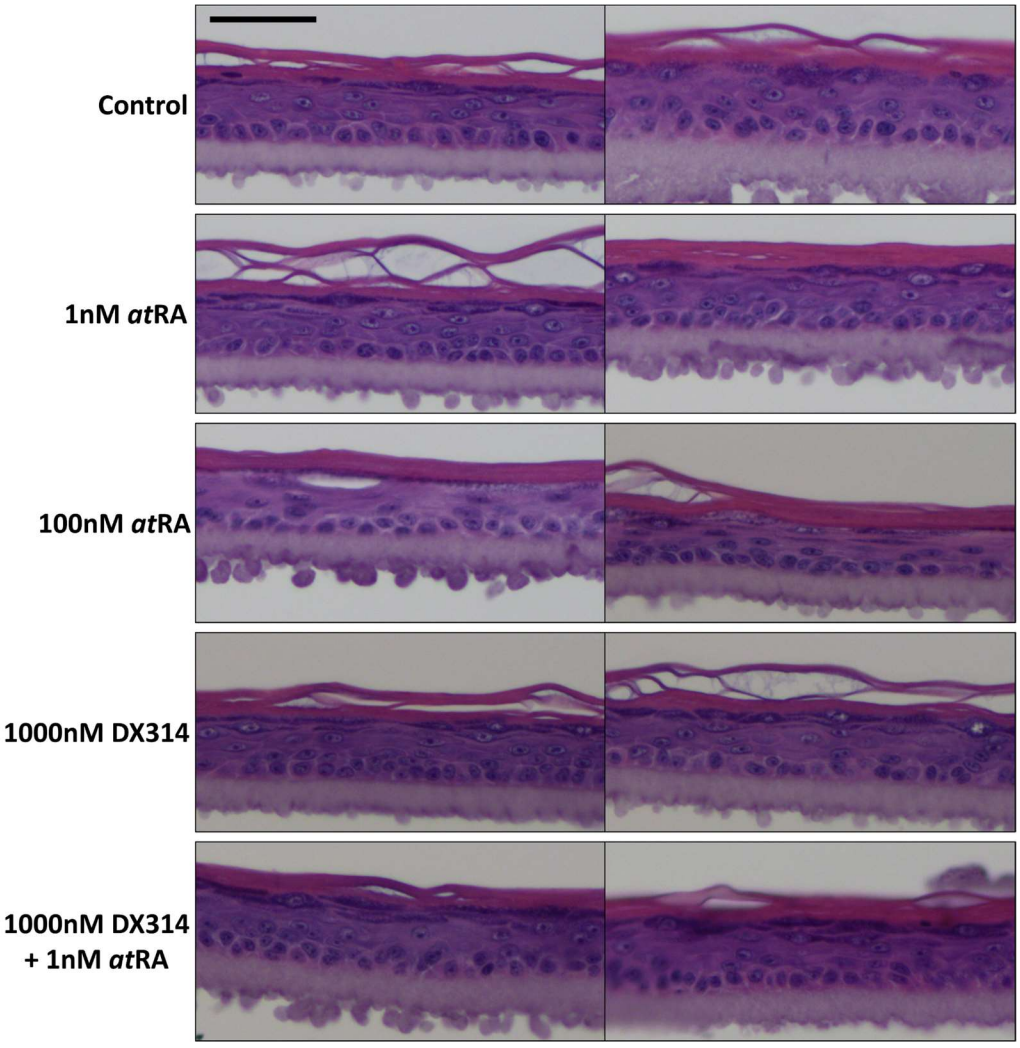

Figure 3.7: Morphology of LI RHE treated with DX314, atRA. HE stained LI RHE treated for 4 days with *at*RA or DX314, with, and without low dose *at*RA.

3.3 DISCUSSION

Darier's disease (DD) and congenital ichthyosis are keratinization disorders with a well-established history of effective treatment by retinoid-based therapies[41,45,47,48,50,88]. As previously discussed, excessive retinoid use often results in adverse effects and drug tolerance despite their proven efficacy. In this series of experiments, we expand upon the work done in our previous studies which show DX314's effects in healthy *in vitro* RHE. With the help of two of our collaborators, we investigated whether DX314 can also mimic the desirable effects of proven therapies in diseased keratinocytes.

In the DD portion of this study, *at*RA treatment resulted in an increase (HBEGF, CYP26A1), or decrease (KRT10), in gene expression consistent with our hypothesis (Figure 3.1). DX314, as well as the potent RAMBA talarozole, were able to significantly potentiate the effects of a low dose *at*RA cotreatment on the gene expression of KRT10 and CYP26A1. Statistically speaking, the expression of HBEGF was only significantly modified by talarozole, however, we do not believe the effect of DX314 should be discounted despite the lack of statistical significance. Due to the rarity of DD, sourcing additional donors is quite difficult, and the necessarily low number of cellular passages required for quality RHE limited the number of replicates possible. These limitations led this experiment to have inadequate statistical power considering the relatively small effect size of the treatments on HBEGF expression. Considering the mean change in HBEGF expression in this experiment is consistent with expectations and our multiple previous studies showing DX314 potentiating the effect of *at*RA its expression, we suggest these results are still in support of our overarching hypothesis.

Histological imaging shows DD RHE having distinct morphological differences compared to healthy RHE (Figure 3.8). We can see that DD RHE lack the columnar keratinocytes characteristic of the SB, have a greatly diminished SG, increased acantholysis (intercellular gaps due to poor cell-cell adhesion), and the presence of corps rond (abnormal keratinocyte, red circle) which are characteristic traits of DD epidermis *in vivo*[45]. This study found that DD RHE morphology is affected by the treatments in a nearly identical manner to our previous studies of healthy RHE. Treatment with a*t*RA caused a loss of the SG, a reduction in epidermal thickness, and denucleation of the SS (Figure 3.2, left column). Both DX314 and talarozole show no significant histological effect alone, however, low-dose *at*RA cotreatment results in the tissue morphology mimicking high-dose *at*RA treated RHE.

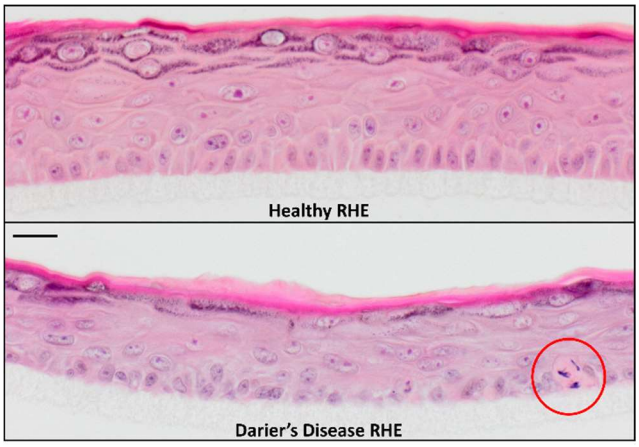

Figure 3.8: RHE grown with healthy (top) or DD (bottom) keratinocytes. Red circle shows a corps rond (round body) keratinocyte, commonly found in DD epidermis. Scale bar = 20µm.

As we would expect, FLG staining correlated with the loss of SG by *at*RA, and as such, also supports a potentiation of *at*RA by RAMBAs, however, we also found that DX314 appears to independently increase the prevalence of FLG (Figure 3.2, middle left column). We did not initially expect this, however FLG's critical role in tight junction formation within the SG may contribute to, and partially explain, DX314's previously

described ability to increase TEER (Figure 2.7, Figure 3.6). Although we did not investigate KRT14 gene expression in DD RHE, we know it to be controlled by RAREs[153] and our previous study showed KRT14 downregulated by *at*RA in healthy RHE (Figure 2.5). For these reasons, we investigated KRT14 localization in DD RHE and found that *at*RA does induce a decrease in KRT14 staining, RAMBAs alone show no significant effect, and RAMBAs cotreated with *at*RA show a decrease in staining (Figure 3.2, middle column). KRT10 is not directly controlled by RAR as it does not contain a RARE promotor, however, its expression is well established as a marker of keratinocyte differentiation and highly sensitive to retinoid treatment. We found KRT10 localization in the control and RAMBA alone groups to begin just above the basal layer keratinocytes and continue into the upper layers of the epidermis (Figure 3.2, middle right column). When treated with *at*RA, or RAMBAs with low-dose *at*RA, we observe a shift in KRT10 localization to only the upper layers of the epidermis with significantly reduced staining in the SS. Additionally, this reduction in KRT10 staining by the treatments is consistent with the observed decrease in KRT10 mRNA expression (Figure 3.1). These studies show the effects observed in healthy RHE are translatable to DD RHE, and that DX314 also potentiates low dose *at*RA in this disease. Together this suggests DX314 may have potential as an effective treatment strategy for Darier's disease patients.

In the congenital ichthyosis portion of this study, we investigated the effects of *at*RA and DX314 in various *in vitro* experiments using keratinocytes donated by two recessive X-linked ichthyosis (RXLI) patients and a lamellar ichthyosis (LI) patient. Investigation of gene expression changes after a 20hr treatment of differentiated monolayer

RXLI-1658 keratinocytes shows DX314, as well as liarozole, potentiating the effects of low-dose *at*RA on HBEGF, KRT10, CYP26A1, and FLG gene expression (Figure 3.3). We did, however, only observe a significant potentiation of HBEGF and CYP26A1 expression at 100nM and 1000nM DX314, while KRT10 and FLG expression were only potentiated with a 1000nM dose. Surprisingly, we also found 1000nM DX314 and 1000nM liarozole independently increasing HBEGF and CYP26A1 expression in the absence of *at*RA cotreatment. This observation is inconsistent with our previous studies which did not see any such effect by RAMBAs alone. It is possible that this is the result of a unique property of monolayer cultures, which is not seen in 3D epidermis; however, we believe it is more likely that a sub-nanomolar concentration of a*t*RA, or a RA precursor, was present in the media of those samples, and was subsequently potentiated by each RAMBA. We also see that 10nM DX314 appears to increase KRT10 and FLG gene expression. Although this increase in structural proteins may be partially contribute to the increase in barrier function previously described, we did not observe an effect on these genes in DD RHE, or in the previous RNAseq study of healthy RHE, so it is likely that this effect is specific to monolayer cultures and does not translate to the 3D epidermis models which better reflect *in vivo* conditions.

Our investigation of RXLI-1653 organotypic rafts also show HBEGF and CYP26A1 gene expression was increased by a*t*RA treatment (Figure 3.4). We also show that both DX314 and liarozole at 1000nM potentiate the effects of low dose *at*RA on these genes together reinforcing our hypothesis. Despite this, we again observe that 1000nM DX314 has a subtle effect on HBEGF expression, while 1000nM liarozole shows a robust

effect on both genes in the absence of *at*RA. These RXLI rafts, as well as the previous RXLI monolayer studies, were performed in unison, so it is possible that the discrepancies of both can be explained by a presence of retinoids in the media, as previously suggested. Replication of these studies was not possible within the timeframe of this dissertation; however, additional experiments have already begun and should help determine if this is indeed a possibility.

Finally, we investigated the gene expression and barrier effects of DX314 in LI-173 RHE. As predicted, gene expression analysis shows an effect by *at*RA, and no effect by DX314 alone on all genes investigated (Figure 3.5). We confirm DX314 potentiates the effects of low-dose *at*RA on the RARE-promoted CYP26A1 and STRA6 genes, however, unlike our previous studies, DX314 was not able to significantly affect the expression of the other genes presented any more than low-dose *at*RA alone. We are unsure as to why these genes were not potentiated by DX314 as we would have expected. It is possible that the genetic differences of this LI donor result in truncated effects relative to the other donors, however, in that case we would expect to be see this reflected in RHE treated with *at*RA alone as well. Another possibility is that RA metabolism in this LI donor has an increased propensity to undergo alternative, compensatory pathways and therefor the specific inhibition of CYP26 does not reduce the inactivation RA enough to affect the expression genes less sensitive to modulation by RA. This may explain why we see the expected effects in CYP26A1 and STRA6 expression, but not the others. Finally, this lack of agreement with previous studies may be significantly more complicated than a single variable can account for and it may be the result of a complicated series of genomic and

non-genomic effects specific to this donor. In any case, we do not believe that this lack of RA potentiation in these specific cases invalidates our general hypothesis. It may merely suggest that, like many other drugs, the efficacy of RAMBAs are subject to interindividual variability and situational differences, meaning they may not universally work in all patients and disorders.

To further gather evidence of the barrier protecting effect of DX314 first observed in our studies of healthy RHE (Section 2.3.2), we measured post-treatment transepithelial electrical resistance (TEER) and trans-epidermal water loss (TEWL). We confirm *at*RA decreases, while DX314 independently increases TEER, suggesting a respective decrease and increase in barrier function, in LI RHE (Figure 3.6a).

We simultaneously investigated the effects treatments have on TEWL which show *at*RA significantly increasing water loss, suggesting a decrease in barrier function (Figure 3.6b). However, our investigation did not find that DX314 had a significant effect on TEWL, nor did it show DX314 mitigating the increase in TEWL by *at*RA. Because water transport across the epidermis is a complicated process, it is possible that changes in TEWL are partially mediated by water transporters such as aquaporins (AQP), rather than a direct reflection of overall barrier integrity. To see if this may be a possibility, we reviewed our previously obtained RNAseq data of healthy RHE. We found three water transporters (AQP3/5/9) were significantly affected by at least one treatment group (Figure 3.9). Notably, we see that all three aquaporins show decreased gene expression in the high dose *at*RA group, AQP3 expression slightly, but significantly, increased in the DX314 group, and AQP3 and AQP5 increased in the DX314 with *at*RA cotreatment RHE. Since altered

expression of AQPs have been correlated with altered TEWL[154,155], a decrease in AQP expression, as seen in high-dose *at*RA, may result in decreased in TEWL. Despite this, we showed high-dose *at*RA significantly increasing TEWL which suggests high-dose *at*RA may disrupt barrier function to a larger extent than the TEWL data alone suggests. More importantly, an increase in AQP expression, as seen in low dose *at*RA, and DX314 with, and without a*t*RA cotreatment, may result in TEWL to increase even if gross barrier function itself is not significantly compromised. This may explain why DX314 did not appear to significantly decrease TEWL, despite appearing to reinforce barrier function in TEER and histological analysis. It should be noted that the AQP expression shown here is from a previous, independent study in healthy RHE, and may not directly translate to the TEWL results of this study. Additionally, we show that there exists an imperfect, but obvious, inverse linear relationship ($R^2 = 0.6568$) between the TEER and TEWL of an RHE (Figure 3.6c). This suggests that, in general, when one measure is altered by an external influence, the other tends to be affected as well.

	AQP3	AQP5	AQP9
1nM atRA	1.19	3.27	-1.11
100nM atRA	-1.38	-4.16	-2.12
1000nM DX314	1.33	1.02	-1.00
1000nM DX314 + 1nM *at*RA	1.61	6.39	-1.15

Figure 3.9: Aquaporins with significant changes in gene expression by DX314, *at*RA. Fold-change in expression of aquaporins (AQP) found to be significantly altered by treatments in healthy RHE by RNAseq. Grey cells indicate non-significant change in expression (significance cutoff: FDR ≤ 0.05)

In summary, these studies of DX314 in diseased keratinocytes show DX314 potentiates the effects of a*t*RA like we previously observed in healthy RHE, however, this was not always the case. DX314 potentiates *at*RA in DD RHE and RXLI organotypic rafts.

In RXLI monolayer cultures, DX314 at higher doses successfully potentiated the effects of low dose *at*RA. Finally, LI RHE did show a DX314 potentiating a*t*RA but only in the expression of certain genes (i.e. CYP26A1, STRA6). Most interestingly, we were able to successfully replicate the barrier reinforcing effects by DX314 first described in our studies of healthy RHE. This indicates that DX314 does in fact display possess some sort of barrier reinforcing property which acts independently of many of the a*t*RA-mediated effects we describe.

We conclude there exists substantial evidence to warrant further investigation into the therapeutic potential of DX314, not only in the treatment of retinoid-responsive skin disorders, but also as a novel therapeutic strategy aimed at protecting a compromised skin barrier.

4. CONCLUSIONS AND FUTURE DIRECTIONS

The primary intention of this research is to assess the therapeutic potential of the novel CYP26B1-selective retinoic acid metabolism blocking agent (RAMBA), DX314 through a series of *in vivo* studies. As the primary disease targets of these compounds are keratinization disorders, this was accomplished by characterizing the biological effects of DX314 in several 2D and 3D cultures of healthy and diseased human keratinocytes. We compare DX314 to several compounds with known therapeutic efficacy including the endogenous retinoid, retinoic acid (RA), and the two well-studied RAMBAs liarozole and talarozole.

Keratinization disorders are a heterogenous family of skin diseases related to abnormal proliferation and differentiation of epidermal keratinocytes. In this study we investigate DX314 in two such disorders, Darier's disease and congenital ichthyosis, however, it should be noted that retinoids have been studied, and/or clinically used in a wide gamut of dermatological disorders (psoriasis, acne, etc.), as well as several other diseases (cancer, neurodegenerative disorders, and more). This wide range of therapeutic applications for compounds affecting retinoid biopathways may allow DX314 to be applied in the treatment of a plethora of other diseases.

As previously discussed, there already exist several different treatments which take advantage of the role retinoids in regulating keratinocyte proliferation and differentiation. The primary strategy of many of these treatments is the direct activation of the target biopathways, typically via retinoic acid receptor (RAR) agonism. Both endogenous (e.g. retinol, retinal, tretinoin) and synthetic (e.g. adapalene, tazarotene, etretinate) retinoids that

utilize this strategy are commonly used, however they can often result in mild-to-severe adverse effects. These adverse effects are often exacerbated by the homeostatic autoregulation mechanisms controlling endogenous retinoids such as metabolic autoinduction (leading to tolerance), and directly influencing the activity or expression of factors directly involved in retinoid biopathways.

The second strategy involves indirectly modulating endogenous retinoid activity by RAMBAs (e.g. liarozole and talarozole) which function by inhibiting RA metabolism. This strategy aims to address many of the issues surrounding direct-acting retinoids in two fundamental ways: 1. They negate the autoinduction of RA-metabolizing enzymes by inhibiting their activity, reducing drug tolerance; 2. Extending endogenous retinoid activity, without needing high-doses of exogenous retinoids, which greatly reduces the risk of adverse effects caused by excessive retinoid use.

Liarozole is the most thoroughly studied RAMBA and underwent clinical studies for skin disorders including ichthyosis and psoriasis, as well as prostate and breast cancer[156]. It was found to be quite effective at alleviating patient symptoms in both ichthyosis (Figure 1.12) and palmoplantar pustular psoriasis[109], however despite advancing to phase III clinical trials, it has not received FDA approval for clinical use, likely due to its lack of CYP26 specificity (inhibitor of steroid biosynthesis, as well as several CYPs)[157]. Relative to liarozole, talarozole is a significantly more potent CYP26 inhibitor, and showed similar promise in the treatment of several skin diseases, however, it too has not proceeded past clinical trials.

Because the first-generation RAMBAs have not been approved for medical use in the US, there remains a need for a highly specific, efficacious treatment alternative that addresses the problems associated with direct retinoid therapy. This lead Diaz et al. to begin developing a library of compounds aimed at specific inhibition of CYP26-mediated RA metabolism, with minimal undesirable non-specific effects. These compounds were designed around the notion that the azole moiety in previous RAMBAs likely contributed to their off-target activity by interacting with the heme found in other CYPs, as well as other endogenous enzymes. The compounds designed by Diaz et al. do not contain an azole group, but still function as CYP26-inhibitors. Early pilot studies identified DX314, among other compounds, as promising leads for further study which led us to run the studies presented in this dissertation.

Altogether, these studies conclusively show DX314 successfully potentiates the effects of *at*RA in *in vitro* models of healthy, Darier's disease, and ichthyotic epidermis, while showing minimal evidence of undesirable off-target activity. Since the primary biological activity of retinoids is related to its nuclear receptor-mediated effects of gene expression, we investigated the gene expression changes of treatments using RT-qPCR and RNA sequencing studies. Several independent experiments comparing the effects of *at*RA and RAMBAs with, and without, low-dose *at*RA confirmed DX314's ability to potentiate the effects of *at*RA on gene expression in a similar manner to well-studied RAMBAs, with minimal observations of expression changes indicating off-target activity (Figure 2.2, Figure 2.5, Figure 2.10, Figure 3.1, Figure 3.3, Figure 3.4). Pathway and upstream regulator analysis were also done on the RNAseq study results (Figure 2.11). The most activated

upstream regulator was tretinoin (i.e. *at*RA) which was predicted to be moderately activated by low-dose *at*RA, highly activated by high-dose *at*RA, not activated by DX314 alone, and very highly activated by DX314 cotreated with low-dose *at*RA. This analysis very strongly supports our hypothesis that DX314 potentiates the effects of *at*RA, without independently acting on RA pathways. Very weak, or in most cases no activity, was predicted on the top 20 pathways and upstream regulators identified by DX314 alone which also support that DX314 does not have significant off-target activity in the absence of RA. DX314 also showed a potentiating effect on low-dose *at*RA in 75% of the pathways and regulators presented also showing strong support of our hypothesis.

To corroborate the observed gene expression changes, we performed histological immunodetection on several respective proteins. Generally, these data show agreement with the expected changes based on gene expression effects (Figure 2.3, Figure 3.2). We did see paradoxical results in CYP26A1 and CYP26B1 immunodetection, which did not appear to be consistent with the mRNA expression changes (Figure 2.4). However, as previously discussed, this inconsistency in the relationship between CYP26 mRNA and protein expression in the epidermis has been previously documented[111,138,139]. Although this effect has not yet been thoroughly investigated, it has been suggested that RA may induce a post-transcriptional mechanism, perhaps by microRNAs, which could influence the subsequent translation of CYP26 and resolve this apparent paradox.

One unexpected, but intriguing discovery in this study is the effect DX314 appears to have on RHE barrier function. The initial observation of this effect was discovered upon analysis treatment-mediated changes on transepithelial electrical resistance (TEER). TEER

informs us of the resistance to ion flow across the tissue, primarily mediated by SG tight junctions and the occlusive properties of the SC, which functions as a quantifiable measure of barrier integrity. We found that when treated alone, DX314 at the highest dose given (1000nM) significantly increases RHE TEER relative to control (Figure 2.6). This contrasts with the decrease in TEER by *at*RA, and no change in TEER by liarozole and talarozole. Additionally, liarozole and talarozole both potentiated the barrier disrupting effects of *at*RA, while DX314 appeared to protect the RHE from the expected *at*RA-induced decrease in TEER.

Histological analysis reveals the significant effect of *at*RA on epidermal morphology including, but not limited to, a significant depletion of the SG which plays a major role in barrier function (Figure 2.8, Figure 2.9, Figure 3.2). We saw very little effect on epidermal morphology when liarozole or talarozole were used alone, and an effect mimicking high-dose *at*RA when cotreated with low-dose *at*RA. DX314 on the other hand, saw minimal depletion of the SG when cotreated with *at*RA which is consistent with the observed effect on TEER. Immunodetection of the keratin aggregating protein filaggrin, which is found in the SG/SC and plays a significant role in epidermal barrier integrity, was increased by DX314 in DD RHE (Figure 3.2). In contrast, FLG staining was greatly reduced in *at*RA treated RHE, and talarozole treated RHE showed no significant change.

Unfortunately, we were not able to replicate this effect on TEER in healthy RHE due to instrument limitations, and attempts to observe significant changes in another measure of barrier function, transepithelial water loss (TEWL), were not successful (Figure 2.7). However, the recent investigation of DX314's effect in LI RHE did replicate this

increase in TEER (Figure 3.6) suggesting this barrier reinforcing effect applies to diseased epidermis as well. Despite certain issues, we believe the combination of the healthy and LI TEER studies, the RHE histology and immunodetection of barrier components, as well as the observation that many cornified envelope precursor family genes of the EDC were not affected by DX314 with *at*RA, but were with *at*RA alone (Figure 2.10), show compelling evidence that DX314 has a protective effect on the barrier function of RHE. Since many skin disorders present with a compromised skin barrier, this discovery, which is clearly not mediated by a potentiation of *at*RA, may in fact be a desirable non-specific effect of DX314. Although we do not identify, or attempt to elucidate, an explanatory mechanism in these studies, further investigation into this should be performed. If the mechanism protecting barrier function can be identified, it may lead to a completely novel class of dermatological drugs aimed at restoring a compromised skin barrier.

We currently have several studies underway which will expand upon the findings of these studies and prepare for the FDA investigative new drug (IND) application we hope to submit. Although we did not see any significant evidence of undesirable off-target activity by DX314, we have performed a small experiment showing that DX314 does not seem to directly activate RARs. We measured the expression of three, RARE-promoted (directly modulated by RAR) genes (STRA6, RBP1, TGM2), and one indirectly RA-regulated gene (HBEGF), in several treatment combinations of *at*RA, DX314, and the pan-RAR antagonist BMS493 (Supplemental Figure 4). We confirmed that *at*RA modulates the expression of these RARE-promoted genes, DX314 does not have any effect alone, but potentiates the effect of low-dose *at*RA, and BMS493 antagonizes these effects indicating

they are likely RAR-mediated. We are currently running a large nuclear receptor functional assay panel to determine if DX314 displays any activity on these receptors. A lack of significant effect by DX314 on these receptors would provide additional evidence that its effect is specific to inhibition of CYP26-mediated RA metabolism. Initial results for this study show that DX314 has no activity on RAR (α, β and γ), PPAR (α, δ and γ), or LXRβ, and can be found in supplemental data (Supplemental Figure 5).

Another major study we are currently running includes the first *in vivo* investigation of topical DX314. This study utilizes the Rhino mouse model which involves a strain of hairless mouse commonly used in the evaluation of retinoid activity on the skin[158–160]. The skin of the Rhino mouse contains keratinized structures (horn-filled utriculi) and dermal cysts which are reduced by retinoid treatment. The magnitude of this reduction can be used to assess a treatment's potential to correct dyskeratosis in keratinization disorders. Additionally, the study will investigate DX314's *in vivo* effect on TEWL to assess any changes in barrier function. This study will provide a significant leap in DX314 research by providing an *in vivo* study of the compound which will provide even greater therapeutic relevance.

Moving forward, we will also be running in-depth drug safety assessments, developing and testing possible topical formulations, and characterizing the pharmacokinetic profile of DX314 as we aim to move into towards clinical trials, and ultimately, approval of this promising therapeutic.

Altogether, we conclude the studies performed in this dissertation provide a compelling basis for further IND-enabling studies and development of DX314 as a novel

therapy in keratinization disorders. We also show DX314 may have therapeutic relevance in the treatment of Darier's disease, a disorder in which RAMBAs have not been studied in the past. Additional studies currently underway will provide significant insight into the translational application of this compound and reinforce the body of promising evidence suggesting DX314's therapeutic potential. Finally, evidence showing DX314 may reinforce skin barrier function and protect from some undesirable effects of retinoid therapy, may provide a completely novel strategy for restoring and protecting a compromised skin barrier. It is our hope that work done here will lead to significant improvements in the quality of life and outcomes of patients suffering from various dermatological disorders.

5. REFERENCES

1. Penzer, R. & Ersser, S. Biology of the Skin. in *Principles of Skin Care* 11–118 (John Wiley & Sons, Incorporated, 2010).
2. De Benedetto, A. *et al.* Tight junction defects in patients with atopic dermatitis. *J. Allergy Clin. Immunol.* **127**, 773-86.e1–7 (2011).
3. Kubo, A., Nagao, K. & Amagai, M. Review series Epidermal barrier dysfunction and cutaneous sensitization in atopic diseases. *J. Clin. Invest.* **122**, 440–7 (2012).
4. Brandner, J. M. & Schulzke, J. D. Hereditary barrier-related diseases involving the tight junction: lessons from skin and intestine. *Cell and Tissue Research* **360**, 723–748 (2015).
5. Fenner, J. & Clark, R. A. F. Anatomy, Physiology, Histology, and Immunohistochemistry of Human Skin. in *Skin Tissue Engineering and Regenerative Medicine* (eds. Albanna, M. Z. & Holmes, J. H.) 1–17 (Elsevier, 2016).
6. Haake, A., Scott, G. A. & Holbrook, K. A. Structure and Function of the Skin: Overview of the Epidermis and Dermis. in *The Biology of the Skin* (eds. Freinkel, R. K. & Woodley, D. T.) 19–46 (The Parthenon Publishing Group, 2001).
7. Mueller, S. N., Zaid, A. & Carbone, F. R. Tissue-resident T cells: dynamic players in skin immunity. *Front. Immunol.* **5**, 332 (2014).
8. Graham-Brown, R., Harman, K. & Johnston, G. *Lecture Notes: Dermatology*. *Lecture Notes Series* (John Wiley & Sons, Incorporated, 2016).
9. Eckhart, L., Lippens, S., Tschachler, E. & Declercq, W. Cell death by cornification. *Biochimica et Biophysica Acta - Molecular Cell Research* **1833**, 3471–3480 (2013).
10. Blanpain, C. & Fuchs, E. Epidermal homeostasis: a balancing act of stem cells in the skin. *Nat. Rev. Mol. Cell Biol.* **10**, 207–217 (2009).
11. Blanpain, C. & Fuchs, E. Plasticity of epithelial stem cells in tissue regeneration. *Science (80-.).* **344**, 1242281–1242281 (2014).
12. Jones, P. H., Simons, B. D. & Watt, F. M. Sic Transit Gloria: Farewell to the Epidermal Transit Amplifying Cell? *Cell Stem Cell* **1**, 371–381 (2007).
13. Simpson, C. L., Patel, D. M. & Green, K. J. Deconstructing the skin: Cytoarchitectural determinants of epidermal morphogenesis. *Nat. Rev. Mol. Cell Biol.* **12**, 565–580 (2011).
14. Moll, R., Divo, M. & Langbein, L. The human keratins: Biology and pathology. *Histochem. Cell Biol.* **129**, 705–733 (2008).
15. Seneschal, J., Clark, R. A., Gehad, A., Baecher-Allan, C. M. & Kupper, T. S. Human epidermal Langerhans cells maintain immune homeostasis in skin by activating skin resident regulatory T cells. *Immunity* **36**, 873–84 (2012).
16. Berger, C. L., Vasquez, J. G., Shofner, J., Mariwalla, K. & Edelson, R. L.

Langerhans cells: Mediators of immunity and tolerance. *Int. J. Biochem. Cell Biol.* **38**, 1632–1636 (2006).

17. Candi, E., Schmidt, R. & Melino, G. The cornified envelope: A model of cell death in the skin. *Nat. Rev. Mol. Cell Biol.* **6**, 328–340 (2005).

18. Brandner, J. M., McIntyre, M., Kief, S., Wladykowski, E. & Moll, I. Expression and localization of tight junction-associated proteins in human hair follicles. *Arch. Dermatol. Res.* **295**, 211–221 (2003).

19. Yuki, T. *et al.* Tight junction proteins in keratinocytes: Localization and contribution to barrier function. *Exp. Dermatol.* **16**, 324–330 (2007).

20. Kurasawa, M., Maeda, T., Oba, A., Yamamoto, T. & Sasaki, H. Tight junction regulates epidermal calcium ion gradient and differentiation. *Biochem. Biophys. Res. Commun.* **406**, 506–511 (2011).

21. Kirschner, N. & Brandner, J. M. Barriers and more: Functions of tight junction proteins in the skin. *Ann. N. Y. Acad. Sci.* **1257**, 158–166 (2012).

22. Menon, G. K., Grayson, S. & Elias, P. M. Ionic calcium reservoirs in mammalian epidermis: Ultrastructural localization by ion-capture cytochemistry. *J. Invest. Dermatol.* **84**, 508–512 (1985).

23. Dlugosz, A. A. & Yuspa, S. H. Coordinate changes in gene expression which Mark the spinous to granular cell transition in epidermis are regulated by protein kinase C. *J. Cell Biol.* **120**, 217–225 (1993).

24. Menon, G. K., Cleary, G. W. & Lane, M. E. The structure and function of the stratum corneum. *Int. J. Pharm.* **435**, 3–9 (2012).

25. Proksch, E., Brandner, J. M. & Jensen, J. M. The skin: An indispensable barrier. *Exp. Dermatol.* **17**, 1063–1072 (2008).

26. Ali, S. M. & Yosipovitch, G. Skin pH: From basic science to basic skin care. *Acta Derm. Venereol.* **93**, 261–267 (2013).

27. Schmid-Wendtner, M. H. & Korting, H. C. The pH of the skin surface and its impact on the barrier function. *Skin Pharmacol. Physiol.* **19**, 296–302 (2006).

28. Deraison, C. *et al.* LEKTI fragments specifically inhibit KLK5, KLK7, and KLK14 and control desquamation through a pH-dependent interaction. *Mol. Biol. Cell* **18**, 3607–19 (2007).

29. Bäsler, K. *et al.* The role of tight junctions in skin barrier function and dermal absorption. *J. Control. Release* **242**, 105–118 (2016).

30. Pasparakis, M., Haase, I. & Nestle, F. O. Mechanisms regulating skin immunity and inflammation. *Nat. Rev. Immunol.* **14**, 289–301 (2014).

31. Gallo, R. L. & Hooper, L. V. Epithelial antimicrobial defence of the skin and intestine. *Nat. Rev. Immunol.* **12**, 503–516 (2012).

32. Wood, L. C., Jackson, S. M., Elias, P. M., Grunfeld, C. & Feingold, K. R. Cutaneous barrier perturbation stimulates cytokine production in the epidermis of mice. *J. Clin. Invest.* **90**, 482–487 (1992).

33. Batista, D. I. S. *et al.* Profile of skin barrier proteins (filaggrin, claudins 1 and 4) and Th1/Th2/Th17 cytokines in adults with atopic dermatitis. *J. Eur. Acad. Dermatology Venereol.* **29**, 1091–1095 (2015).

34. Baek, J. H., Lee, S. E., Choi, K. J., Choi, E. H. & Lee, S. H. Acute modulations in stratum corneum permeability barrier function affect claudin expression and epidermal tight junction function via changes of epidermal calcium gradient. *Yonsei Med. J.* **54**, 523–528 (2013).

35. Sugawara, T. *et al.* Tight junction dysfunction in the stratum granulosum leads to aberrant stratum corneum barrier function in claudin-1-deficient mice. *J. Dermatol. Sci.* **70**, 12–18 (2013).

36. Akiyama, M. The roles of ABCA12 in epidermal lipid barrier formation and keratinocyte differentiation. *Biochim. Biophys. Acta - Mol. Cell Biol. Lipids* **1841**, 435–440 (2014).

37. Zimmerli, S. C. & Hauser, C. Langerhans cells and lymph node dendritic cells express the tight junction component claudin-1. *J. Invest. Dermatol.* **127**, 2381–2390 (2007).

38. Kubo, A., Nagao, K., Yokouchi, M., Sasaki, H. & Amagai, M. External antigen uptake by Langerhans cells with reorganization of epidermal tight junction barriers. *J. Exp. Med.* **206**, 2937–2946 (2009).

39. Horimukai, K. *et al.* Transepidermal water loss measurement during infancy can predict the subsequent development of atopic dermatitis regardless of filaggrin mutations. *Allergol. Int.* **65**, 103–108 (2016).

40. Elkeeb, R., Hui, X., Chan, H., Tian, L. & Maibach, H. I. Correlation of transepidermal water loss with skin barrier properties in vitro: Comparison of three evaporimeters. *Ski. Res. Technol.* **16**, 9–15 (2010).

41. Lucker, G. P. H. *et al.* Topical liarozole in ichthyosis: A double-blind, left-right comparative study followed by a long-term open maintenance study [2]. *Br. J. Dermatol.* **152**, 566–569 (2005).

42. McKusick-Nathans Institute of Genetic Medicine, Johns Hopkins University (Baltimore, M. Online Mendelian Inheritance in Man, OMIM. (2018). Available at: https://omim.org/.

43. Vahlquist, A., Gånemo, A. & Virtanen, M. Congenital ichthyosis: An overview of current and emerging therapies. *Acta Dermato-Venereologica* **88**, 4–14 (2008).

44. Rajpopat, S. *et al.* Harlequin ichthyosis: A review of clinical and molecular findings in 45 cases. *Arch. Dermatol.* **147**, 681–686 (2011).

45. Cooper, S. M. & Burge, S. M. Darier's disease: epidemiology, pathophysiology, and

management. *Am. J. Clin. Dermatol.* **4**, 97–105 (2003).

46. Savignac, M., Edir, A., Simon, M. & Hovnanian, A. Darier disease: A disease model of impaired calcium homeostasis in the skin. *Biochim. Biophys. Acta - Mol. Cell Res.* **1813**, 1111–1117 (2011).

47. Dicken, C. H. *et al.* Isotretinoin treatment of Darier's disease. *J. Am. Acad. Dermatol.* **6**, 721–726 (1982).

48. Lucker, G., van de Kerkhof, P., Castelijns, F. & Steijlen, P. Topical treatment of Darier's disease with 13- cis -retinoic acid. A clinical and immunohistochemical study. *J. Dermatolog. Treat.* **7**, 227–230 (1996).

49. Steijlen, P. M. *et al.* Topical treatment of ichthyoses and Darier's disease with 13-cis-retinoic acid - A clinical and immunohistochemical study. *Arch. Dermatol. Res.* **285**, 221–226 (1993).

50. Casals, M., Campoy, A., Aspiolea, F., Carrasco, M. A. & Camps, A. Successful treatment of linear Darier's disease with topical adapalene. *J. Eur. Acad. Dermatol. Venereol.* **23**, 237–8 (2009).

51. Bieber, T. Atopic dermatitis. *Ann. Dermatol.* **22**, 125–37 (2010).

52. Boguniewicz, M. & Leung, L. Y. Atopic Dermatitis: A Disease of Altered Skin Barrier and Immune Dysregulation. *Immunol. Rev.* **242**, 233–246 (2012).

53. Eichenfield, L. F. *et al.* Guidelines of care for the management of atopic dermatitis: Section 1. Diagnosis and assessment of atopic dermatitis Work Group. *J. Am. Acad. Dermatol.* **70**, 338–351 (2014).

54. Bussmann, C., Weidinger, S. & Novak, N. Genetics of atopic dermatitis. *J. Dtsch. Dermatol. Ges.* **9**, 670–6 (2011).

55. Cork, M. J. *et al.* New perspectives on epidermal barrier dysfunction in atopic dermatitis: Gene-environment interactions. *J. Allergy Clin. Immunol.* **118**, 3–21 (2006).

56. De Vuyst, E., Salmon, M., Evrard, C., Lambert de Rouvroit, C. & Poumay, Y. Atopic Dermatitis Studies through In Vitro Models. *Front. Med.* **4**, (2017).

57. De Vuyst, É., Mound, A., Lambert de Rouvroit, C. & Poumay, Y. Modelling atopic dermatitis during the morphogenetic process involved in reconstruction of a human epidermis. *Curr. Res. Transl. Med.* **64**, 179–183 (2016).

58. Orfanos, C. E., Zouboulis, C. C., Almond-Roesler, B. & Geilen, C. C. Current use and future potential role of retinoids in dermatology. *Drugs* **53**, 358–388 (1997).

59. Menter, A. *et al.* Guidelines of care for the management of psoriasis and psoriatic arthritis: Section 1. Overview of psoriasis and guidelines of care for the treatment of psoriasis with biologics. *J. Am. Acad. Dermatol.* **58**, 826–50 (2008).

60. Dawson, A. L. & Dellavalle, R. P. Acne vulgaris. *BMJ* **346**, f2634 (2013).

61. Al Tanoury, Z., Piskunov, A. & Rochette-Egly, C. Vitamin A and retinoid signaling: genomic and nongenomic effects. *J. Lipid Res.* **54**, 1761–75 (2013).

62. Balmer, J. E. & Blomhoff, R. Gene expression regulation by retinoic acid. *J. Lipid Res.* **43**, 1773–1808 (2002).

63. Huang, P., Chandra, V. & Rastinejad, F. Retinoic acid actions through mammalian nuclear receptors. *Chemical Reviews* **114**, 233–254 (2014).

64. Fisher, G. J. & Voorhees, J. J. Molecular mechanisms of retinoid actions in skin. *Faseb J.* **10**, 1002–1013 (1996).

65. Rittié, L., Varani, J., Kang, S., Voorhees, J. J. & Fisher, G. J. Retinoid-induced epidermal hyperplasia is mediated by epidermal growth factor receptor activation via specific induction of its ligands heparin-binding EGF and amphiregulin in human skin in vivo. *J. Invest. Dermatol.* **126**, 732–9 (2006).

66. Das, B. C. *et al.* Retinoic acid signaling pathways in development and diseases. *Bioorg. Med. Chem.* **22**, 673–683 (2014).

67. Roos, T. C., Jugert, F. K., Merk, H. F. & Bickers, D. R. Retinoid metabolism in the skin. *Pharmacol. Rev.* **50**, 315–333 (1998).

68. Mihály, J., Gamlieli, A., Worm, M. & Rühl, R. Decreased retinoid concentration and retinoid signalling pathways in human atopic dermatitis. *Exp. Dermatol.* **20**, 326–330 (2011).

69. Duell, E. A., Åström, A., Griffiths, C. E. M., Chambon, P. & Voorhees, J. J. Human skin levels of retinoic acid and cytochrome P-450-derived 4-hydroxyretinoic acid after topical application of retinoic acid in vivo compared to concentrations required to stimulate retinoic acid receptor-mediated transcription in vitro. *J. Clin. Invest.* **90**, 1269–1274 (1992).

70. Fisher, G. J. *et al.* Immunological identification and functional quantitation of retinoic acid and retinoid X receptor proteins in human skin. *J. Biol. Chem.* **269**, 20629–35 (1994).

71. Radoja, N. *et al.* Specific organization of the negative response elements for retinoic acid and thyroid hormone receptors in keratin gene family. *J. Invest. Dermatol.* **109**, 566–572 (1997).

72. Di, W. *et al.* Keratinocyte-specific retinoid regulation of human Cellular Retinoic Acid Binding Protein-II (hCRABPII) gene promoter requires an evolutionary conserved DR1 retinoic acid-responsive element. *J. Invest. Dermatol.* **111**, 1109–1115 (1998).

73. Loudig, O., Maclean, G. A., Dore, N. L., Luu, L. & Petkovich, M. Transcriptional co-operativity between distant retinoic acid response elements in regulation of Cyp26A1 inducibility. *Biochem. J.* **392**, 241–248 (2005).

74. Bernard, F. X., Pedretti, N., Rosdy, M. & Deguercy, A. Comparison of gene expression profiles in human keratinocyte mono-layer cultures, reconstituted

epidermis and normal human skin; Transcriptional effects of retinoid treatments in reconstituted human epidermis. *Exp. Dermatol.* **11**, 59–74 (2002).

75. Briata, P., D'Anna, F., Franzi, A. T. & Gherzi, R. AP-1 activity during normal human keratinocyte differentiation: evidence for a cytosolic modulator of AP-1/DNA binding. *Exp. Cell Res.* **204**, 136–46 (1993).

76. Elias, P. M. Retinoid effects on the epidermis. *Dermatologica* **175 Suppl**, 28–36 (1987).

77. Zouboulis, C. C. *et al.* The human sebocyte culture model provides new insights into development and management of seborrhoea and acne. *Dermatology* **196**, 21–31 (1998).

78. Trautmann, A., Akdis, M., Blaser, K. & Akdis, C. A. Role of dysregulated apoptosis in atopic dermatitis. *Apoptosis* **5**, 425–429 (2000).

79. Feng, X. *et al.* Suprabasal expression of a dominant-negative RXRα mutant in transgenic mouse epidermis impairs regulation of gene transcription and basal keratinocyte proliferation by RAR-selective retinoids. *Genes Dev.* **11**, 59–71 (1997).

80. Li, M. *et al.* RXR-alpha ablation in skin keratinocytes results in alopecia and epidermal alterations. *Development* **128**, 675–688 (2001).

81. Okano, J. *et al.* Increased retinoic acid levels through ablation of Cyp26b1 determine the processes of embryonic skin barrier formation and peridermal development. *J. Cell Sci.* **125**, 1827–1836 (2012).

82. Attar, P. S. *et al.* Inhibition of Retinoid Signaling in Transgenic Mice Alters Lipid Barrier Function. *Mol. Endocrinol.* **11**, 792–800 (1997).

83. Dawson, H. D., Collins, G., Pyle, R., Key, M. & Taub, D. D. The retinoic acid receptor-α mediates human T-cell activation and Th2 cytokine and chemokine production. *BMC Immunol.* **9**, 1–14 (2008).

84. Stephensen, C. B., Borowsky, A. D. & Lloyd, K. C. K. Disruption of Rxra gene in thymocytes and T lymphocytes modestly alters lymphocyte frequencies, proliferation, survival and T helper type 1/type 2 balance. *Immunology* **121**, 484–498 (2007).

85. Stephensen, C. B. *et al.* Vitamin A Enhances in Vitro Th2 Development Via Retinoid X Receptor Pathway. *J. Immunol.* **168**, 4495–4503 (2002).

86. Aukrust, P. *et al.* Decreased vitamin A levels in common variable immunodeficiency: Vitamin A supplementation in vivo enhances immunoglobulin production and downregulates inflammatory responses. *Eur. J. Clin. Invest.* **30**, 252–259 (2000).

87. Núñez, V. *et al.* Retinoid X receptor alpha controls innate inflammatory responses through the up-regulation of chemokine expression. *Proc. Natl. Acad. Sci. U. S. A.* **107**, 10626–31 (2010).

88. Lucker, G. P. H., Heremans, A. M. C., Boegheim, P. J., Van De Kerkhof, P. C. M. & Steijlen, P. M. Oral treatment of ichthyosis by the cytochrome P-450 inhibitor liarozole. *Br. J. Dermatol.* **136**, 71–75 (1997).

89. Bovenschen, H. J. *et al.* Oral retinoic acid metabolism blocking agent Rambazole for plaque psoriasis: an immunohistochemical study. *Br. J. Dermatol.* **156**, 263–70 (2007).

90. Kuijpers, A. L. A. *et al.* The effects of oral liarozole on epidermal proliferation and differentiation in severe plaque psoriasis are comparable with those of acitretin. *Br. J. Dermatol.* **139**, 380–389 (1998).

91. Berth-Jones, J., Todd, G., Hutchinson, P. E., Thestrup-Pedersen, K. & Vanhoutte, F. P. Treatment of psoriasis with oral liarozole: a dose-ranging study. *Br. J. Dermatol.* **143**, 1170–6 (2000).

92. Noy, N. & Blaner, W. S. Interactions of retinol with binding proteins: studies with rat cellular retinol-binding protein and with rat retinol-binding protein. *Biochemistry* **30**, 6380–6386 (1991).

93. Kurlandsky, S. B., Duell, E. A., Kang, S., Voorhees, J. J. & Fisher, G. J. Auto-regulation of retinoic acid biosynthesis through regulation of retinol esterification in human keratinocytes. *J. Biol. Chem.* **271**, 15346–15352 (1996).

94. Foti, R. S. Characterization of xenobiotic substrates and inhibitors of CYP26A1 , CYP26B1 and CYP26C1 using computational modeling and in vitro analyses Université de Nice-Sophia Antipolis. (Université de Nice-Sophia Antipolis Thèse, 2016).

95. Li, E. & Norris, A. W. Structure/function of cytoplasmic vitamin A-binding proteins. *Annu. Rev. Nutr.* **16**, 205–34 (1996).

96. Guengerich, F. P. Cytochrome P450 and Chemical Toxicology. **450**, 70–83 (2008).

97. Thatcher, J. E. & Isoherranen, N. The role of CYP26 enzymes in retinoic acid clearance. *Expert Opin. Drug Metab. Toxicol.* **5**, 875–86 (2009).

98. Taimi, M. *et al.* A novel human cytochrome P450, CYP26C1, involved in metabolism of 9-cis and all-trans isomers of retinoic acid. *J. Biol. Chem.* **279**, 77–85 (2004).

99. Wang, Y., Zolfaghari, R. & Catharine, R. A. Cloning of rat cytochrome P450RAI (CYP26) cDNA and regulation of its gene expression by all-trans-retinoic acid in vivo. *Arch. Biochem. Biophys.* **401**, 235–243 (2002).

100. Loudig, O. *et al.* Cytochrome P450RAI(CYP26) promoter: a distinct composite retinoic acid response element underlies the complex regulation of retinoic acid metabolism. *Mol. Endocrinol.* **14**, 1483–1497 (2000).

101. Abu-Abed, S. S. *et al.* Mouse P450RAI (CYP26) expression and retinoic acid-inducible retinoic acid metabolism in F9 cells are regulated by retinoic acid receptor γ and retinoid X receptor α. *J. Biol. Chem.* **273**, 2409–2415 (1998).

102. Lampen, A., Meyer, S. & Nau, H. Effects of receptor-selective retinoids on CYP26 gene expression and metabolism of all-trans-retinoic acid in intestinal cells. *Drug Metab. Dispos.* **29**, 742–747 (2001).

103. Ozpolat, B., Mehta, K. & Lopez-Berestein, G. Regulation of a highly specific retinoic acid-4-hydroxylase (CYP26A1) enzyme and all-trans-retinoic acid metabolism in human intestinal, liver, endothelial, and acute promyelocytic leukemia cells. *Leuk. Lymphoma* **46**, 1497–1506 (2005).

104. Heise, R. *et al.* Skin retinoid concentrations are modulated by CYP26AI expression restricted to basal keratinocytes in normal human skin and differentiated 3D skin models. *J. Invest. Dermatol.* **126**, 2473–2480 (2006).

105. Verfaille, C. J., Borgers, M. & van Steensel, M. A. M. Retinoic acid metabolism blocking agents (RAMBAs): a new paradigm in the treatment of hyperkeratotic disorders. *J. der Dtsch. Dermatologischen Gesellschaft = J. Ger. Soc. Dermatology JDDG* **6**, 355–364 (2008).

106. Bossche, H. Vanden, Koymans, L. & Moereels, H. P450 inhibitors of use in medical treatment: Focus on mechanisms of action. *Pharmacol. Ther.* **67**, 79–100 (1995).

107. Van Wauwe, J. *et al.* Liarozole, an inhibitor of retinoic acid metabolism, exerts retinoid-mimetic effects in vivo. *J. Pharmacol. Exp. Ther.* **261**, 773–9 (1992).

108. Kang, S., Duell, E. A., Kim, K. J. & Voorhees, J. J. Liarozole inhibits human epidermal retinoic acid 4-hydroxylase activity and differentially augments human skin responses to retinoic acid and retinol in vivo. *J. Invest. Dermatol.* **107**, 183–187 (1996).

109. Bhushan, M. *et al.* Oral liarozole in the treatment of palmoplantar pustular psoriasis: A randomized, double-blind, placebo-controlled study. *Br. J. Dermatol.* **145**, 546–553 (2001).

110. Stoppie, P. *et al.* R115866 inhibits all-trans-retinoic acid metabolism and exerts retinoidal effects in rodents. *J. Pharmacol. Exp. Ther.* **293**, 304–312 (2000).

111. Pavez Loriè, E. *et al.* Topical treatment with CYP26 inhibitor talarozole (R115866) dose dependently alters the expression of retinoid-regulated genes in normal human epidermis. *Br. J. Dermatol.* **160**, 26–36 (2009).

112. Verfaille, C. J. *et al.* Oral R115866 in the treatment of moderate to severe plaque-type psoriasis. *J. Eur. Acad. Dermatology Venereol.* **21**, 1038–1046 (2007).

113. Geria, A. N. & Scheinfeld, N. S. Talarozole, a selective inhibitor of P450-mediated all-trans retinoic acid for the treatment of psoriasis and acne. *Curr. Opin. Investig. Drugs* **9**, 1228–37 (2008).

114. Diaz, P. *et al.* Development and Characterization of Novel and Selective Inhibitors of Cytochrome P450 CYP26A1, the Human Liver Retinoic Acid Hydroxylase. *J. Med. Chem.* **59**, 2579–2595 (2016).

115. Foti, R. S., Diaz, P. & Douguet, D. Comparison of the ligand binding site of

CYP2C8 with CYP26A1 and CYP26B1: a structural basis for the identification of new inhibitors of the retinoic acid hydroxylases. *J. Enzyme Inhib. Med. Chem.* **6366**, 1–14 (2016).

116. Diaz, P., Isoherranen, N., Buttrick, B. & Guilloteau, N. Specific Inhibitors of Cytochrome P450 26 Retinoic Acid Hydroxylase. (2018).

117. Lutz, J. D. *et al.* Expression and functional characterization of cytochrome P450 26A1, a retinoic acid hydroxylase. *Biochem. Pharmacol.* **77**, 258–268 (2009).

118. Frankart, A. *et al.* Epidermal morphogenesis during progressive in vitro 3D reconstruction at the air-liquid interface. *Exp. Dermatol.* **21**, 871–875 (2012).

119. Poumay, Y. *et al.* A simple reconstructed human epidermis: Preparation of the culture model and utilization in in vitro studies. *Arch. Dermatol. Res.* **296**, 203–211 (2004).

120. De Vuyst, E. *et al.* Reconstruction of normal and pathological human epidermis on polycarbonate filter. *Methods Mol. Biol.* **1195**, 191–201 (2014).

121. Giltaire, S. *et al.* The CYP26 inhibitor R115866 potentiates the effects of all-trans retinoic acid on cultured human epidermal keratinocytes. *Br. J. Dermatol.* **160**, 505–513 (2009).

122. Willems, E., Leyns, L. & Vandesompele, J. Standardization of real-time PCR gene expression data from independent biological replicates. *Anal. Biochem.* **379**, 127–129 (2008).

123. Minner, F., Herphelin, F. & Poumay, Y. Study of Epidermal Differentiation in Human Keratinocytes Cultured in Autocrine Conditions. in *Biology of the Integument* 71–82 (2010). doi:10.1007/978-1-60761-380-0_6

124. Kim, D. *et al.* Transcript-level expression analysis of RNA- seq experiments with HISAT , StringTie and Transcript-level expression analysis of RNA-seq experiments with HISAT , StringTie and Ballgown. *Nat. Protoc.* **11**, 1650–1667 (2016).

125. Pertea, M. *et al.* StringTie enables improved reconstruction of a transcriptome from RNA-seq reads. *Nat. Biotechnol.* **33**, 290–295 (2015).

126. Love, M., Anders, S. & Huber, W. Differential analysis of RNA-Seq data at the gene level using the DESeq package. 1–32 (2013).

127. Love, M. I., Huber, W. & Anders, S. Moderated estimation of fold change and dispersion for RNA-seq data with DESeq2. *Genome Biol.* **15**, 1–21 (2014).

128. Bolger, A. M., Lohse, M. & Usadel, B. Trimmomatic: A flexible trimmer for Illumina sequence data. *Bioinformatics* **30**, 2114–2120 (2014).

129. Kim, D., Langmead, B. & Salzberg, S. L. HISAT: a fast spliced aligner with low memory requirements. *Nat. Methods* **12**, 357–360 (2015).

130. Andrews, S. FastQC: A quality control tool for high throughput sequence data.

(2010).

131. Li, H. *et al.* The Sequence Alignment/Map format and SAMtools. *Bioinformatics* **25**, 2078–2079 (2009).

132. Kim, B., Langmead, B. & Salzberg, S. genome_tran. (2017). Available at: ftp://ftp.ccb.jhu.edu/pub/infphilo/hisat2/data/grch38_tran.tar.gz. (Accessed: 25th June 2018)

133. RCoreTeam. R: A Language and Environment for Statistical Computing. (2018).

134. Klaus, B. Differential expression analysis of RNA – Seq data using DESeq2. 1–24 (2014).

135. Durinck, S., Spellman, P. T., Birney, E. & Huber, W. Mapping identifiers for the integration of genomic datasets with the R/Bioconductor package biomaRt. *Nat. Protoc.* **4**, 1184–91 (2009).

136. Zhu, A., Ibrahim, J. G. & Love, M. I. Heavy-tailed prior distributions for sequence count data: removing the noise and preserving large differences. *Bioinformatics* 1–9 (2018). doi:10.1093/bioinformatics/bty895

137. Krämer, A., Green, J., Pollard, J. & Tugendreich, S. Causal analysis approaches in ingenuity pathway analysis. *Bioinformatics* **30**, 523–530 (2014).

138. Pavez Loriè, E., Chamcheu, J. C., Vahlquist, A. & Törmä, H. Both all-trans retinoic acid and cytochrome P450 (CYP26) inhibitors affect the expression of vitamin A metabolizing enzymes and retinoid biomarkers in organotypic epidermis. *Arch. Dermatol. Res.* **301**, 475–485 (2009).

139. Pavez Loriè, E. *et al.* Expression of retinoid-regulated genes in lamellar ichthyosis vs. healthy control epidermis: Changes after oral treatment with liarozole. *Acta Derm. Venereol.* **89**, 12–20 (2009).

140. Kang, S. *et al.* Application of retinol to human skin in vivo induces epidermal hyperplasia and cellular retinoid binding proteins characteristic of retinoic acid but without measurable retinoic acid levels or irritation. *J. Invest. Dermatol.* **105**, 549–556 (1995).

141. Aström, A., Pettersson, U., Chambon, P. & Voorhees, J. J. Retinoic acid induction of human cellular retinoic acid-binding protein-II gene transcription is mediated by retinoic acid receptor-retinoid X receptor heterodimers bound to one far upstream retinoic acid-responsive element with 5-base pair spacing. *J. Biol. Chem.* **269**, 22334–9 (1994).

142. Lalevée, S. *et al.* Genome-wide in silico identification of new conserved and functional retinoic acid receptor response elements (direct repeats separated by 5 bp). *J. Biol. Chem.* **286**, 33322–34 (2011).

143. de Thé, H., Vivanco-Ruiz, M. M., Tiollais, P., Stunnenberg, H. & Dejean, A. Identification of a retinoic acid responsive element in the retinoic acid receptor beta gene. *Nature* **343**, 177–80 (1990).

144. Tomic-Canic, M., Sunjevaric, I., Freedberg, I. M. & Blumenberg, M. Identification of the retinoic acid and thyroid hormone receptor-responsive element in the human K14 keratin gene. *J. Invest. Dermatol.* **99**, 842–7 (1992).

145. Aström, A., Pettersson, U. & Voorhees, J. J. Structure of the human cellular retinoic acid-binding protein II gene. Early transcriptional regulation by retinoic acid. *J. Biol. Chem.* **267**, 25251–5 (1992).

146. Vasios, G. W., Gold, J. D., Petkovich, M., Chambon, P. & Gudas, L. J. A retinoic acid-responsive element is present in the 5' flanking region of the laminin B1 gene. *Proc Natl Acad Sci U S A* **86**, 9099–9103 (1989).

147. Fisher, G. J. *et al.* All-trans retinoic acid induces cellular retinol-binding protein in human skin in vivo. *J. Invest. Dermatol.* **105**, 80–86 (1995).

148. Laursen, K. B., Kashyap, V., Scandura, J. & Gudas, L. J. An alternative retinoic acid-responsive Stra6 promoter regulated in response to retinol deficiency. *J. Biol. Chem.* **290**, 4356–4366 (2015).

149. Kypriotou, M., Huber, M. & Hohl, D. The human epidermal differentiation complex: Cornified envelope precursors, S100 proteins and the 'fused genes' family. *Exp. Dermatol.* **21**, 643–649 (2012).

150. Digiovanna, J. J., Mauro, T., Milstone, L. M., Schmuth, M. & Toro, J. R. Systemic retinoids in the management of ichthyoses and related skin types. *Dermatol. Ther.* **26**, 26–38 (2013).

151. Vahlquist, A. *et al.* Oral liarozole in the treatment of patients with moderate/severe lamellar ichthyosis: Results of a randomized, double-blind, multinational, placebo-controlled phase II/III trial. *Br. J. Dermatol.* **170**, 173–181 (2014).

152. Zheng, D. *et al.* Topical delivery of siRNA-based spherical nucleic acid nanoparticle conjugates for gene regulation. *Proc. Natl. Acad. Sci.* **109**, 11975–11980 (2012).

153. Presland, R. B., Tomic-Canic, M., Lewis, S. P. & Dale, B. A. Regulation of human profilaggrin promoter activity in cultured epithelial cells by retinoic acid and glucocorticoids. *J. Dermatol. Sci.* **27**, 192–205 (2001).

154. Ågren, J. *et al.* Transepidermal water loss in developing rats: Role of aquaporins in the immature skin. *Pediatr. Res.* **53**, 558–565 (2003).

155. Lee, Y. *et al.* Changes in transepidermal water loss and skin hydration according to expression of aquaporin-3 in psoriasis. *Ann. Dermatol.* **24**, 168–174 (2012).

156. Njar, V. C. O. *et al.* Retinoic acid metabolism blocking agents (RAMBAs) for treatment of cancer and dermatological diseases. *Bioorganic Med. Chem.* **14**, 4323–4340 (2006).

157. Nelson, C. H., Buttrick, B. R. & Isoherranen, N. Therapeutic potential of the inhibition of the retinoic acid hydroxylases CYP26A1 and CYP26B1 by xenobiotics. *Curr. Top. Med. Chem.* **13**, 1402–28 (2013).

158. Mezick, J. A., Bhatia, M. C. & Capetola, R. J. Topical and systemic effects of retinoids on horn-filled utriculus size in the rhino mouse. A model to quantify 'antikeratinizing' effects of retinoids. *J. Invest. Dermatol.* **83**, 110–3 (1984).

159. Kligman, L. H. & Kligman, A. M. The effect on rhino mouse skin of agents which influence keratinization and exfoliation. *J. Invest. Dermatol.* **73**, 354–358 (1979).

160. Hsia, E., Johnston, M. J., Houlden, R. J., Chern, W. H. & Hofland, H. E. J. Effects of topically applied acitretin in reconstructed human epidermis and the rhino mouse. *J. Invest. Dermatol.* **128**, 125–30 (2008).

161. Jing, J. *et al.* Physiologically Based Pharmacokinetic Model of All-trans-Retinoic Acid with Application to Cancer Populations and Drug Interactions. *J. Pharmacol. Exp. Ther.* **361**, 246–258 (2017).

6. APPENDICES

6.1 SUPPLEMENTAL DATA

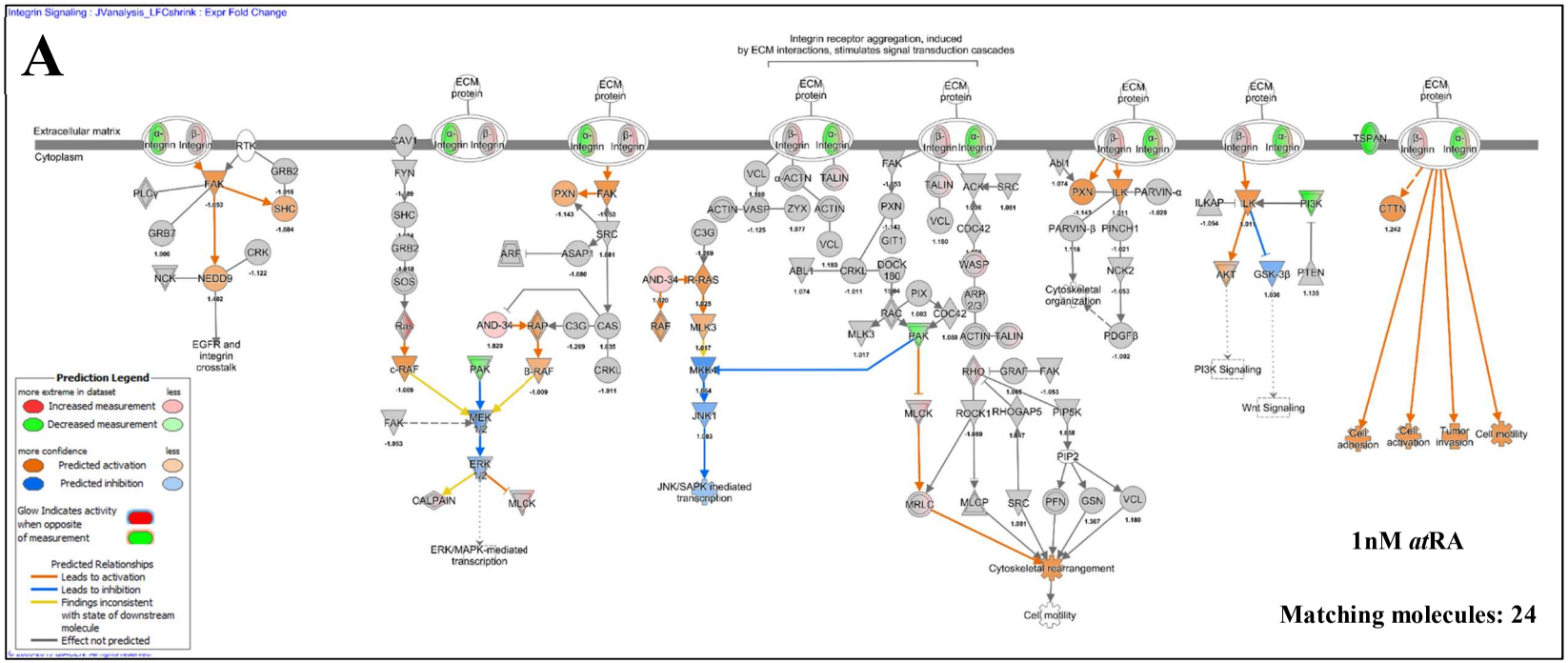

Supplemental Figure 1: Integrin signaling pathways. IPA predicted activity of canonical pathway components based on differential expression analysis by RNAseq: (a) 1nM *at*RA, (b) 100nM *at*RA, (c) 1000nM DX314, (d) 1000nM DX314 + 1nM *at*RA, which have 24, 78, 0, and 46 matching molecules, respectively. Values below each molecule shows respective fold-change in RNA expression from control.

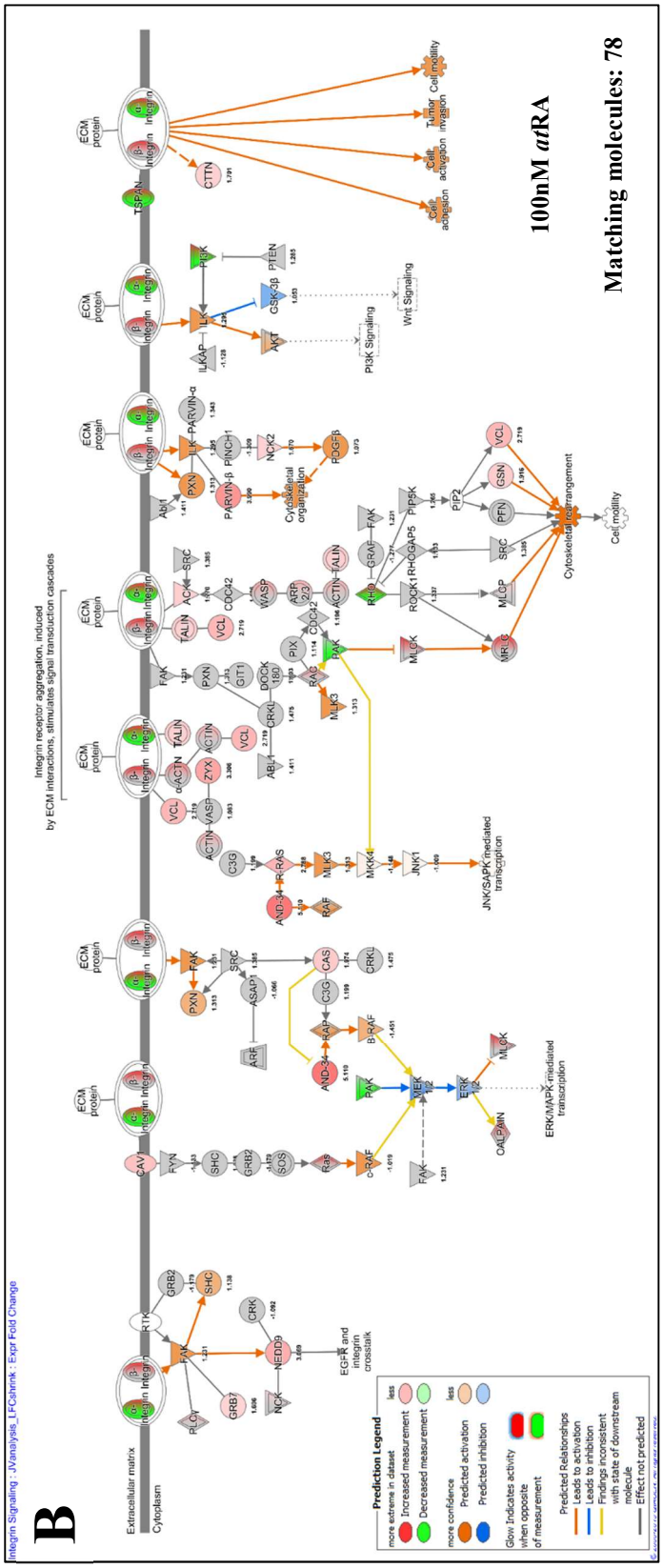

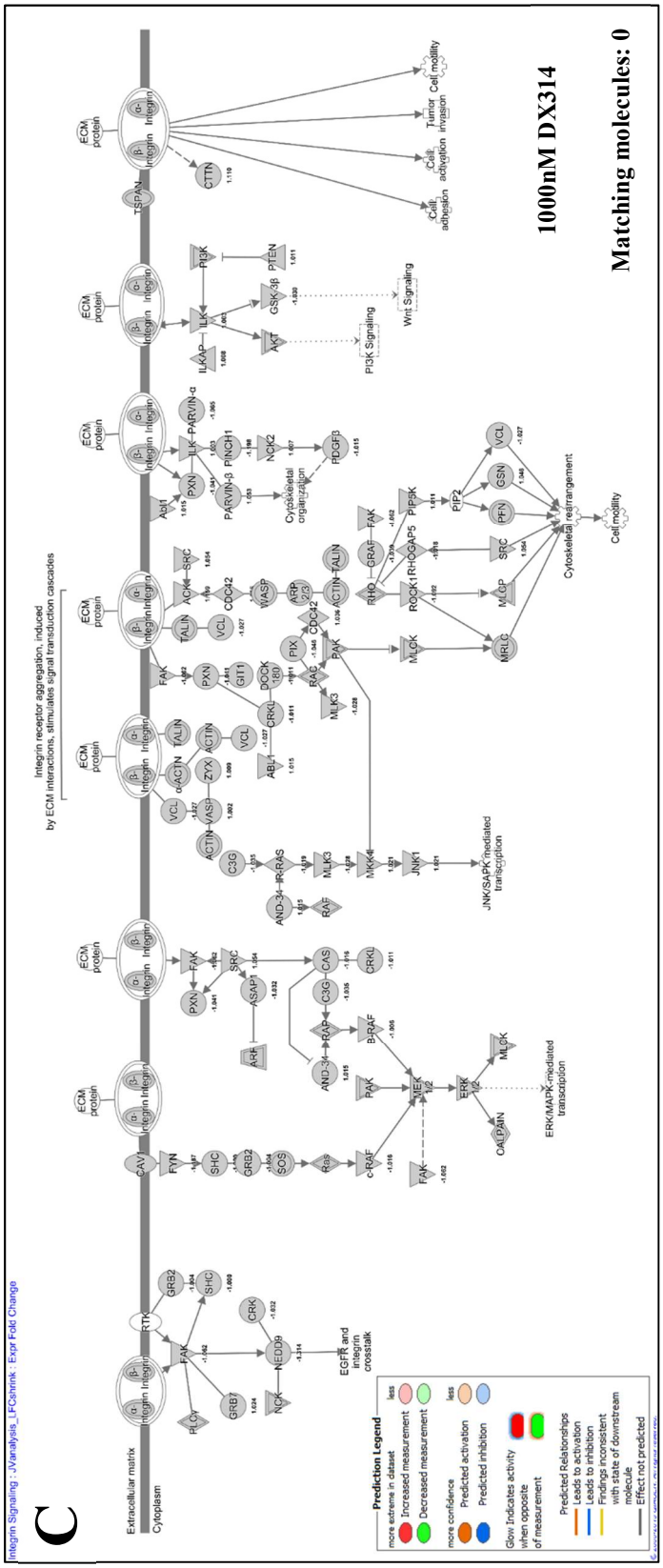

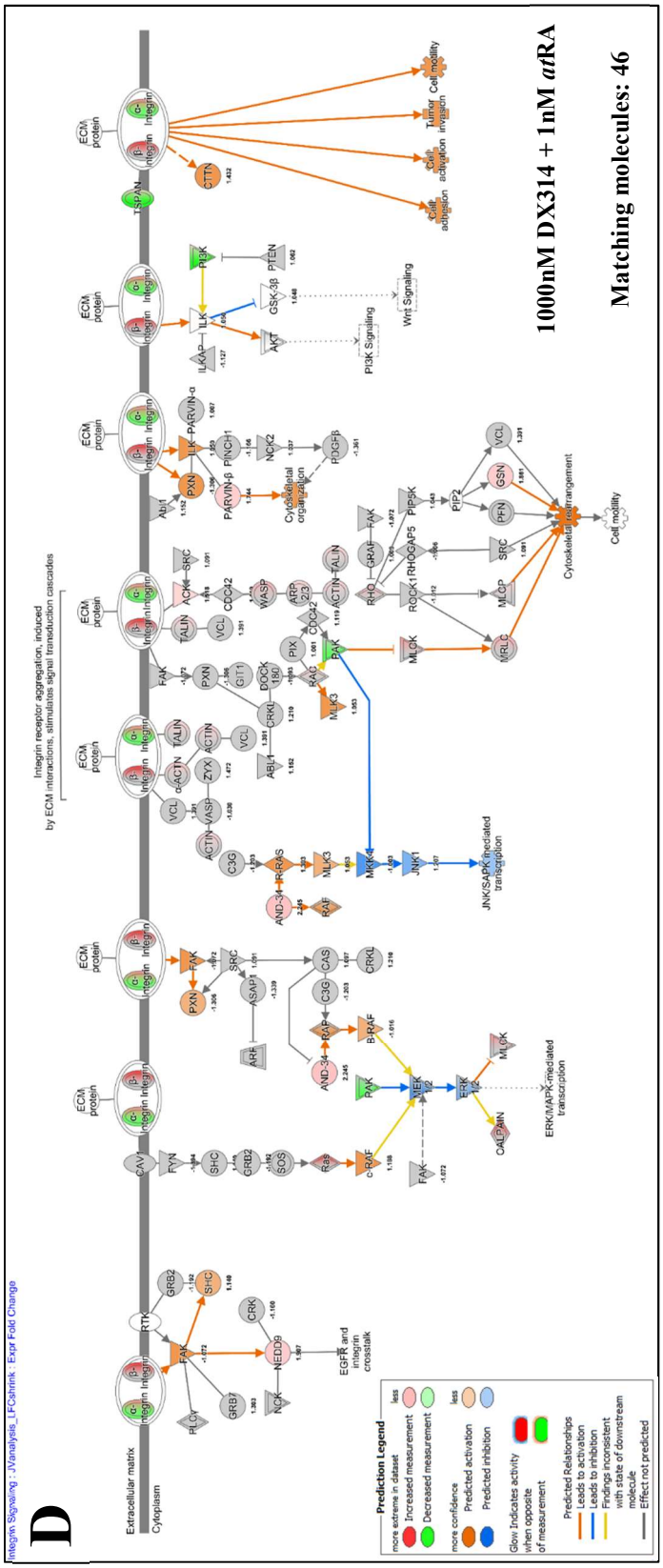

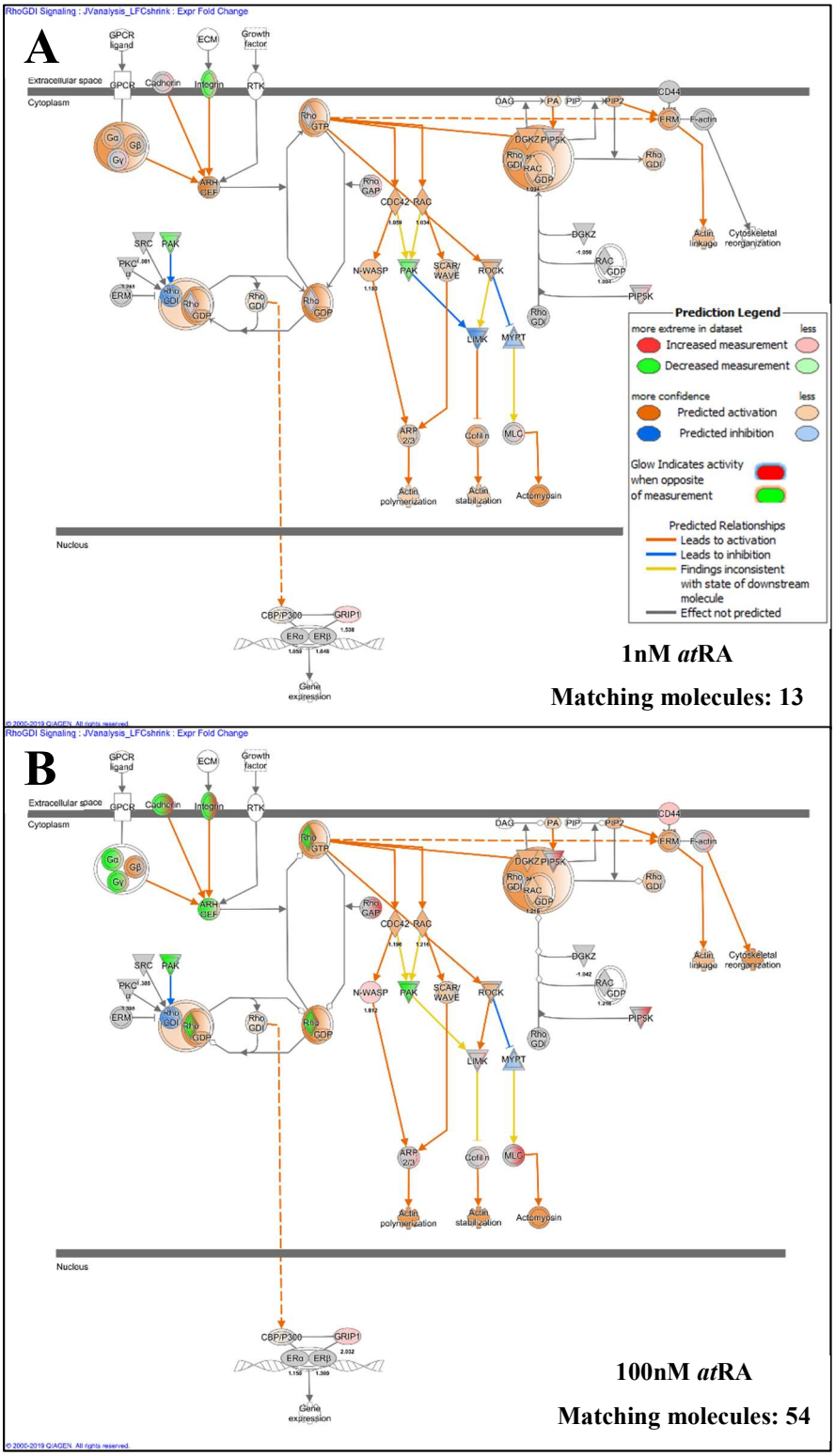

Supplemental Figure 2: RhoDGI Signaling Pathway. IPA predicted activity of canonical pathway components based on differential expression analysis by RNAseq: (a) 1nM *at*RA, (b) 100nM *at*RA, (c) 1000nM DX314, (d) 1000nM DX314 + 1nM *at*RA. Values below each molecule shows respective fold-change in RNA expression from control.

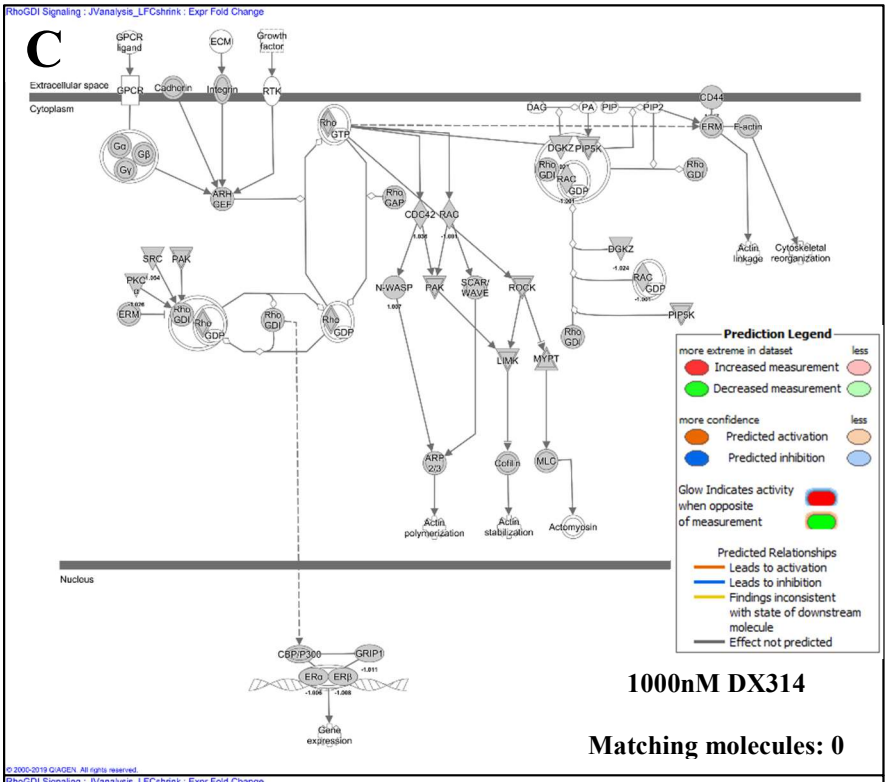

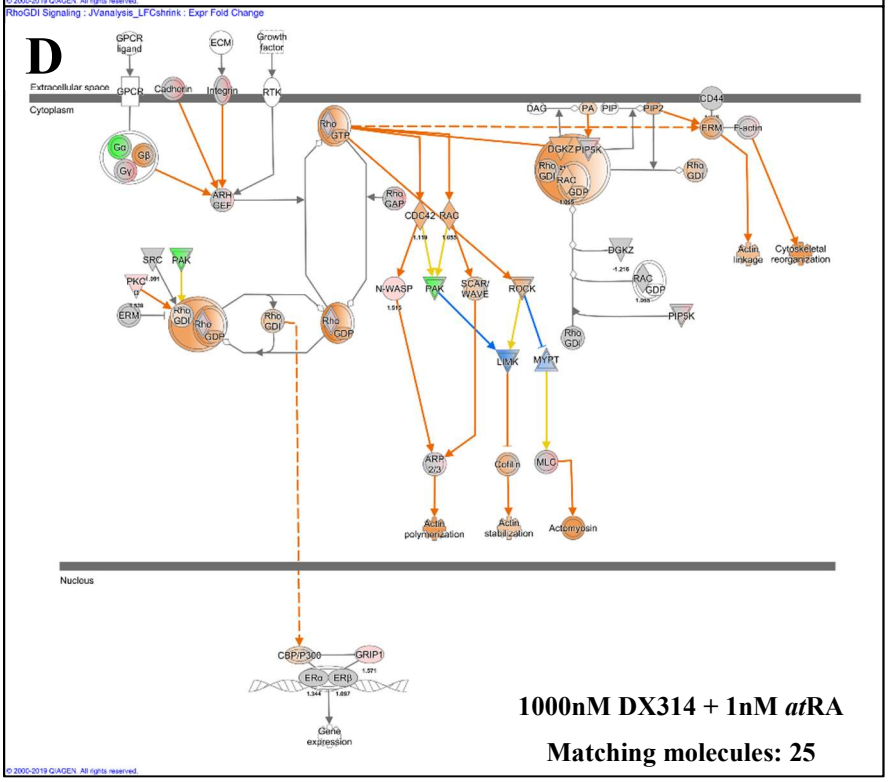

A

1nM *at*RA

Matching molecules: 15

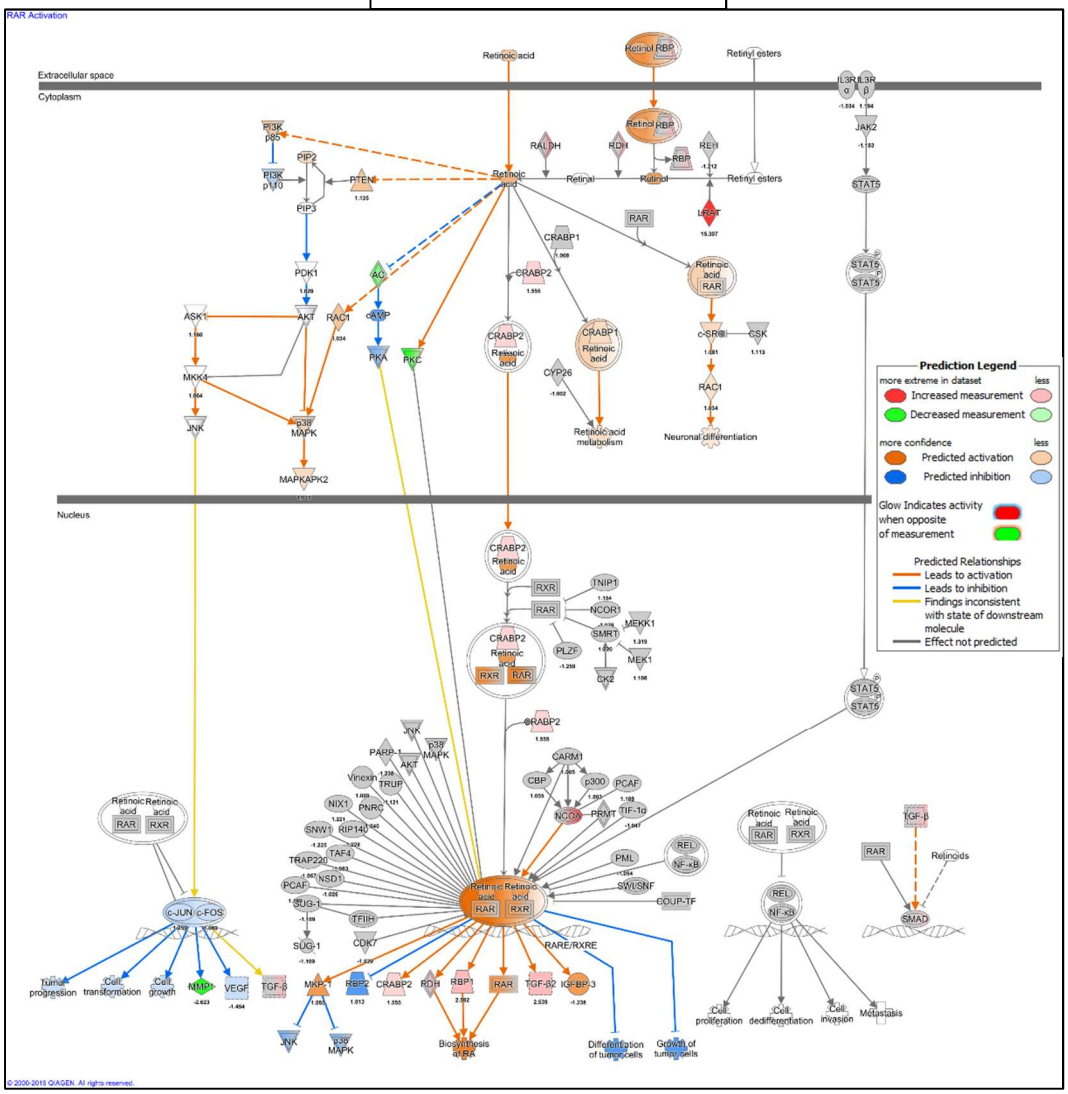

Supplemental Figure 3: RAR Activation Pathway. IPA predicted activity of canonical pathway components based on differential expression analysis by RNAseq: (a) 1nM *at*RA, (b) 100nM *at*RA, (c) 1000nM DX314, (d) 1000nM DX314 + 1nM *at*RA. Values below each molecule shows respective fold-change in RNA expression from control.

B

100nM *at*RA

Matching molecules: 53

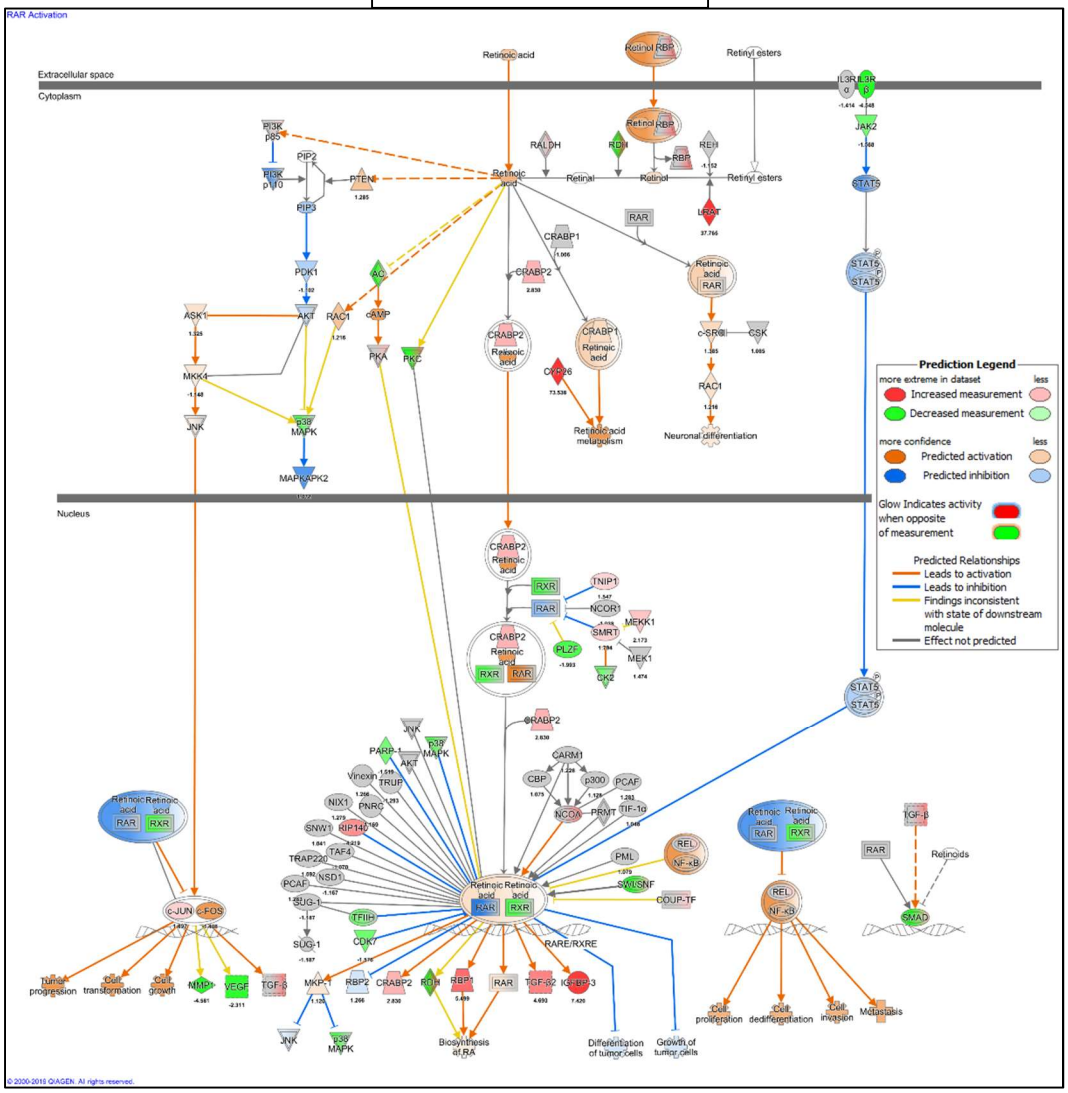

C

1000nM DX314

Matching molecules: 4

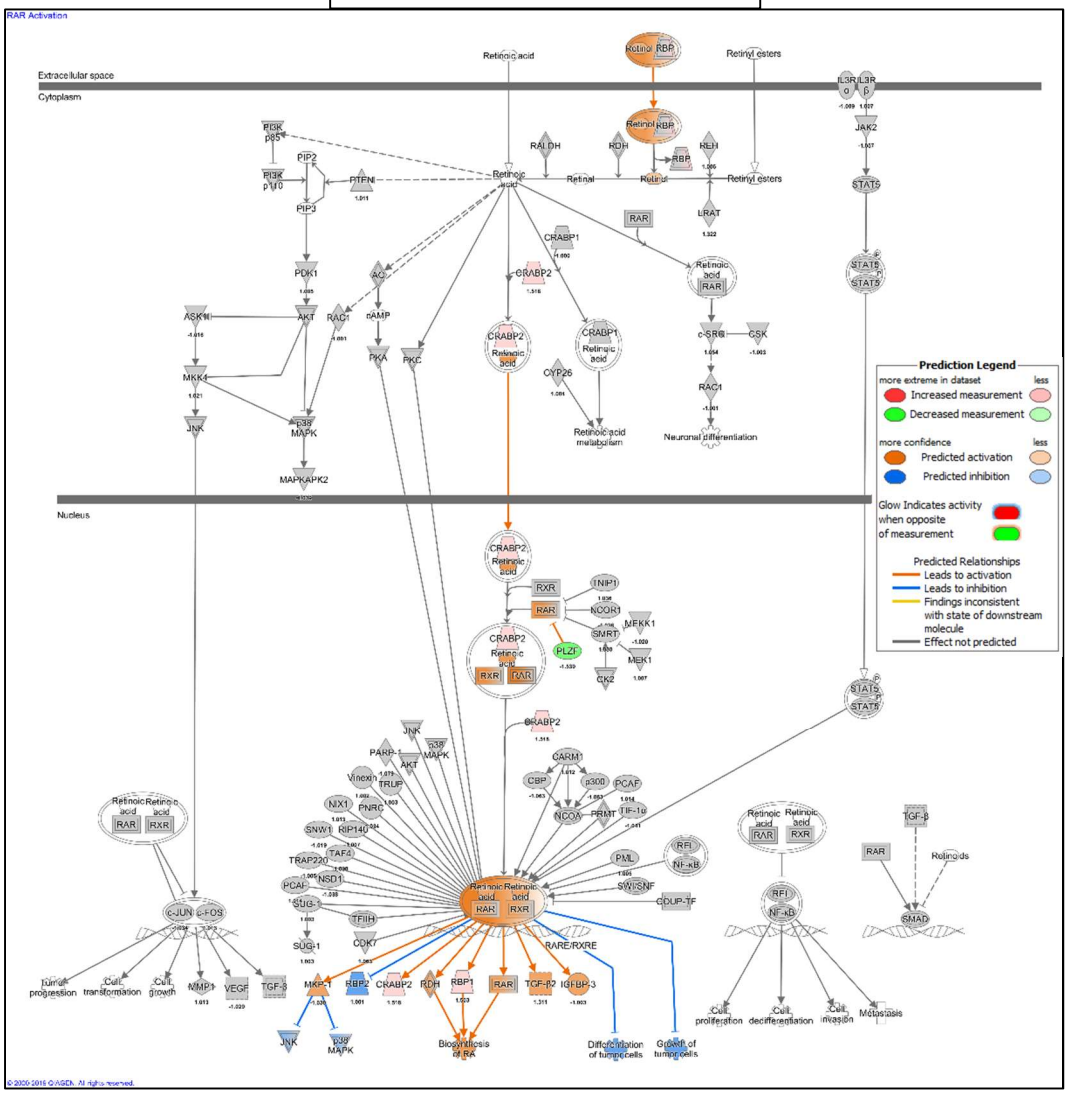

D

1000nM DX314 + 1nM *at*RA

Matching molecules: 29

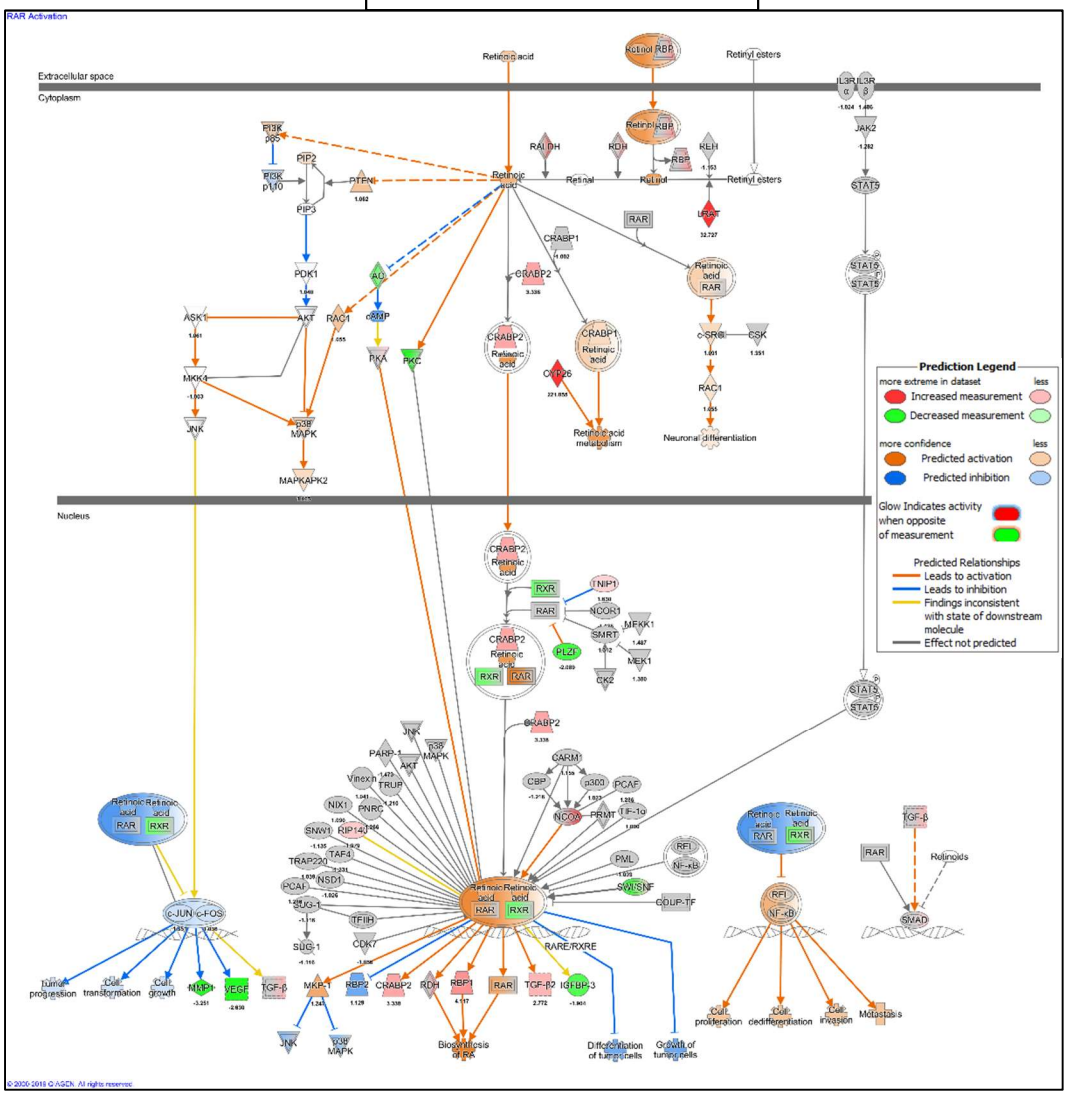

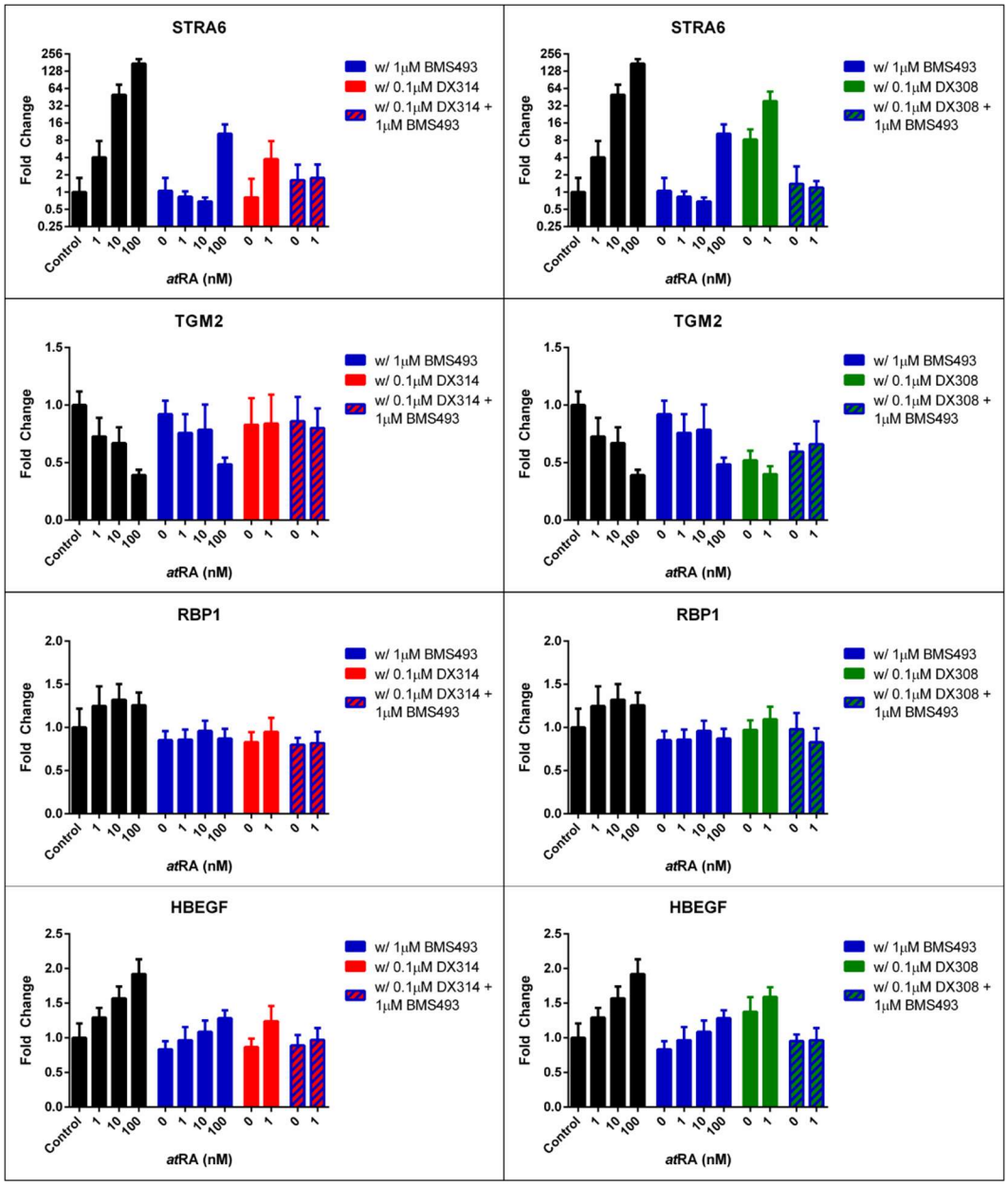

Supplemental Figure 4: Effect of pan-RAR antagonist BMS493 on gene expression effects by atRA, RAMBAs. Effects of candidate RAMBAs DX314 (left column) or DX308 (right column) with, or without, low dose *at*RA, on HBEGF, and RARE-promoted (STRA6, TGM2, RBP1) gene expression compared to *at*RA. All treatments are also done in the presence, or absence, of pan-RAR antagonist BMS493. This study was performed in autocrine monolayer cultures of healthy keratinocytes. Bars show mean ± 95% CI.

	EC50 (nM)						
	RARα	RARβ	RARγ	PPARα	PPARδ	PPARγ	LXRβ
DX314	IA	IA	IA	IA	IA	IA	IA
DX308	9040	>10,000	IA	IA	IA	IA	IA
AM580	0.18	7.6	24.5	-	-	-	-
Tazarotene	32.5	3.3	25.5	-	-	-	-
BRL49653	-	-	-	IA	IA	168.5	IA
GW7647	-	-	-	52	3697	1333	IA
GW3965	-	-	-	IA	IA	IA	221.3
GW501516	-	-	-	IA	1.3	IA	IA

Supplemental Figure 5: Nuclear Receptor EC50 Screening of DX314, DX308. Performed by Syneos Health using HeLa lec2P/9XGAL4 cell lines transfected with expression vector for respective nuclear receptor. IA = Inactive.

Note: This data shows the preliminary data of an ongoing study and may not represent the final study results.